University of Alberta

Transverse Relaxation of Rat Optic Nerve

by

Isidro Bonilla   ©

A thesis submitted to the Faculty of Graduate Studies and Research in partial fulfillment
of the requirements for the degree of Master of Science

In the

Department of Biomedical Engineering

Edmonton, Alberta

Fall 2004

Canada

Acknowledgements

I would like to thank my family for all their love and support, you have always been with me and you always encourage me to accomplish my goals; my dad and my mom who have thought me a lot about commitment and responsibility; my sister for her cheering; my nephew Jose Luis for very "long" and cute conversations consisting of "hola and ok bye". I want to thank my girlfriend (& family) for her love, support and patience. Yes, I can be moody when I am stressed but you know how to make me happy again ☺. Doing stuff with you is the "best day of my day besitos".

I would like to thank my supervisor Dr. Richard E. Snyder for all his support and help during my studies. Thanks for teaching me about planning my experiments and being more concise with my scientific writing ("remember you are not writing a novel get to the point soon"). Also thanks to Keith who thought me a lot about SMIS and NNLS. I really appreciate the time that Monica and Frances spent reviewing my thesis, your comments were very helpful. I thank my teachers in NMR Drs. Allen, Beaulieu and Wilman, I enjoyed the classes; they were hard but you always found the way in which we could understand the NMR concepts. Thanks to Dan for keeping the magnets in excellent conditions for our experiments. I am grateful for the opportunity to be part of this department and for meeting very nice people; Amir my officemate, who has been a very good friend and who likes to talk a lot like me hehe. Atiyah, thanks for answering my questions about MR and coils, it was always fun to try to fix the world and end up talking about soccer. Jacob sap joe!. Luis, my Mexican buddy, the doctor that I think in his other life was an engineer. Kim, it was nice to know that if we have to work until late you will be there. Robby we still have to go for a round of squash. Yussuf, I hope I follow your commitment and go to the gym.

Thanks to all the people in the department Alison, Chango, Daniel san, Jane, Jason, Lindsey, Myrlene, Peter, Sasha and Steven (Topito). A special recognition to Maisie, Brenda and Carol for keeping the department running efficiently and being very helpful with students needs.

Thanks to all my friends in Juarez and Monterrey, even if sometimes we spend several months without seen each other, we kept the friendship no matter what!. Thanks to the country racquet club's boys for all your support and funny e-mails that helped me keep on going. I have met very nice people in Edmonton, thanks to you all. For the Mexican gang it was fun to hang out with you guys.

Table of Contents

List of Tables

Chapter 1- Introduction and Background

Chapter 2- Methods and Materials

Chapter 3- Experiments to Determine the Existence of Three T_2 Spectral Components

Chapter 4- Experiments to Establish the Component-Compartment Relationship

Chapter 5- Water Compartments and T_2 Components of the Optic Nerve

List of Figures

Chapter 1- Introduction and Background

Chapter 2- Methods and Materials

Chapter 3- Experiments to Determine the Existence of Three T_2 Spectral Components

Chapter 4- Experiments to Establish the Component-Compartment Relationship

Chapter 5- Water Compartments and T_2 Components of the Optic Nerve

LIST OF SYMBOLS AND ABREVIATIONS

ADC   Apparent Diffusion Coefficient

B   Net magnetic field vector

$\mathbf{B}_0$ External static magnetic field vector

B_0 Magnitude of $\mathbf{B}_0$

$\mathbf{B}_{eff}$ Effective magnetic field in the rotating frame

$\mathbf{B}_1$ Externally applied radio-frequency magnetic field vector

B_1 Amplitude of B_1 field

BPP   Bloembergen, Purcell and Pound

C   Concentration of paramagnetic agent

CNS   Cental Nervous System

CPMG   Carr-Purcell-Meiboom-Gill

CSF   Cerebrospinal Fluid

DNA   Desoxyreibonucleic acid

FID   Free Induction Decay

fMRI   Functional Magnetic Resonance Imaging

Gd-DTPA	Gadolinium-diethylenetriaminepentaacetic acid
h	Planck's constant
$\hbar$	Planck's constant divided by 2π
^{1}H	Hydrogen nuclei
Hz	Hertz
I	Spin angular moment operator
I	Spin quantum number
k	Boltzmann's constant
m	Quantum magnetic number
M	Magnetization vector
M_z	Magnetization in z-axis
M_0	Longitudinal Magnetization
M_{xy}	Transverse Magnetization
MET_2	Multi-exponential transverse relaxation
MHz	Megahertz
MRA	Magnetic Resonance Angiography
MRI	Magnetic Resonance Imaging
MRS	Magnetic Resonance Spectroscopy
MS	Multiple Sclerosis

NMR	Nuclear Magnetic Resonance
NNLS	Non Negative Least Square
PNS	Peripheral Nervous System
RF	Radio Frequency
SNR	Signal to Noise Ratio
SE	Spin Echo
T	Absolute temperatue, or Tesla
T_1	Longitudinal relaxation time
T_2	Transverse relaxation time
T_2^*	Time constant characterizing decay of FID in an inhomogeneous static magnetic field
TE	Echo Time
TR	Sequence repetition time
TI	Inversion recovery time
ΔB	Magnetic field inhomogeneity
ΔE	Energy difference between spin orientation states
α	Flip angle
α_1	Relaxivity for longitudinal relaxation
α_2	Relaxivity for Transverse relaxation

γ	Gyromagnetic ratio
μ	Magnetic moment
τ	Torque or time
ν	Magnetic resonance frequency
ω_1	Angular frequency of the RF pulse
ω_0	Larmor frequency (resonance frequency)
$(90°)_x$	90° RF pulse in the x direction in the rotating frame
$(180°)_y$	180° RF pulse in the y direction in the rotating frame

Chapter 1

Introduction and Background

1.1- Introduction to the Thesis

Nuclear magnetic resonance (NMR) has evolved into amazing and exciting medical applications such as: 1) Magnetic Resonance Imaging (MRI), in which images of the body can be produced in a non-invasive way from signal obtained from nuclei of the tissue, commonly hydrogen, giving valuable diagnostic information about anatomical disorders or pathologies, 2) Magnetic Resonance Spectroscopy (MRS), which can non-invasively determine the presence of different metabolites in tissue, 3) Functional Magnetic Resonance Imaging (fMRI), which identifies active regions of the brain based on blood flow, and 4) Magnetic Resonance Angiography (MRA), which produces quality images of the blood vessels to determine more accurately diseases related to blood flow. The above modalities observe tissue at a macroscopic scale; they obtain signal from voxels ≥ 1 mm^3. We want to approach NMR in a different way, using it to determine micro-anatomical information in tissue based upon a NMR property known as relaxation. Often, diseased and other altered states of tissue present modifications in their micro-anatomical structures; these changes may alter the relaxation times of the tissue [1]. Thus, if relaxation may be understood and measured *in vivo*, it may provide useful diagnosis information.

Relaxation depends upon interaction of the nuclei with their environment; in this study we analyze signal from ^{1}H (proton) present in water. There are two types of relaxation: i) longitudinal, which occurs as a consequence of thermal energy dissipation and ii) transverse, a phenomenon that this thesis is based on, which occurs as a consequence of nuclear spin interactions. Nervous tissue contains differing micro-anatomical water compartments, that is, regions within the tissue in which the molecular environment of the water differs from that of another. From an NMR point of view, these compartments in the case of the peripheral nervous system (PNS) are the myelin, axoplasm,

extracellular space (ECS) and Schwann cells engulfed by the perineurial sheath; for the case of the central nervous system (CNS) the compartments are myelin, axoplasm, glial cells and ECS covered by meningeal sheaths of dura. Assuming the majority of the water remains in a specific compartment for at least a few hundred milliseconds, each compartment may be characterized by a different water proton transverse-relaxation (T_2) time. A given tissue may thus contain multiple T_2 times or components that can be obtained through measurement, either *in vivo* or *in vitro*, of a T_2-relaxation spectrum, each component associated with one or more micro-anatomical compartments. Thus, measurements of T_2 relaxation times and spectra *in vivo* may be able to identify specific compartments in nerves that could be related to diseased states (such as pathologies related with demyelination).

Amphibian and rat sciatic nerve have been studied both *in vivo* using MRI and *in vitro* using excised tissue samples [2-6]. Both species of nerve have been found to exhibit a three-component T_2-relaxation spectrum. Studies of amphibian nerve have suggested the relationship between the components of the T_2 spectrum and the compartments of the nerve, that is, which micro-anatomical compartment gives rise to a given spectral component [6, 7]. The establishment of this relationship may provide valuable information about specific regions of the nerve. Preliminary studies in our laboratory performed using standard *in-vitro* techniques have found rat optic nerve to be characterized by a three-component T_2-relaxation spectrum [8, 9]. However, white matter, studied by MRI, exhibits only a two-component T_2 spectrum [10], and excised bovine optic nerve studied *in vitro* has also been reported to exhibit only two components [11]. This raises the question as to whether a fundamental difference exists between the T_2 spectra of peripheral and optic nerve, the latter physiologically similar to central nervous tissue, or whether differences in optic-nerve component numbers relate to experimental measurement techniques or species.

In this study, rat optic nerve was analyzed *in vitro* because it is considered an extension of the CNS and the risk of damaging the nerve is less than using the whole brain or white matter tracks. While to be of clinical value T_2 spectra must be measured *in vivo* using

MRI techniques, *in-vitro* measurements of excised tissue offer distinct advantages in terms of understanding the spectra. Experiments *in vitro* may provide information that is not possible to obtain *in vivo*, providing a good approach to understanding the different compartments of nervous tissue [12]. Chapter 1 of this thesis presents an overview of NMR and nerve anatomy. Chapter 2 defines the methods followed to accomplish the main objectives of this study. Chapter 3 determines whether rat optic nerve is characterized by a 2- or 3-component T_2-relaxation spectrum and chapter 4 determines whether the spectral components are characterized by a similar relationship to the micro-anatomical compartments as found in amphibian sciatic nerve. This latter objective was accomplished through the addition of paramagnetic ions to the bathing solution, which reduce the T_2-relaxation time of the water compartments to which they have access [13-15], and through cellular swelling resulting from the addition of glutamate to the buffer solution. An assignment between the micro-anatomical compartments of the nerve and T_2 components is suggested. Chapter 5 presents an extensive discussion of the results and chapter 6 deals with the conclusion of our studies.

1.2- Principles of NMR

1.2.1- Basic NMR Theory

In order to perform an NMR experiment we need nuclei that have a nuclear magnetic moment (μ). Protons and neutrons form the nuclei of elements. Protons give the nuclei the positive charge and their atomic number. The sum of the number of protons and neutrons is the mass number.

It is important to know the number of protons and neutrons in the nuclei. If the nuclei are even-even, which means the nuclei have an even number of protons and of neutrons, the circulating currents in the nucleus cancel each other and no nuclear magnetic moment is obtained. On the other hand, if the nuclei have an odd number of protons, neutrons, or both, the currents do not cancel each other and a nuclear magnetic moment will be generated. Table 1.1 shows this information for different elements [16].

Table 1.1- Characteristics of the nuclei of different elements present in biological systems and their Naturally Occurring Fractions (NOF). Also are shown the Nuclear Magnetic Moment (NMM).						
Element	Mass No.	Protons	Neutrons	Classification	NMM	NOF
Hydrogen	1	1	0	Odd-even	Yes	99.98%
Carbon	12	6	6	Even-even	No	98.9%
	13	6	7	Even-odd	Yes	1.1%
Nitrogen	14	7	7	Odd-odd	Yes	99.63%
Oxygen	16	8	8	Even-even	No	99.96%
Sodium	23	11	12	Odd-even	Yes	100%
Phosphorus	31	15	16	Odd-even	Yes	100%

Living organisms are largely made out of water. Approximately 70% of the total volume in the human body is water. It is a wonderful coincidence that hydrogen, which is present in great percentages in the human body, has a nuclear magnetic moment that makes it viable for NMR experiments because it is possible to obtain enough signal to examine living organisms based on NMR studies.

The internal properties of the nucleus give rise to a nuclear characteristic called "spin angular momentum"; the spin angular momentum operator I is measured in units of $\hbar$, where $\hbar = h / 2\pi$ (h = Planck's constant = 6.63×10^{-34} J s). The magnitude of the spin angular momentum is $\hbar(I (I+1))^{1/2}$, where I is known as the spin quantum number or spin of the nucleus. For even-even nuclei, where the internal circulations cancel each other, the spin angular momentum is zero. For the other nuclei I can take half integer or integer values [1]. There is a unique relationship between the nuclear magnetic moment (μ) and I, involving the gyromagnetic ratio, γ, which is expressed in the next equation:

$$\mu = \gamma \, \hbar \, I \qquad (1.1)$$

When a nucleus of spin I is placed in a magnetic field, the energy of interaction between the magnetic moment μ and the magnetic field B_0 can be represented by the dot product as:

$$E = - \mu \cdot B = - \gamma \, \hbar \, B_0 \, m \qquad (1.2)$$

where m, the quantum magnetic number, can take the values I = -I, -I+1,.....I. The total number of energy levels is 2I+1. Hydrogen, for example, with a spin of ½, can occupy 2(½) + 1 = 2 energy states [17]. In the antiparallel state, where the spins align against the magnetic field, it is possible to determine the energy related with the spin −½ by substituting m = -½ in Eq. (1.2):

$$E_{anti} = (\gamma \hbar B_0) / 2 \qquad (1.3)$$

For the parallel state, spins aligned with the magnetic field, a similar equation can be obtained with the spin ½ and substituting m = ½ into Eq. (1.2):

$$E_{parallel} = -(\gamma \hbar B_0) / 2 \qquad (1.4)$$

The energy of separation between the equally spaced levels is thus

$$\Delta E = \gamma \hbar B_0 \qquad (1.5)$$

which corresponds to a frequency, based upon the Bohr relationship, of

$$\nu = \Delta E / h = \gamma B_0 / 2\pi \qquad (1.6)$$

Knowing that $\nu = \omega_0 / 2\pi$, we can obtain the frequency of nuclear precession known as the **Larmor frequency** [16]:

$$\omega_0 = \gamma B_0 \qquad (1.7)$$

The precessional frequency of hydrogen protons at a magnetic field of 3 Tesla, the field strength used in our studies, is $\omega_0 = \gamma B_0 = 42.55$ (MHz/T) * 3 (T) = 127.7 MHz. Each nuclear species resonates at a different Larmor frequency at a given field strength, which means that a specific RF coil is needed to measure signal from each type of nucleus. The gyromagnetic ratios are not the same for different nuclei; in Table 1.2 are listed these values for a number of biologically important nuclei [18].

Table 1.2- Gyromagnetic ratios for different nuclei			
Nucleus	Symbol	I	γ (MHz/T)
Proton	^{1}H	$^1/_2$	42.55
Deutron	^{2}H	1	6.54
Carbon	^{13}C	$^1/_2$	10.68
Nitrogen	^{14}N	1	3.07
	^{15}N	$^1/_2$	4.31
Oxygen	^{17}O	$^5/_2$	5.77
Sodium	^{23}Na	$^3/_2$	11.25
Phosphorus	^{31}P	$^1/_2$	17.23
Chlorine	^{35}Cl	$^3/_2$	4.17
	^{37}Cl	$^3/_2$	3.47
Potassium	^{39}K	$^3/_2$	1.98

After explaining the behavior of a single spin in a magnetic field, we have to understand what happens to several spins in a real NMR experiment. At the beginning of the experiments we can pretend that the system is just a bag full of little nuclear magnets. In the absence of any external interactions this bag can be represented as in fig. 1.1.
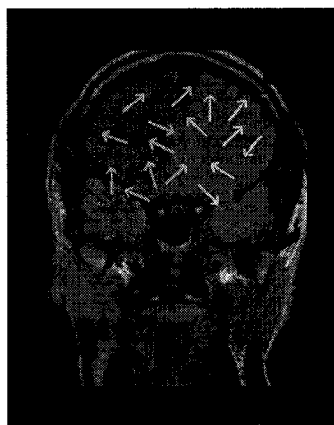
Fig 1.1- Representation of the magnetic dipoles (arrows) with no magnetic field applied to the system. Note that all the dipoles have random orientations. The net magnetization is equal to zero.

To perform an NMR experiment we have to place the sample into the magnet bore to make it experience the large homogenous and static magnetic field B_0, which will align all the magnetic dipoles either parallel or anti-parallel to the main magnetic field as it is shown in fig. 1.2.
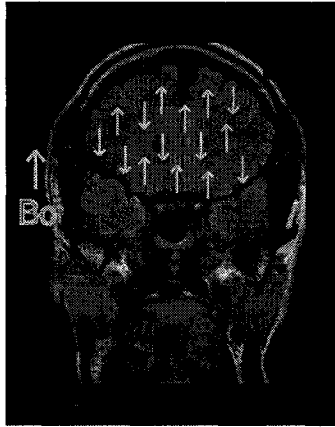
Fig. 1.2 -Representation showing magnetic dipoles (arrows) aligning parallel and anti-parallel to the main magnetic field, B_0.

The alignment of magnetic dipoles for ^1H nuclei occurs as a consequence of the presence of two energy states, low (parallel with the main magnetic field, B_0) and high (anti-parallel with B_0) (fig 1.3) [16]. To determine a ratio between the orientation of the magnetic dipoles parallel or anti-parallel with the main magnetic field, the following equation can be applied, which arises from the classical Boltzmann statistics [1]:

$$\frac{n_\downarrow}{n_\uparrow} = \exp(-\frac{\Delta E}{kT})$$

(1.8)

where T is in Kelvin, ΔE is the energy difference between the two orientation states and k is the Boltzmann constant ($k = 1.38 \times 10^{-23}$ J$\cdot$K^{-1}).
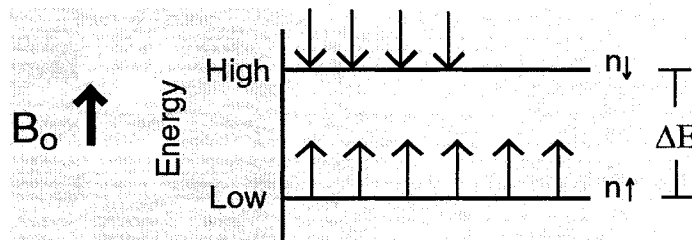
Fig.1.3– Diagram of the two energy states, showing greater population of spins in the low energy state than in the high.

The protons are continually oscillating back and forth between the two states, but at any given instant there are more protons aligned with the field. If the magnitude of the external B_0 field increases, the difference in energy levels and the protons aligned with the field increases, resulting in a greater signal.

The individual magnetic dipoles of the nuclei do not align parallel or anti-parallel with B_0. The magnetic dipoles align parallel with the angular momentum vectors, which are actually oriented at an angle to the main field. A constant projection, μ_z, which may be positive or negative depending on the spin, will be present. The interaction of the magnetic moment μ with B_0 will cause it to precess about the field direction in the form of a cone (fig. 1.4) [1]. This precession is possible because the main field produces a torque determined by the equation:

$$\frac{d}{dt}(\hbar\mathbf{I}) = \mu \times \mathbf{B}_0 \tag{1.9}$$

The cross product indicates that the torque applied to μ is perpendicular to the plane containing μ and B_0 [19].
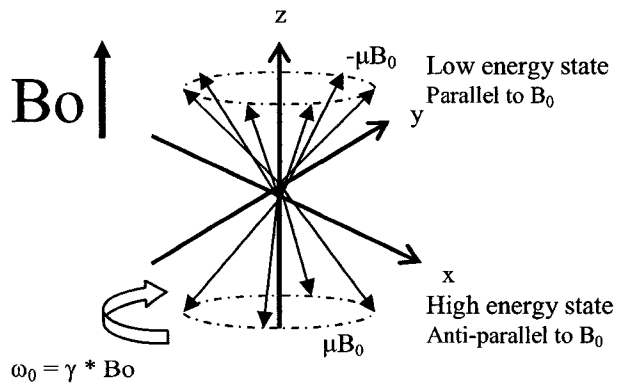
Fig.1.4- Interaction between the main magnetic field B_0 and several spins, giving rise to a precession represented by ω_0.

There are more nuclear moments in the low energy level (preferred state) aligned with the main magnetic field, which produces a net magnetization along the z-axis. The net magnetization results when all the parallel magnetic moments are subtracted from the anti-parallel, giving rise to the net magnetization vector **M** in the z direction (fig. 1.5), where **B₀** is assumed to be oriented along the positive z-axis of the coordinate system. The net magnetization of the sample results from the sum of the magnetic moment vectors within the sample and it is shown in the equation:

$$\mathbf{M}=\Sigma\ \mu \tag{1.10}$$
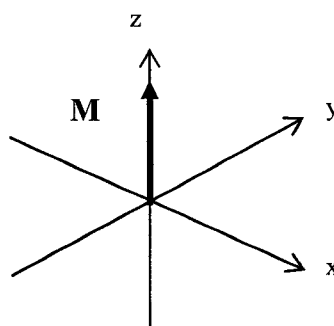
Fig. 1.5- Diagram of the net magnetization along the z-axis.

1.2.2- Excitation Process and Rotating Frame

To perform an NMR experiment it is necessary to have a uniform homogenous main magnetic field, **B₀**, which will be used to align the dipole moments of the sample, and another magnetic field, **B₁(t)**, used to excite the nuclei and provide energy to the system. This excitation is brought about when the net equilibrium magnetization **M** is deflected from its thermal equilibrium position along the positive z-axis, which by convention is the direction of the main magnetic field, **B₀**. In general, this means that the resultant magnetization will have a transverse component (M_{xy}) as well as a z component (M_z). In a manner similar to a single nuclear magnetic moment that experiences a torque due to **B₀** (Eq. 1.9) and precesses, **M** in a field **B** will experience a torque given by the following cross product [1]:

$$\frac{d}{dt}(I\hbar) = \frac{d}{dt}\left(\frac{\mathbf{M}}{\gamma}\right) = \mathbf{M} \times \mathbf{B} \tag{1.11}$$

where $\mathbf{B} = \mathbf{B_0} + \mathbf{B_1}(t)$. To excite the protons, we need to apply an additional magnetic field to $\mathbf{B_0}$, called $\mathbf{B_1}(t)$, which varies with time and rotates around the z-axis in the same sense as M_{xy} with the same frequency ω_0. After the pulse is turned off, $\mathbf{M}$ will be precessing in the xy plane at the frequency ω_0. However, M_{xy} does not remain in the transverse plane indefinitely, it decreases in size and M_z recovers back to thermal equilibrium. This phenomenon is called relaxation and will be explained in section 1.2.4.

If we include both fields $\mathbf{B_0}$ and $\mathbf{B_1}$ into the equation of motion Eq. 1.11 where: $\mathbf{B_0} = (0, 0, B_0)$ and $\mathbf{B_1}(t) = (B_1\cos\omega t, B_1\sin\omega t, 0)$, equation 1.11 becomes:

$$dM_x/dt = \gamma(M_y B_0 - M_z B_1\sin\omega t) \tag{1.12}$$

$$dM_y/dt = \gamma(M_z B_1\cos\omega t - M_x B_0) \tag{1.13}$$

$$dM_z/dt = \gamma(M_x B_1\sin\omega t - M_y B_1\cos\omega t) \tag{1.14}$$

In order to simplify the mathematics of the interaction of $\mathbf{B_1}$ and $\mathbf{B_0}$ with the system, the equations of motion established for a laboratory reference frame will be changed to a frame that rotates in synchronism with $\mathbf{B_1}(t)$. The new rotating frame (described in the equations by a prime (') suffix) is displaced from the reference frame by ωt. The new equations are as follows:

$$M_x' = M_x \cos\omega t + M_y \sin\omega t \tag{1.15}$$

$$M_y' = -M_x \sin\omega t + M_y \cos\omega t \tag{1.16}$$

$$M_z' = M_z \tag{1.17}$$

The new equations of motion in the rotating frame are:

$$dM_x'/ dt = (\gamma\, B_0 + \omega)\, M_y' \tag{1.18}$$

$$dM_y'/dt = -(\gamma\, B_0 + \omega)\, M_x' + \gamma\, B_1\, M_z' \tag{1.19}$$

$$dM_z'/dt = -\gamma\, B_1\, M_y' \tag{1.20}$$

These components can be combined in a single equation of motion in the rotating frame:

$$d\mathbf{M'}\,/dt = -\gamma\, \mathbf{M'} \times \mathbf{B}_{eff} \tag{1.21}$$

where

$$\mathbf{B}_{eff} = B_1\, \mathbf{i'} + (B_0 + \omega/\gamma)\, \mathbf{k'} \tag{1.22}$$

In the rotating frame $\mathbf{B}_{eff}$ is the static magnetic field that represents the time dependant combination of $\mathbf{B_1}$ and $\mathbf{B_0}$. Now, in the rotating frame $\mathbf{M'}$ will precess on the surface of a cone around an effective field $\mathbf{B}_{eff}$ at $\omega_{eff} = \gamma\, \mathbf{B}_{eff}$, where $\mathbf{B}_{eff}$ is the vector resultant of the rotating field $B_1\, \mathbf{i'}$ and the off resonant field $(B_0 + \omega/\gamma)\, \mathbf{k'}$.

When $\mathbf{B_1}$ (t) rotates in a negative sense at $-\omega$, the term $(B_0 + \omega/\gamma) = 0$. This means that the system is exactly on resonance and $\mathbf{B}_{eff} = B_1\, \mathbf{i'}$. In the exact resonance condition the effective field is parallel to the $\mathbf{B_1}$ field and the magnetization vector rotates in the plane z'y' about $B_1\, \mathbf{i'}$ at a frequency $\omega_1 = \gamma\, B_1$. Generally speaking, if the system is not in resonance and the reference frame is rotating at a frequency ω, the magnetization vector $\mathbf{M}$ rotates at a frequency $\omega_{eff} = \gamma\, \mathbf{B}_{eff}$ in a cone around $\mathbf{B}_{eff}$; if the system is in resonance $\omega = -\omega_0$, $\mathbf{B}_{eff} = \mathbf{B_1}$ and the magnetization $\mathbf{M}$ rotates in the y'z' plane. Figure 1.6 shows a diagram of this system [1].
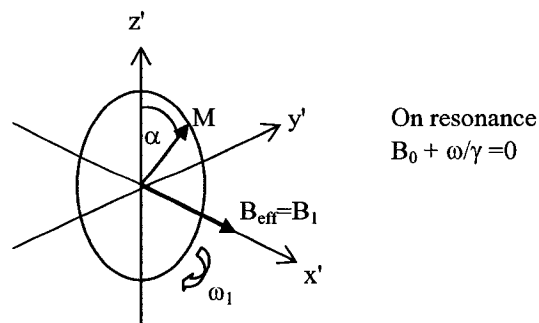
Fig. 1.6- Diagram showing the system excited by a pulse in resonance, where $\mathbf{M}$ rotates through an angle α of an RF pulse of duration t, and $\mathbf{Beff} = \mathbf{B_1}$.

The change experienced by the net magnetization vector, **M**, from its thermal equilibrium depends on the strength of the **B₁** (t) RF pulse and its duration t_{RF}. The flip angle, α, is the angular displacement of the magnetization vector **M** away from its original thermal equilibrium position:

$$\alpha = \omega_{eff} t_{RF} = \gamma\, B_1\, t_{RF} \qquad\qquad (1.23)$$

During an NMR experiment when the RF field **B₁** (t) is turned off at a time $t_{RF} = (\pi/2) / (\gamma\, B_1)$, a 90° pulse is obtained. This means **M** has been placed along the y' axis in the rotating frame and if the RF coil detector is placed along this axis, this pulse (90° or $\pi/2$), results in maximal signal. The longitudinal magnetization is transferred completely into the transverse plane. If the time of the pulse used is twice, then a 180° or π pulse is obtained, which inverts all the longitudinal magnetization to the negative z-axis. To detect signal in NMR experiments the signal should be in the transverse plane. In the NMR field 90° and 180° are the most common RF excitations for NMR pulse sequences.

Assertive utilization of these and other pulses may have important implications in order to obtain valuable information from living tissue. To achieve 90° or 180° pulses the **B₁** (t) strength needed is a very small percentage of the main magnetic field **B₀**. This is because **B₁** is rotating at the Larmor frequency as a time varying magnetic field, which induces phase coherence in the precession of the individual magnetic moments about **B₀**, making them change states with less energy.

1.2.3- Bloch Equations

In 1946 Bloch came up with the equation that describes the behavior of the nuclear magnetization in a magnetic field [20]:

$$\frac{d\mathbf{M}(t)}{dt} = \gamma(\mathbf{M}(t) \times \mathbf{B}) - \frac{M_x(t)}{T_2}\mathbf{i} - \frac{M_y(t)}{T_2}\mathbf{j} + \frac{M_o - M_z}{T_1}\mathbf{k} \qquad (1.24)$$

where **M**(t) is the total magnetization vector, M_0 is the equilibrium magnetization, **B** is the total magnetic field vector, **i**, **j**, and **k** are unitary vectors, and T_1 and T_2 are the

longitudinal and transverse relaxation times, respectively. The z direction is assigned to be parallel with the main magnetic field $\mathbf{B_0}$.

If we neglect the influence of the T_1 and T_2 relaxation times in the system by assuming they are infinitely long, the Bloch equation becomes:

$$\frac{d\mathbf{M}(t)}{dt} = \gamma(\mathbf{M}(t) \times \mathbf{B})$$ (1.25)

Now, in the real NMR experiment where T_1 and T_2 have finite values, it is possible to extract the rate of change of the transverse magnetization component from Eq. 1.24 as

$$\frac{d\mathbf{M}_{xy}}{dt} = -\frac{\mathbf{M}_{xy}}{T_2}$$ (1.26)

In the same manner, we can extract the longitudinal magnetization component shown by this equation

$$\frac{d\mathbf{M}_z}{dt} = \frac{\mathbf{M}_o - \mathbf{M}_z}{T_1}$$ (1.27)

Longitudinal and transverse relaxation will be discussed more extensively in the next section (1.2.4). The relaxation times T_1 and T_2 are merely phenomenological and were not derived from fundamental principles; however, Bloch certainly suggested that longitudinal relaxation T_1 results from thermal interactions and transverse relaxation T_2 from inter-nuclear interactions.

1.2.4- Relaxation

By the middle of the 20th century, scientists working in the relaxation behavior of protons would never imagine that this phenomenon would be the basic mechanism to obtain contrast between different tissues and identify pathologies in MRI studies. Nowadays, the relaxation behavior is still not quite understood, however, the basic principles discovered in the 1950's are still applicable. Bloch stated that longitudinal relaxation occur as a

consequence of thermal energy dissipation and transverse relaxation from proton nuclear spin interactions [17]. To determine water content and other biophysical characteristics of tissue, Shaw and Odeblad started to use proton NMR technology to develop their experiments [21, 22]. Bloembergen, Purcell and Pound (BPP) established the foundations of the relaxation characteristics in liquids; this principle is important in understanding the relationship between molecular motion and relaxation properties [1].

The relaxation phenomenon has proven to play a key role in the diagnosis of pathologies in MRI. Thus, it is important to explain more about longitudinal and transverse relaxation. In order to obtain longitudinal (spin-lattice) relaxation during NMR experiments, energy absorbed by the excited protons should be transferred from the spin system to the surrounding lattice, giving rise to the reestablishment of thermal equilibrium.

On the other hand, the transverse T_2 or spin-spin relaxation can occur either with or without energy dissipation because it refers to the temporary and random interaction between spins that cause a cumulative loss in phase. The T_2 values are always less than or equal to T_1. In most cases for biological tissues, T_2 values are approximately 5 to 10 times shorter than T_1 values, because the transverse relaxation is affected by more parameters than the longitudinal. The relaxation phenomenon in general is originated by fluctuating magnetic fields in the sample.

1.2.4.1- Transverse Relaxation

As was mentioned before, T_2 relaxation results as a consequence of intrinsic processes in the system that causes the main magnetization to lose its phase coherence in the transverse plane. This results from spins creating fluctuating variations in the local magnetic field. As a result of the movement of protons, their individual local magnetic fields start to interact with each other. This interaction is responsible for the relaxation process. If the field of one proton affects the field of another, then the second proton will precess at a slightly different frequency and gain or lose phase compared with the other

spins; during this process no net absorption or emission of energy occurs. This is the basic principle behind transverse relaxation (fig. 1.7).
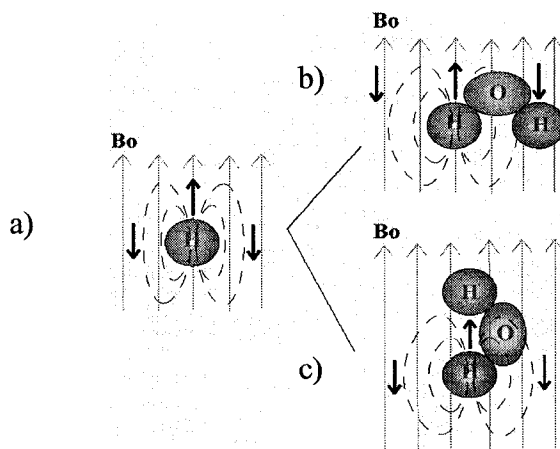
Fig. 1.7– Diagram of the dipole-dipole interaction in a moving water molecule showing different positions. In a), the hydrogen (H) placed in a magnetic field B_0, the dotted lines represent the local magnetic field of the proton. In b), diagram showing (with arrows) the direction of the field (decreased) that the second H experiences due to the interaction with the first H. In c), the water molecule has moved 90°. The direction of the field that the second H experiences increases due to the interaction with the first hydrogen.

Spins tumbling in the sample generate fluctuating magnetic fields that may alter the Larmor frequency. When molecules are rigidly bound, their random motions are very slow, such as in membranous tissue and phospholipids. In this type of environment, the T_2 relaxation time is extremely efficient, with T_2 values on the order of microseconds. Protons with these characteristics cannot be detected during NMR experiments because the signal decays extremely fast.

Now, analyzing the other case when molecules experience a rapid motion, as it is the case of water, spins do not experience alterations in their local magnetic field (field averages to zero). For this reason in molecules moving rapidly the relaxation process is very inefficient, and as a consequence the T_2 times are very long (on the order of seconds). In order to obtain a better understanding of transverse relaxation, a mathematical explanation will be described. Generally speaking, the transverse magnetization M_{xy} in tissues decays to zero before the longitudinal magnetization M_0 has reached thermal equilibrium; it is not possible to have any transverse signal if equilibrium has been achieved.

When spatial and temporal magnetic field non-uniformities exist, the microscopic field b(x,y,z,t), which is time dependent and causes an irreversible decay in the transverse signal, is added to the main magnetic field as:

$$\mathbf{B} = \mathbf{B_0} + b(x,y,z,t) \tag{1.28}$$

This alteration in the field causes the spin moments to precess at different frequencies. However, this is not the only reason for transverse decay. Static inhomogeneites that produce alterations in the main magnetic field can be added to the equation as $\beta(x,y,z)$:

$$\mathbf{B} = \mathbf{B_0} + b(x,y,z,t) + \beta(x,y,z) \tag{1.29}$$

The term $\beta(x,y,z)$ is not time dependent and also creates dephasing of the spins. Both terms $b(x,y,z,t)$ and $\beta(x,y,z)$ together produce a decay in the transverse magnetization characterized by T_2^*. However, the term $\beta(x,y,z)$ can be reversed with a spin echo leading to exponential decay due to a true T_2 instead of T_2^*. Now, we see that the magnetic field experienced by the sample, $\mathbf{B}$, is composed of $\mathbf{B_0}$ and fluctuating and static local magnetic fields originated by spin interactions and magnetic field inhomogeneities, represented by $b(x,y,z,t)$ and $\beta(x,y,z)$, respectively.

The Bloch equations of motion are good in the interpretation of transverse relaxation. Solving Eq. (1.26) for the transverse magnetization M_{xy} varying with time under T_2 relaxation effects we obtain:

$$M_{xy}(t) = M_0 \cdot e^{-t/T_2} \cdot \sin\alpha \tag{1.30}$$

where M_0 is the longitudinal magnetization in thermal equilibrium and α is the RF flip angle used for excitation of the sample. A variety of flip angles are used for different experiments in NMR. For simplicity we assume $\alpha=90°$, then we obtain:

$$M_{xy}(t) = M_0 \cdot e^{-t/T_2} \tag{1.31}$$

The transverse magnetization is characterized by an exponential decay in which the T_2 value is the time after excitation when the amplitude of the signal has been reduced to 36.8% of its original value; this is when $t = T_2$ (fig. 1.8).
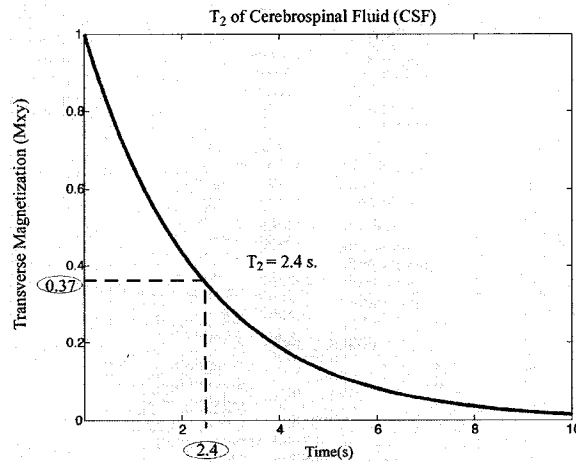
Fig. 1.8- Diagram showing the T_2 value in a mono-exponential decay curve of cerebrospinal fluid (CSF).

Note that M_{xy} can be composed of multiple T_2 components. To analyze multiple components in tissue Eq. 1.31 is modified to obtain

$$M_{xy}(t) = \sum_i S_i \cdot e^{-t/T_2(i)} \qquad (1.32)$$

where T_2 (i) is the *i-th* T_2 components of magnitude S_i and Σ S_i is equal to M_0. This equation deals with multi-compartment tissues, which originate multi-component T_2 spectra. Thus, a relationship between the spectral components and the water compartments of the tissue can be established.

1.2.4.2- Dipole-Dipole Interactions

The individual magnetic field originated by a proton can be analogous to a small bar magnet, which is called a magnetic dipole. Dipole-dipole or magnetic interactions between protons constitute the most important characteristic for T_2 relaxation in tissues. Mathematical concepts to understand dipole-dipole interactions were developed by Bloembergen, Purcell and Pound in 1948 [17]. Their analysis revealed that the motion,

the distance, and the angle of the spins interacting in a sample are the basic characteristics for dipole-dipole interactions.

Nuclear spins interact with each other depending on their distance, a characteristic called dipole-dipole coupling. The energy of this interaction is modeled by this equation:

$$E = \frac{A}{r^3}(1 - 3\cos^2\theta)$$

(1.33)

where θ is the angle between the main magnetic field B_0 and the vector joining the spins, and r is the distance between the two spins (fig. 1.9). The parameter A depends on the magnetic moments of the coupled spins and their orientations, aligned with the field or against the field. When a molecule moves rapidly in a solution the angle θ changes, generating a fluctuating magnetic field at each nucleus. This changing magnetic field originates relaxation in the sample.
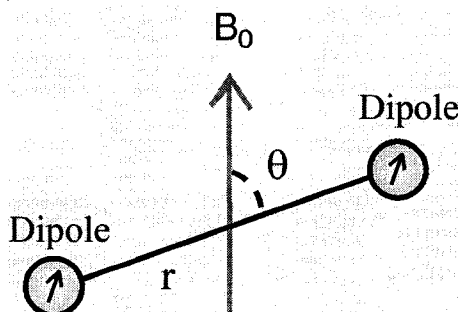
Fig. 1.9– Diagram of a dipole-dipole interaction in a main magnetic field, B_0, showing the separation r and angle θ.

The strength of the interactions depends on the distance between the nuclei ($\propto 1/r^3$). If the distance, r, is greater than 2 or 3 angstrom (Å) the field strength is too weak to cause a dipole-dipole interaction, therefore a good interaction between nuclei will be present if the distance is shorter than 2-3 Å. Based on the localization of the two protons in comparison to B_0, the field of the first proton may either increase or decrease the field

that the second proton is experiencing. This phenomenon is an important characteristic for transverse relaxation decay in NMR experiments.

1.2.4.3- Longitudinal Relaxation

Longitudinal relaxation (T_1) is the process in which spins move from a high energy state to a low energy state, aligning with B_0. Longitudinal interaction is the result of the excited system returning to thermal equilibrium. Regrowth of longitudinal magnetization requires transfer of energy from the nuclear spins to the environment. Longitudinal relaxation can only occur when a proton encounters another magnetic field fluctuating near the Larmor frequency. This fluctuating field is caused by a dipole-dipole interaction. To be efficient at T_1 relaxation the molecules must be tumbling and resonating close to the Larmor frequency. Water molecules tumble very fast, and water is very inefficient at T_1 relaxation. However, when the motion of water is restricted, partially bound to proteins or other molecules, the tumbling might be reduced near the Larmor frequency. Then the relaxation time in these cases will be effective with shorter T_1 values.

To determine the magnitude of the longitudinal magnetization at a certain time t it is necessary to refer to Eq. (1.27). Solving this equation for longitudinal magnetization after an RF pulse with flip angle α is applied we obtain

$$M_z(t) = M_0 + [M_0(0)\cos\alpha - M_0]e^{-t/T_1} \qquad (1.34)$$

where M_0 is the longitudinal magnetization, $M_z(0)$ is the magnitude of the longitudinal magnetization at time 0 and T_1 is the time after the excitation pulse when 63.2% of the longitudinal magnetization has recovered alignment with B_0 (fig. 1.10). Modifying Eq. (1.34) as a function of time (t) after a 90° pulse we obtain:

$$M_z(t) = M_0(1 - e^{-t/T_1}) \qquad (1.35)$$
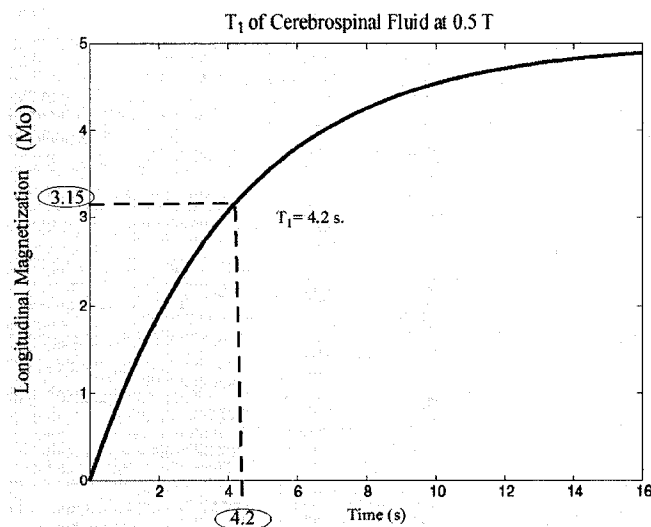
Fig. 1.10 – Graph of the longitudinal relaxation (T_1) time for CSF. At time equal to 4.2 s., the longitudinal magnetization has recovered $\approx$ 63% of its original magnitude.

1.2.5- Free Induction Decay

When the RF transmitter is turned off during an NMR experiment after a single 90° pulse, the longitudinal magnetization is flipped completely into the transverse plane. Then, a signal known as a Free Induction Decay (FID) can be observed. The initial amplitude of the signal is determined by the magnetization vector, M, which has been placed in the transverse plane (xy). The equations previously mentioned describe the recovery of M_z and the dissipation of M_{xy} in the rotating frame. Now, the transverse magnetization M_{xy} precesses around the z axis at the Larmor frequency ω_0. Following Faraday's law of electromagnetic induction, the motion of this magnetization generates an electromotive force (EMF) in the receiver coil placed around the sample of interest that is able to detect signal. The FID decays exponentially and the actual signal is oscillating at the resonance frequency. Usually the FID will arise from a 90° pulse, however, the FID can be generated by any pulse (there will be a component of the magnetization in the transverse plane) except for a 180° pulse because this pulse places the magnetization vector along the negative z-axis, not leaving any magnetization in the transverse plane.

The FID signal in a system with a single component resonating at a frequency ω_0 is determined by

$$S(t) = M_o \sin\alpha \cdot e^{-t/T_2} \cdot e^{-iw_o t} \tag{1.36}$$

where M_0 is the longitudinal magnetization, α is the flip angle and T_2 is the transverse relaxation time. The amplitude of the signal depends on the flip angle and the longitudinal magnetization in thermal equilibrium and can be expressed as

$$A = M_o \sin \alpha \tag{1.37}$$

If nothing affects the homogeneity of the main magnetic field, $\mathbf{B_0}$, the transverse magnetization decays characterized by the relaxation time T_2. However, in reality, $\mathbf{B_0}$ is not perfectly homogenous. There are many factors creating imperfections in the homogeneity of the field, such as manufacturing problems or tissues with different magnetic susceptibilities. This inhomogeneity in the main magnetic field affects the signal causing it to dissipate at a faster rate than the Bloch equations would predict.

1.2.6- Field Inhomogeneity

To analyze the inhomogeneities in the system, the main magnetic field will take the form $(\mathbf{B_0} + \beta)$ as was mentioned before (section 1.2.4.1), where the field inhomogeneity is represented by β and is much smaller than $\mathbf{B_0}$. As a consequence of field inhomogeneities the spins resonate at slightly different frequencies, getting out of phase, and their magnetic moments will cancel each other leading to decay in the detected signal. The signal decay in the presence of field inhomogeneites is characterized by a time constant known as T_2^*. In a homogenous field the FID is characterized by the transverse relaxation time T_2 which is intrinsic to the molecular structure and dynamics of the sample, however, T_2^* additionally takes into account contributions from the field inhomogeneities.

Figure 1.11 shows an FID curve characterized by T_2 and T_2^* decays. It is possible to express T_2^* as:

$$1 / T_2^* = 1 / T_2 + \gamma \, \Delta \, B_0 \qquad (1.38)$$
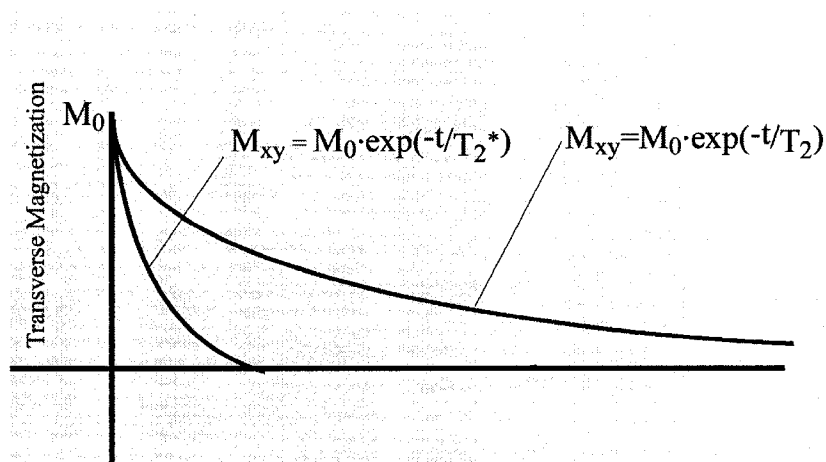
Fig. 1.11- Representation of an FID curve characterized by T_2 decay and also, a signal decay characterized by T_2^*.

1.2.7- Spin Echo

The true transverse relaxation decay can be recovered by the effect of successive RF pulses; this action is called spin echo and it is used to measure T_2 relaxation times (fig. 1.12). The RF excitation scheme is represented as follows:

$$90°\text{-}\ \tau\text{-}\ 180°\ \text{-}\ 2\ \tau\ \text{-}\ 180°\text{-}\ 2\tau\ \text{-}180°\text{-}....$$

(where $TE = 2\tau$, the echo time)

The first RF pulse is used to tip the longitudinal magnetization into the transverse plane. An FID signal is generated due to T_2^* characteristics, and the individual spins lose their phase coherence and dephase. However, if a second RF pulse of 180° (π) is applied to the system at a time τ after the first pulse has been applied the spins will recover the phase and the signal affected by field inhomogeneities will be recovered at time TE as a spin echo (SE). The transverse decay caused by magnetic field inhomogeneities is reversible;

when the180° pulse is applied the phase dispersion that has been accumulated in the second half of the echo time (TE) reverses exactly in coherence, canceling the phase accumulated in the first half of the echo time, making it possible to reverse the dispersion of the magnetization. The echo time is the time between excitation and the peak of the echo.

The spins whose local magnetic fields do not change during the RF excitation and the echo formation are the only ones capable of rephasing using the spin-echo technique. The transverse-relaxation (T_2) decay occurs as a consequence of time dependent changes in the local magnetic field experienced by each proton. These changes in the phase of the spins under T_2 interactions cannot be refocused using a spin echo.

1.2.8- The CPMG Sequence

Note that in a spin-echo experiment following a 90° pulse about the x-axis, if instead of a single $(180°)_x$ pulse, where the subscript x indicates that B_1 is along the x-axis, an echo train of $(180°)_x$ evenly spaced pulses at TE intervals is applied, a Car-Purcell (CP) sequence is obtained, which can be used in the measurement of T_2 times. When spin-echo experiments started to be more popular in the 1950's after Hahn came up with the brilliant idea of spin echo [23], Carr, Purcell and colleagues used to set the RF pulses to be all applied along the same axis [24]. Soon after they realized that with this method the T_2 values obtained from their experiments were very short. The reason for these short values was because of imperfections in the set up of the 180° pulses, which generate a cumulative phase error making the signal decay faster. To overcome this problem in the late 1950's, Meiboom and Gill proposed a sequence in which the 180° pulses in the echo train were phased shifted in a direction orthogonal (90°) with respect to the initial 90° pulse (fig. 1.12). After application of this method in a (SE) sequence it was shown that these types of errors could be effectively reduced [25]. To honor the main scientists that worked in development of this sequence CPMG stands for (Carr-Purcell-Meiboom-Gill).
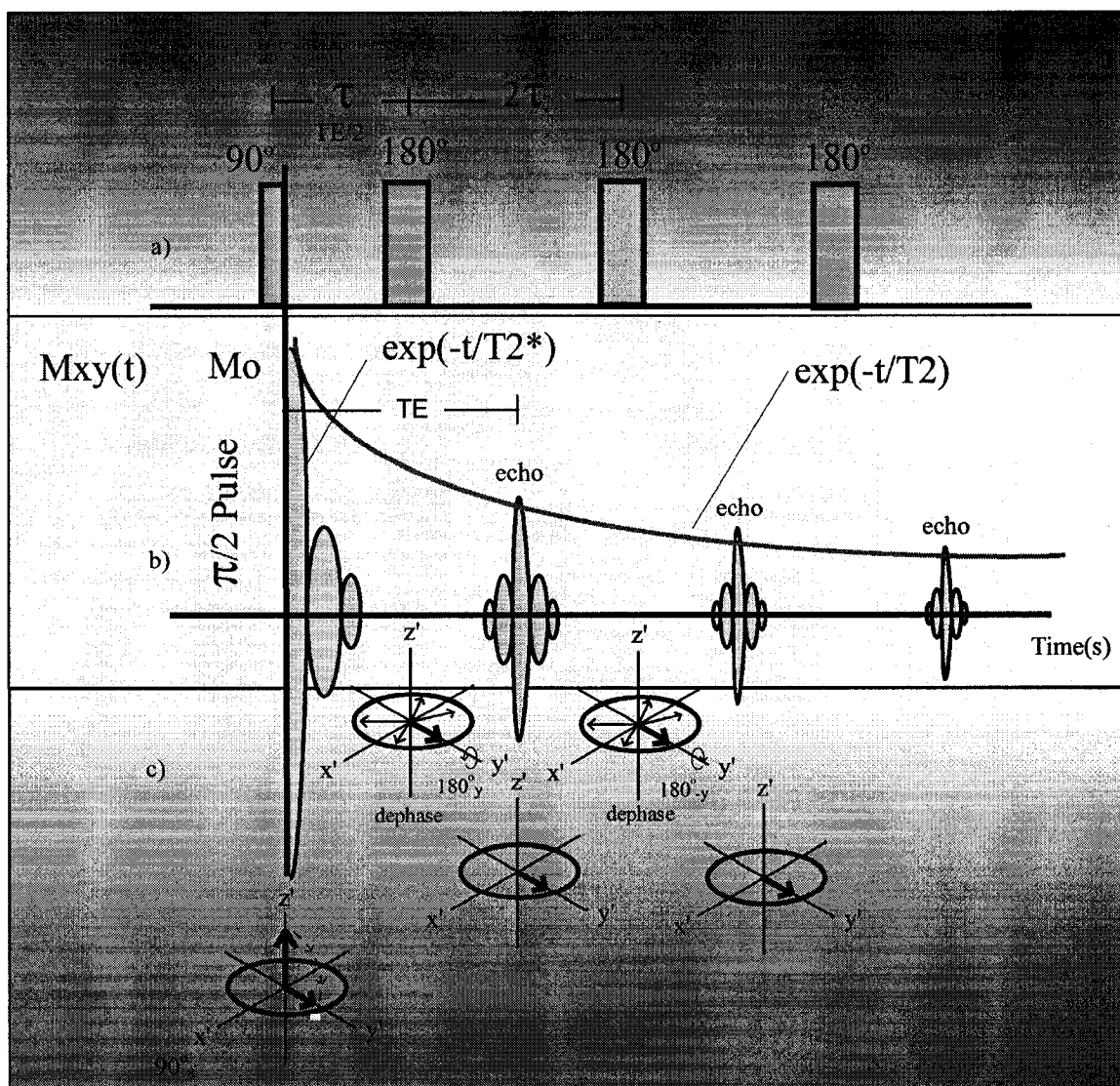
Fig 1.12– Diagram of a CPMG sequence used to generate an FID curve showing a) CPMG pulse sequence, b) FID curve and c) the formation of echoes. In this diagram the 90° pulse is applied along the x-axis, therefore for a CPMG sequence the 180° pulses would be applied along ±y-axis.

1.3- Nervous Tissue

The understanding of NMR principles and the mechanisms underlying T_2-relaxation of tissue (explained in previous sections) are valuable in understanding the T_2 spectrum of the optic nerve. This information can be related with the micro-anatomical water compartments of the tissue, for this the anatomy of the nerve has to be explored.

1.3.1- The Peripheral Nerve

Peripheral nerves are composed primarily by three different structures: 1) the epineurium, 2) the endoneurium and 3) the perineurium (fig. 1.13) [26]. A fascicle is a perineurium and all the material contained therein. The frog sciatic nerve contains only one fascicle. On the other hand, mammalian sciatic nerve is characterized by several fascicles.
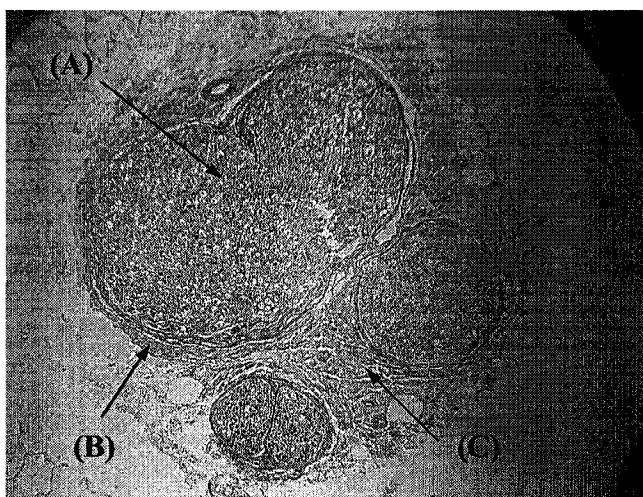
Fig. 1.13– Light microscopy of human peripheral nerve showing (A) the endoneurium, (B) the perineurium and (C) the epineurium.

The epineurium is the connective tissue that is found in the outermost region of multifasciculated nerves; all this connective tissue surrounds the fascicles of nerve fibers. The epineurium and the endoneurium have very similar structures of extracellular elements composed mainly by collagenous fibrils. However, the cellular populations in

both sections of the nerve are quite different; fibroblasts, macrophagues and mast cells are present in the epineurium in greater numbers.

The perineurium surrounds the endoneurium and consists of flattened layers of cells and connective tissue, it works as a barrier to isolate the endoneurium from the epineurium. The extracellular part of the perineurium is clearly connective tissue, however, its cellular organization is not comparable to any other one in the body. Because the perineurium works as a diffusion barrier it has a unique structure that allow ions to pass through. The endoneurium is the connective tissue engulfed by the perineurium, which provides an optimal environment for the axons and other cells. In the peripheral nervous system (PNS) Schwann cells are responsible for the myelination of axons. Bundles of nerve fibers (axons) carry sensory information and motor commands in the PNS. Such bundles with associated blood vessels and connective tissues are called peripheral nerves.

1.3.2- White Matter

The white matter of the CNS is composed of numerous axons covered by myelin. This myelin layer is responsible for the color of white matter. White matter contains many glial cells (astrocytes, oligodendrocytes, microlglia and ependymal cells) but it does not contain cell bodies of neurons. Neuronal cell bodies constitute gray matter, which give rise to the axons present in white matter [27].

One of the most important functions of glial cells in white matter is that they regulate the extracellular environment of ions and transmitters, provide structural and nutritive support of neurons, guide migrating neurons during development, and play an important role in repair and regeneration. Oligodendrocytes are glial cells responsible for the ensheathment of axons with myelin [27-30].

White matter has a high lipid content. White matter has a water content of 72 % and gray matter of 82 %. The non-myelinated structures in white matter are composed of about 80% water [31].

1.3.3- Optic Nerve

From its development and structure, the optic nerve must be regarded as an extension of the central nervous system rather than as a true nerve (fig. 1.14). The optic nerve is formed by numerous axons that originate in the retinal ganglion cells. These axons travel from the eye through the orbit, following intracranially paths until they combine with counterparts from the opposite eye to form the optic chiasm [32]. In the adult state, the optic nerve is ensheathed in meningeal coverings rather than in perineurium. The optic nerve is the structure of the central nervous system responsible for transmitting the information from the retina to the brain. It is formed by i) axons that conduct nerve impulses, ii) glial cells (astrocytes, oligodendrocytes and microglia), iii) blood vessels and iv) connective tissue. The axons are covered by a myelinated sheath except at the nodes of Ranvier. Myelination is not necessary for vision, but it makes it more efficient. Results from R. C. Wiggins indicate that the distribution of myelinated fibers is relatively uniform in the rat optic nerve [33]. The section analyzed in our studies was from the base of the orbital bulb to the chiasm.
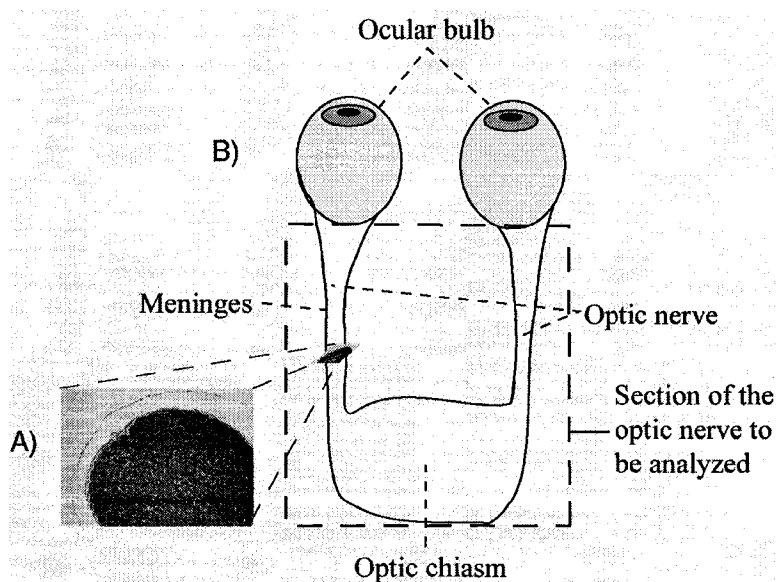
Fig. 1.14- Diagram of the optic nerve anatomy showing A) a transverse section of the optic nerve and B) the principal structures of the nerve. Note that the ocular bulbs are removed from the optic nerves for our studies.

Each optic nerve consists of thousands of axons. Figure 1.15 shows different regions of the optic nerve. The intraocular portion of the optic nerve fiber is non-myelinated; this characteristic helps retinal photoreceptors to function in an efficient way. There is a transition from myelinated axons to unmyelinated axons at the lamina cribrosa (the supporting structure for the optic nerve where it leaves the eye). Unmyelinated axons are divided into fascicles by astrocytes. Posterior to the lamina cribrosa, oligodendrocytes ensheath the axons in concentric wrappings of myelin. The optic nerve is closely interconnected with the pia mater, from which it obtains its blood supply; also, it is protected by the arachnoid and surrounded by dura mater. The membranous layers in the optic nerve play a very important role in this study, because they will be responsible for the diffusion of the paramagnetic agents (or other solutes) used to identify micro-anatomical structures based on NMR studies.
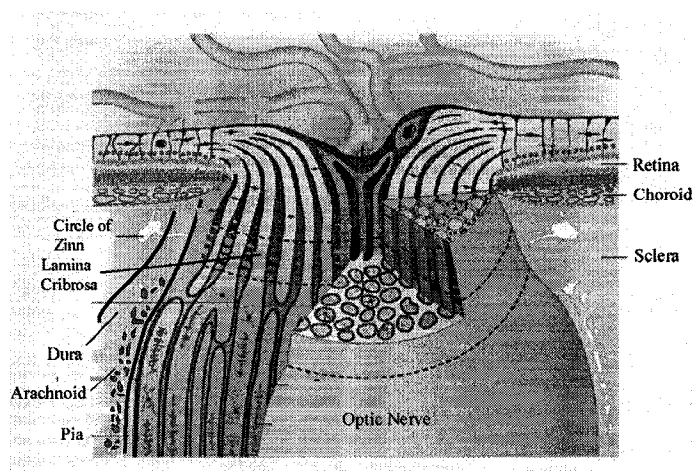
Fig. 1.15- Diagram showing different structures of the optic nerve and the meninges.

The optic nerve is covered with the same meningeal layers as the rest of the central nervous system [32]. The pia and arachnoid layers are mainly formed by collagen. The innermost layer in the optic nerve, the pia mater, provides pathways directed into the nerve, which are responsible for blood vessel distribution and separation of the fibers into discrete bundles of axons. The pia extends from the lamina cribrosa all the way back to the optic chiasm. The arachnoid is superficial to the pia and surrounds it. The outermost layer of the meninges, the dura mater, forms the outer covering of the optic nerve.

The optic nerve was chosen for our studies because it is considered an extension of the central nervous system and the risk of tissue damage in excising it is less than that of excising white matter. The optic nerve is engulfed by dura matter, therefore, it is possible to place it in the perfusion chamber (device used to perform the NMR experiments, detailed description in section 2.2) while maintaining its shape and structure. On the other hand, it was observed that excised white matter tracts from rat spinal cord vanished at the time they were placed in the perfusion chamber for NMR experiments.

1.3.4- The Axon

The axon is the part of the neuron responsible for propagation of an action potential. An axon can be myelinated or unmyelinated. The cytoplasm of the axon, or axoplasm, is constituted of neurotubules, neurofibrils, small vesicles, mitochondria, lysosomes and various enzymes. The axoplasm is surrounded by the axolemma. The axon hillock is a thickened section of the neuron where the axon in a multipolar neuron attaches to the soma [27]. The axon may have different branches, which are used to communicate with different cells. The synaptic terminals are located at the end of the axon, a specific region where communication between neurons and cells take place (fig. 1.16).
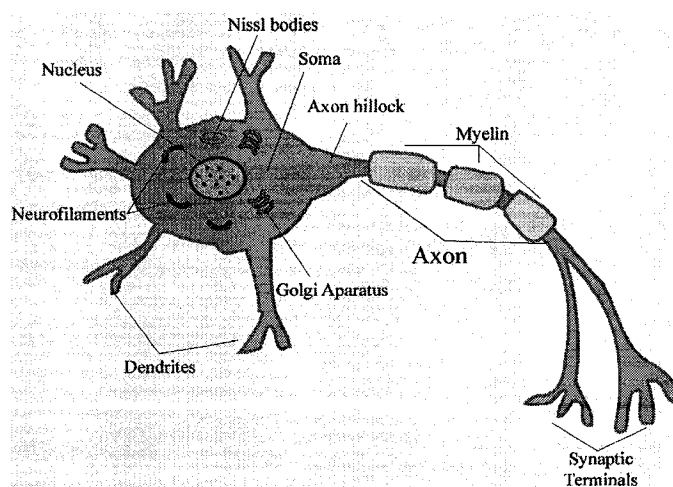
Fig. 1.16- Diagrammatic view of a multipolar neuron showing the axon and major organells.

1.3.5- Oligodendrocytes and Astrocytes

Oligodendrocytes are the predominant glial cells in white matter. Usually they are found between myelinated axons. These cells are responsible of forming the myelin in the CNS. A single oligodendrocyte provides the myelin for many internodal segments of different axons simultaneously. One Oligodendrocyte may be responsible for the production and maintenance of up to 50 nerve fibers. This characteristic is very important in demyelintating diseases because damage to a few oligodendrocytes may have a large implication in demyelination of neural fibers.

Astrocytes are the largest and most numerous gial cells. Astrocytes have a variety of functions, many of which are not well understood. However some of the known functions are: i) maintaining the blood-brain barrier (these cells create a blood brain barrier that isolates the CNS from the general circulation), ii) creating a structure for the CNS (provide a structural framework for neurons of the brain and spinal cord), iii) guiding neuron development and iv) controlling the interstitial environment.

1.3.6- Myelin

Myelin is an essential component of the nerve for normal functioning. In the central nervous system (CNS) and peripheral nervous system (PNS) myelin is present in large quantities.

Myelin is tightly wrapped around axons forming a multilamellar membranous structure, which has a very high lipid content. The myelin bilayer is composed of saturated fatty acids with very long chain lengths. This fatty acid composition leads to a closely packed, highly stable membrane structure (fig 1.17) [31]. A membranous structure containing long chains of fatty acids is more tightly held than those containing shorter fatty chains. The binding interactions between lipid molecules depend on the length of the chain, the longer the hydrocarbon chain the stronger the interaction strength.
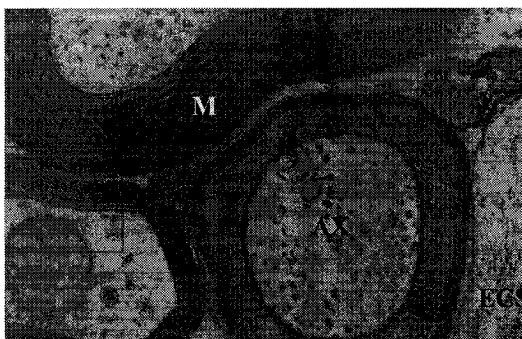
Fig 1.17- Electron micrograph of a peripheral nerve showing different compartments, axoplasm (AX), myelin (M) and extracellular space (ECS). Modified from [34].

The nodes of Ranvier are segmented parts of the axons that are not wrapped by myelin; this segment allows the axon to repolarize [35] and conduct the electrical pulse in a way known as "saltatory" conduction [36].

In the PNS, myelin is formed by Schwann cells while in the CNS it is formed by oligodendrocytes cells. Myelination of the nervous fibers follow these rules: i) tracts in the nervous system becomes myelinated at the time they become functional, ii) myelination starts to be formed in the PNS before it starts in the CNS, iii) myelination in central sensory areas tends to precede myelination in central motor areas, iv) myelination in the brain occurs in areas of primary function earlier than in association areas and v) most tracts become myelinated in the direction of the impulse conduction. Myelin is one of the membranes richest in lipids, containing 70-80 % lipid by dry weight. It is also a structure that contains only 40 % water [31].

Nerve fibers communicate with other nerve fibers by transmitting information via electrical impulses called action potentials, which are conducted in an all-or-none fashion (electrical impulse is propagated or not). In myelinated axons the nodes of Ranvier are the only sections where the axonal membrane is in contact with the extracellular space. Myelin sheath has a much higher resistance and much lower capacitance than the axonal membrane. This is why, when the membrane at the node is excited, the ionic flow cannot go through the myelin and therefore flows out the sheath through the next node of

Ranvier and depolarizes the membrane there. This is the way electrical impulses travel as "saltatory" conduction, meaning the impulse jumps from node to node making the conduction velocity considerably faster. Also, it saves energy because only the sections at the nodes of Ranvier need to be depolarized and repolarized for impulse conduction. Myelin is very important for nervous fibers in transmitting the action potential in an efficient and rapid way.

1.4- Multi-component T_2 Relaxation and Water Compartments

Tissue characterization based on NMR experiments is very well documented [3, 37-44]. There is supportive evidence that differences in the transverse-relaxation (T_2) times of water in nervous tissue originates from different water compartments (fig. 1.17) within the micro-anatomical structures. It is known that myelin acts as a diffusion barrier between the extracellular space and the axons making it possible to obtain proton signal from different compartments. The use of multi-component T_2 relaxation information in studying nerve has been of particular interest because of its potential to identify the presence and possibly quantify the volume of myelin or other substances in nerve. Magnetic resonance relaxometry has been used to study myelin disorders, hypomyelination, and demyelination [45-47]. Also, T_2 components assigned to water in the intra- and extracellular space may be used in assessing inflammatory and edematous changes [48]. Unfortunately, accurate multi-component T_2 measurements are generally difficult to obtain *in vivo* [45]. The correct assignment of components and compartments using NMR techniques is important to determine tissue characterization and diagnosis discrimination between different cellular mechanisms of disease. Differences in the molecular environment of tissue are the main source that gives rise to the origin and variation of contrast in MRI; therefore, studies related to micro-anatomical structures are of general interest and significant value. The main objective of this study is to identify the different T_2 times and component sizes that characterize the T_2 spectrum of the rat optic nerve and to establish a relationship between water compartments and T_2 components of the nervous tissue.

1.5- Bibliography

1.   Bronskill, M.J. and P. Sprawis, *The Physics of MRI. 1992 AAPM Summer School Proceedings*. 1992.

2.   Does, M.D., et al., *Multi-component T_1 relaxation and magnetisation transfer in peripheral nerve*. Magnetic Resonance Imaging, 1998. 16(9): p. 1033-41.

3.   Does, M.D. and J.C. Gore, *Compartmental study of T_1 and T_2 in rat brain and trigeminal nerve in vivo*. Magnetic Resonance in Medicine, 2002. 47(2): p. 274-83.

4.   Does, M.D. and R.E. Snyder, *T_2 relaxation of peripheral nerve measured in vivo*. Magnetic Resonance Imaging, 1995. 13(4): p. 575-80.

5.   Beaulieu, C., F.R. Fenrich, and P.S. Allen, *Multicomponent water proton transverse relaxation and T_2-discriminated water diffusion in myelinated and nonmyelinated nerve*. Magnetic Resonance Imaging, 1998. 16(10): p. 1201-10.

6.   Wachowicz, K. and R.E. Snyder, *Assignment of the T_2 components of amphibian peripheral nerve to their microanatomical compartments*. Magnetic Resonance in Medicine, 2002. 47(2): p. 239-45.

7.   Peled, S., et al., *Water diffusion, T_2, and compartmentation in frog sciatic nerve*. Magnetic Resonance in Medicine, 1999. 42(5): p. 911-8.

8.   Bonilla, I., Wachowicz, K., Snyder, R.E., *T_2 spectrum of mammalian optic nerve*. ISMRM 11th Meeting, 2003: p. 1452.

9.   Wachowicz, K., and Snyder, R. E., *A Look at the Transverse Relaxation Spectra of Mammalian Optic Nerve at 3.0 T*. ISMRM 10th Meeting, 2002: p. 1211.

10.   Whittall, K.P., et al., *In vivo measurement of T_2 distributions and water contents in normal human brain*. Magnetic Resonance in Medicine, 1997. 37(1): p. 34-43.

11.   Stanisz, G.J. and R.M. Henkelman, *Diffusional anisotropy of T_2 components in bovine optic nerve*. Magnetic Resonance in Medicine, 1998. 40(3): p. 405-10.

12.   Menon, R.S., M.S. Rusinko, and P.S. Allen, *Proton relaxation studies of water compartmentalization in a model neurological system*. Magnetic Resonance in Medicine, 1992. 28(2): p. 264-74.

13.   Laniado, M., et al., *First use of GdDTPA/dimeglumine in man*. Physiological Chemistry & Physics & Medical NMR, 1984. 16(2): p. 157-65.

14.   Mendonca-Dias, M.H., E. Gaggelli, and P.C. Lauterbur, *Paramagnetic contrast agents in nuclear magnetic resonance medical imaging*. Seminars in Nuclear Medicine, 1983. 13(4): p. 364-76.

15.   Saeed, M., M.F. Wendland, and C.B. Higgins, *Contrast media for MR imaging of the heart*. Journal of Magnetic Resonance Imaging, 1994. 4(3): p. 269-79.

16.   Gillies, R.J., *NMR in Physiology and Biomedicine*. 1994.

17.   Elster, A.D., *Questions and Answers in Magnetic Resonance Imaging*. 1994.

18.   Suetens, P., *Fundamental of Medical Imaging*. 2002: Cambridge University Press.

19.   Farrar, T.C. and E.D. Becker, *Pulse and Fourier Transform NMR Introduction to Theory and Methods*. 1971.

20.   Bloch, F., *Nuclear Induction*. Phys Rev, 1946. 70(460).

21.   Shaw, T.M., R.H. Elsken, and C.H. Kunsman, *Proton magnetic resonance absorption and water content of biological materials*. Physiol. Rev., 1953. 85(708).

22. Odeblad, E. and G. Lindstrom, *Some preliminary observation on PMR in biological samples*. Acta. Radiol., 1955. **43**(469).

23. Hahn, E.L., *Spin Echoes*. Phys Rev, 1950. **80**: p. 580-594.

24. Carr, H.Y. and E.M. Purcell, *Effects of diffusion on free precession in nuclear magnetic resonance experiments*. Phys Rev, 1954. **94**(630).

25. Meiboom, S. and D. Gill, *Modified spin-echo method for measuring nuclear relaxation times*. Rev. Sci. Instrum., 1958. **29**: p. 688-693.

26. Landon, D.N., *The Peripheral Nerve*. 1976.

27. Martini, F.H., *Fundamentals of Anatomy and Physiology*, ed. 4th. 1998: Prentice Hall.

28. Matute, C., et al., *On how altered glutamate homeostasis may contribute to demyelinating diseases of the CNS*. Advances in Experimental Medicine & Biology, 1999. **468**: p. 97-107.

29. Black, J.A., et al., *A quantitative study of developing axons and glia following altered gliogenesis in rat optic nerve*. Brain Research, 1986. **380**(1): p. 122-35.

30. Perez-Cerda, F. and C. Matute, *Excitotoxicidad oligodendroglial y desmielinizacion en el nervio optico*. Archivos de la Sociedad Espanola de Oftalmologia, 2000. **75**(5): p. 301-4.

31. Knaap, M.S.V.d. and J. Valk, *Magnetic Resonance of Myelin, Myelination and Myelin Disorders*. 1995.

32. Paxinos, G., *The Rat Nervous System*. Vol. 1. 1985.

33. Wiggins, R.C., et al., *Myelination of the rat optic nerve during postnatal undernourishment and recovery: a morphometric analysis*. Brain Research, 1984. **308**(2): p. 263-72.

34. Kessler, J., *Computer Assisted Teaching System University of Vermont, College of Medicine. Electron Micrographs of the Peripheral Nervous System*. 2000.

35. Rall, W., *Core conductor theory and cable properties of neurons*. The Nervous System, ed. In E. R. Kandell. Vol. 1. 1977: American Physiological Society. 39-97.

36. Hodgkin, A., *The conduction of the Nervous Impulse*, ed. c. Thomas. 1964.

37. English, A.E., M.L. Joy, and R.M. Henkelman, *Pulsed NMR relaxometry of striated muscle fibers*. Magnetic Resonance in Medicine, 1991. **21**(2): p. 264-81.

38. Estilaei, M., et al., *1H NMR measurements of wet/dry ratio and T_1, T_2 distributions in lung*. Journal of Magnetic Resonance, 1997. **124**(2): p. 410-9.

39. Gareau, P.J., et al., *In vivo measurements of multi-component T_2 relaxation behaviour in guinea pig brain*. Magnetic Resonance Imaging, 1999. **17**(9): p. 1319-25.

40. Graham, S.J. and M.J. Bronskill, *MR measurement of relative water content and multicomponent T_2 relaxation in human breast*. Magnetic Resonance in Medicine, 1996. **35**(5): p. 706-15.

41. Graham, S.J., P.L. Stanchev, and M.J. Bronskill, *Criteria for analysis of multicomponent tissue T_2 relaxation data*. Magnetic Resonance in Medicine, 1996. **35**(3): p. 370-8.

42. Harrison, R., M.J. Bronskill, and R.M. Henkelman, *Magnetization transfer and T_2 relaxation components in tissue*. Magnetic Resonance in Medicine, 1995. **33**(4): p. 490-6.

43.   Larsson, H.B., et al., *In vivo determination of T1 and T2 in the brain of patients with severe but stable multiple sclerosis*. Magnetic Resonance in Medicine, 1988. **7**(1): p. 43-55.

44.   Menon, R.S. and P.S. Allen, *Application of continuous relaxation time distributions to the fitting of data from model systems and excised tissue*. Magnetic Resonance in Medicine, 1991. **20**(2): p. 214-27.

45.   Lancaster, J.L., et al., *Three-pool model of white matter*. Journal of Magnetic Resonance Imaging, 2003. **17**(1): p. 1-10.

46.   Gay, C.T., et al., *Magnetic resonance imaging demonstrates incomplete myelination in 18q- syndrome: evidence for myelin basic protein haploinsufficiency*. American Journal of Medical Genetics, 1997. **74**(4): p. 422-31.

47.   Stanisz, G., M. Bronskill, and R. Henkelman, *The effect of demyelination on T1, T2 relaxation and magnetization transfer in white matter*. 8th Annual Meeting of ISMRM, 2000. **1119**.

48.   Fenrich, F.R., C. Beaulieu, and P.S. Allen, *Relaxation times and microstructures*. NMR in Biomedicine, 2001. **14**(2): p. 133-9.

Chapter 2

Methods and Materials

In this chapter we present the methods and materials used in our experiments. We intend to explain how we performed our experiments from the moment we excised the rat optic nerve until the moment we generated a T_2 spectrum. Also, it is explained how we analyze and plot the data.

2.1- Optic Nerve Excision

Sprague Dawley rats, males weighting approximately 300-400 gms were chosen for this study. Ethical approval by the Health Science Animal Policy and Welfare Committee of the University of Alberta was obtained. A total of thirty-two rats were used for different experiments, and all data was collected at room temperature. The rats were euthanised with CO_2 and their optic nerves excised for analysis *in vitro*. The left and right optic nerves join in the chiasm; these sections together with the ocular bulbs were carefully removed from the animal. The connective tissue and fat surrounding the nerves was carefully removed to leave the nerve clean and ready for NMR studies; the ocular bulbs were removed carefully with minimal damage. The duration of the excision and cleaning procedure for each optic nerve was approximately 1.5 hrs, during which time the tissue was constantly bathed with a standard buffer solution (see below) to avoid dehydration. The dimensions of the optic nerves were ≈0.5 mm in diameter and ≈1.3 cms in length (fig. 2.1).
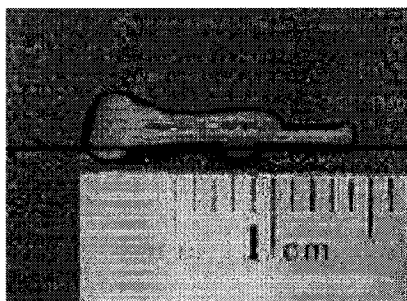
Fig. 2.1- Photograph of the rat optic nerve.

2.2- Perfusion Chamber

The standard way of performing an NMR experiment *in vitro* is to place a sample and bathing solution in an NMR tube in the magnet and acquire the data. If a different bathing solution were needed, the sample would have to be removed from the tube and a new solution added. All this handling and movement of the sample may cause inconsistency in the results. To avoid this situation, we performed the majority of our experiments with a perfusion chamber made out of interlocking polyethylene tubing. Once the samples were placed in a perfusion chamber centered in a small solenoid RF coil (fig. 2.2), a dual infusion pump was used to circulate the solution through the system (fig. 2.3).

In the perfusion chamber a physiologically appropriate standard buffer solution with a pH of 7.4, consisting of 130-mM NaCl, 3-mM KCl, 2-mM $MgSO_4$, 2-mM $CaCl_2$, 10-mM Dextran and 10-mM Hepes, flowed at a rate of 6.5 ml/hr [1].

Flow rates >4 ml/hr are sufficient for the oxygen requirements of mammalian nerve tissue. The flow may cause the component sizes of the tissue to change, and this change may result in signal loss from the standard buffer solution flowing outside the sensitive area of the RF coil after the excitation or from imperfect reception of excitation and inversion pulses. At 6.5 ml/hr the component sizes of the tissue and the standard buffer were similar to those found in a static solution. The perfusion chamber is a very useful technique that allows changing the buffer composition on-the-fly. This is important because paramagnetic agents added to the buffer solution may provide relevant information of the nervous tissue, keeping the environment relatively unchanged. During some studies paramagnetic agents were added to the solution to establish the real number of components in the T_2 spectrum of the optic nerve or to determine their relationship with the nerve water compartments. It takes 2-3 minutes to obtain a 99% replacement of the previous buffer when switching from one solution to another. When a static solution is used for NMR experiments of tissue, there is a risk that the environment surrounding the sample may be unable to meet the oxygen requirements.

Although excised tissue can never completely represent tissues *in vivo*, the data acquired from *in-vitro* experiments may be of significant relevance. It is important at the time of examining the samples *in vitro* to provide them with an environment as close as possible to that *in vivo*. Therefore, the perfusion chamber is an optimal device that offers a continuous supply of oxygen and nutrients to the tissue. There are three types of experiments we performed *in vitro:* 1) using a standard NMR test tube where the sample is placed inside the magnet, 2) using a perfusion chamber with a single-coil system for transmission and reception of the signal and 3) using a perfusion chamber with a two-coil system where one coil is used to transmit and the other one to receive the signal (fig. 2.2). The majority of the experiments were performed with a single coil system.
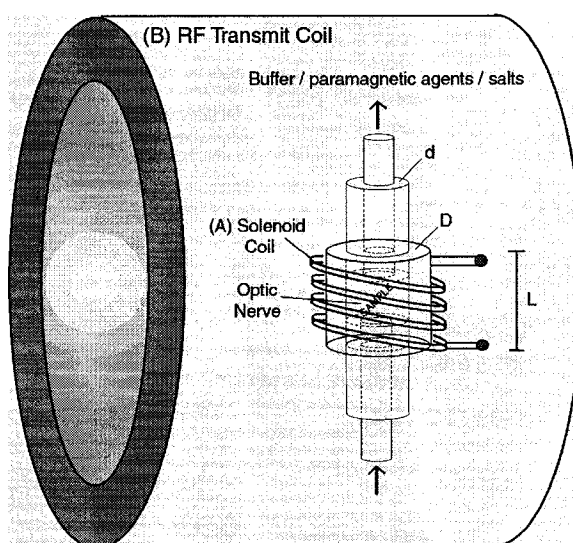
Fig.2.2 - Diagram of the perfusion chamber system used inside the magnet. The two-coil system uses (B) to transmit and (A) to receive. The single coil system uses (A) to transmit and receive. This system allows switching of the buffer solution to different perfusates on-the-fly The length of the chamber is approximately 1 cm. The outer diameter (D) has a dimension of ≈ 6 mm and the inner diameter (d) of ≈ 3 mm. The chamber is constructed of interlocking sections of polyethylene.

2.3- Solenoid RF Coil

An RF coil (fig 2.2) is used to generate the time varying magnetic field, $B_1(t)$. This magnetic field has to be at the Larmor frequency of the proton spins in order to accomplish excitation of the system. Once B_1 is turned on, depending on its duration, the

flip angle will vary as is shown by Eq. (1.23). The 4-loop solenoid RF coil should tightly fit the perfusion chamber in order to obtain an optimal SNR. Before setting up the π and $^{\pi}/_2$ RF pulses, the coil was tuned and shimmed manually. A typical line width after shimming was approximately 25 Hz. The $\mathbf{B_1}$ magnetic field rotates the longitudinal magnetization into the transverse plane from where it is possible to obtain signal from the sample [2]. To obtain the transverse relaxation decay of the nervous tissue we used the CPMG sequence (see below).
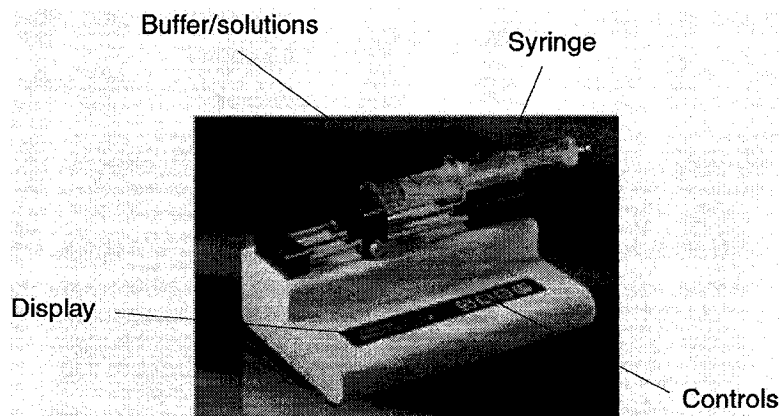
Fig 2.3- Dual infusion pump system used to obtain a flow of 6.5 ml/hr. The standard buffer and other solutions are contained in the syringes; tubing goes from the perfusion chamber to the tip of the syringes. During an experiment both syringes are working and the tubing is switched depending on which solution is needed.

2.4- Bathing Solutions and Paramagnetic Agents

Paramagnetic agents have an effect on the T_1 and T_2 relaxation times of the nuclei that they interact with. It is possible to determine the relaxation times when a paramagnetic agent is added to a solution. In order to obtain this information we need to know the relaxation time of the solution itself and the relaxivity of the paramagnetic agent. It has been shown that relaxation rates can be calculated as follows [3]:

$$\left(\frac{1}{T_{1,2}}\right)_{wanted} = \left(\frac{1}{T_{1,2}}\right)_{known} + \left(\frac{1}{T_{1,2}}\right)_{ca} \tag{2.1}$$

where $T_{1,2\ wanted}$ stands for the relaxation time expected after the paramagnetic agent is added to the solution, $T_{1,2\ known}$ refers to the relaxation time of the normal tissue before

the addition of the paramagnetic agent and $T_{1,2\,ca}$ refers to the relationship between the concentration of paramagnetic agent (C) and the specific relaxivity ($\alpha_{1,2}$) of the paramagnetic agent defined as:

$$\left(\frac{1}{T_{1,2}}\right)_{ca} = \alpha_{1,2} \cdot [C] \tag{2.2}$$

It is important to know the relaxivities of different elements. This information is useful in order to calculate the correct concentrations of paramagnetic agents to be used during NMR experiments (Table 2.1) [3].

Table 2.1- Different elements and their specific relaxivities		
Cation	α_1 (/mM/sec)	α_2 (/mM/sec)
Ni^{2+}	0.5	0.5
Cu^{2+}	0.53	0.56
Mn^{2+}	6.67	50
Cr^{3+}	3.13	3.13
Gd^{3+}	5.0	4.5

It is important to use the appropriate concentration of paramagnetic agents to be efficient and also avoid large quantities that may alter drastically the environment of the nervous tissue. When using different paramagnetic agents or salts in the buffer solution, the concentration of NaCl was reduced in the standard buffer solution in order to maintain an appropriate osmotic pressure.

2.5- Use of Paramagnetic Agents or Solutions to Establish the Correct Number of Components in the T_2 Spectrum

Since the T_2 time of the water buffer is longer than that of any T_2 time of the nerve, it may produce an artifactual component that might otherwise be attributed to the nerve. In order to eliminate this possibility two approaches were used: $FeCl_3$ and fluorinert.

2.5.1- Iron Chloride

Even a molecule as small as $FeCl_3$, although it penetrates deeply into the perineurium within a few minutes, takes hours to reach the endoneurium [4]. Iron chloride, $FeCl_3$, is used as a paramagnetic agent principally for bowel opacification [5]. In this study iron chloride is used because it takes a long time to diffuse through the perineurium. With this characteristic it is possible to reduce the relaxation time of the buffer to less than 5 ms and still have signal from the nerve. In rat optic nerve the outer membranous layer (dura) that protects the nervous tissue is expected to behave similar to that of perineurium. The appropriate concentration of iron chloride needed to reduce the relaxation time of the buffer to < 5 ms was determined to be 15-mM. This concentration effectively removes the signal of the buffer from that originating from the nerve. As a result of the null diffusion of the paramagnetic agent into the nerve, it was possible to see the signal from the nervous tissue without any artifactual contamination that may be created by the buffer. Figure 2.4 is a picture that represents how the paramagnetic agent remains outside the nerve, just affecting the buffer solution.
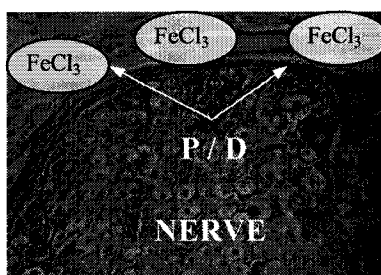
Fig. 2.4- Light micrograph of peripheral nerve. The iron chloride ($FeCl_3$) does not diffuse into the nerve. The perineurium (P) in sciatic nerve or the dura (D) in optic nerve acts as a diffusion barrier, therefore, the buffer solution is the only one affected by the paramagnetic agent.

2.5.2- Fluorinert

To determine the true number of components in the T_2 spectrum of the optic nerve, we used a fluorinated liquid, which does not give rise to any proton NMR signal. This substance does not contain any ^1H, therefore it is invisible for an NMR proton experiment [6] and keeps the nervous tissue in good condition, avoiding dehydration [7]. This characteristic is useful for our studies because without the signal from the buffer we

eliminate the possibility that a buffer water artifact may cause the appearance of the long-lived component.

2.6- The Use of Paramagnetic Agents to Establish the Component-Compartment Relationship

When paramagnetic agents that diffuse into the nerve are added to the buffer solution, the paramagnetic agents diffuse in the different compartments of the nerve beginning with the extracellular space (ECS) of the tissue. Following the switch from a standard buffer solution to one containing certain paramagnetic agents the first thing to happen is that the buffer solution goes to a shortened T_2 time within 2-4 minutes. After approximately four minutes the agent starts to lower the magnitude of the signal from the ECS then the axoplasm and myelin. This characteristic has been observed in the frog sciatic nerve [8]. The effects of the paramagnetic agent in the different water compartments of the nerve may provide important information in defining the relationship between compartments and components of the T_2 spectrum. Figure 2.5 shows the way we believe the paramagnetic agents diffuse into the water compartments of the nerve.
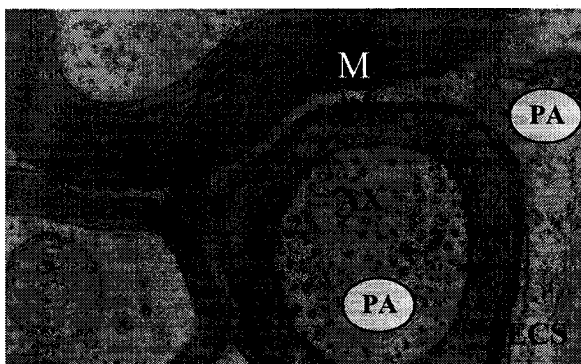
Fig.2.5- Diagram of how it is believed the paramagnetic agent (PA) diffuses into the nerve. First it diffuses into the extracellular space (ECS), which is the closer compartment to the perineurium or dura, and then it might diffuse to the axoplasm (AX) through the Nodes of Ranvier. Myelin (M) may act as a diffusion barrier. It is expected to see these types of changes in the T_2 times and magnitudes of the components when they start to be affected by the paramagnetic agents in NMR experiments.

2.6.1- Manganese

Manganese, Mn^{2+}, or more accurately $MnCl_2$, has been used in frog sciatic nerve studies to lower the relaxation time of the extracellular space component [8]. Mn^{2+} has a very high specific relaxivity (α_2 of 50) [3], which makes this element very suitable to be used as a paramagnetic agent. A small quantity of $MnCl_2$ will have a great impact on the relaxation time of a solution. This is important, as it is not necessary to add great quantities of this agent to the buffer in order to reduce its relaxation time. $MnCl_2$ is toxic for medical use; however, this is not an issue for use in-vitro experiments. Manganese diffuses into the peripheral nerve [9], a characteristic that is useful in the development of our experiments. It was determined that the appropriate concentration to use in the experiments is 10-mM of $MnCl_2$. This concentration reduced the relaxation time of the buffer to < 3 ms.

2.6.2- Gadolinium (Gd-DTPA)

Gadolinium is a toxic element in its natural state, so it is chelated to diethylenetriamine pentaacetic acid (DTPA) to modify its toxicity and other physiological properties that make it viable for medical use [10, 11]. The chemical structure of GD-DTPA is shown in fig. 2.6.
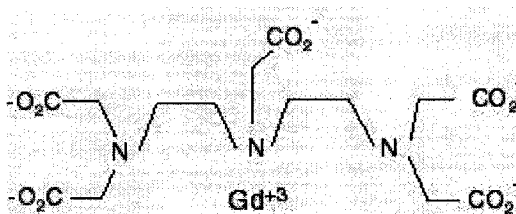
Fig. 2.6- Chemical structure of the commercial Gd-DTPA contrast agent supplied by Magnevist.

Gadolinium as well as manganese diffuses into nerve [8]. This paramagnetic agent diffuses at a slower rate than manganese [8, 12, 13], and its relaxation characteristic is less effective as well. This is why a higher concentration of Gd-DTPA had to be added to

the solution in order to decrease its relaxation time to < 5 ms. Based on Eqs. (2.1 & 2.2) the appropriate concentration of gadolinium needed to reduce the relaxation time of the buffer to <5ms was calculated. Therefore, based on experiments and analysis, concentrations in the range 20 - 35 mM were chosen.

2.7- Induction of Cell Swelling

As was mentioned above, the use of paramagnetic agents may provide valuable information to establish a relationship between the water compartments and the T_2 spectral components of the nerve. However, in addition to the paramagnetic agents, we decided to use glutamate, which induces cell swelling, making it possible to extract additional information from the T_2 spectrum. Cell swelling would be expected to increase the magnitude of the T_2 component related to the axoplasm.

2.7.1- Glutamate

The rat optic nerve is considered as mammalian white matter lacking neuronal cell bodies and synapses [14]. Glutamate is one of the most active and important neurotransmitters in optic nerve; glutamate transporters are responsible for keeping the resting extracellular glutamate concentration low. This is required for normal neurotransmission and prevents the extracellular concentration of glutamate from reaching toxic levels that may damage the cells [15]. There are studies suggesting that problems with glutamate signaling may contribute to the development of some white matter pathologies [16]. There is supportive evidence to the idea that glutamate works as an intercommunication signal between axons and glial cells because glutamate transporters were found in oligodendrocytes in experiments performed *in vitro* and *in situ* [17].

Glutamate transporters localized in neuronal, axonal and glial cell membranes remove glutamate from the extracellular space, this was found even in non-synaptic regions such as the optic nerve. It has been suggested that neurons may communicate with glial cells

along their axons through the reversal of glutamate transporters localized at the nodes of Ranvier. This characteristic, together with the fact that the activation of glutamate receptors can induce toxicity in oligodendroglial cells, strongly suggest that the extracellular glutamate concentration is regulated by transporters in order to prevent damage to oligodendrocyte cells and demyelination [17].

For experiments performed in *situ* in the rat optic nerve it was found that glutamine synthetase (a key enzyme in glutamate metabolism) was present in oligodendrocytes [17]. Also, it was determined that glutamate transporters are present in higher quantities in oligodendrocytes than in astrocytes suggesting that oligodendrcytes of the optic nerve may participate in the glutamate-glutamine transformation cycle in order to provide axons with glutamine as a potential source for glutamate [17].

In the optic nerve, oligodendrocytes are the cells that engulf axons with myelin. If their function is disrupted as a consequence of cell swelling, demyelination will occur [18]. The results presented by Domerq strongly suggest that oligodendrocytes as well as glutamate transporters contribute to the maintenance of low levels of extracellular glutamate [17]. This function is very important because high levels of glutamate induce cell swelling and death. Experiments in rat cerebrum indicate that after the addition of glutamate, the apparent diffusion coefficients (ADC) measured in the brain changes as a result of a water shift from the extracellular to the intracellular space [19]. Recent studies by Kriegler and Chiu have demonstrated a physiological signaling between axon and neighboring glia in the rat optic nerve by detecting activation of glutamate receptors [14]. The optic nerve possesses glutamate receptors and transporters [20].

In physiological conditions, millimolar concentrations of glutamate are released from axons to the extracellular space during and after propagation of action potentials [21, 22]. It has been suggested that the transmembrane ionic shifts observed after glutamate release are accompanied by water movement from the extra- to the intra-cellular space, and that activation of glutamate receptors may result in rapid cellular swelling. It is known that cellular swelling as a consequence of high concentrations of glutamate in the extracellular

space is a complex process at the molecular level. It was determined in experiments by Vargova that 10-mM of glutamate induced cell swelling in the CNS [23].

2.8- Parameters for CPMG Pulse Sequence

Experiments were performed on a SMIS 3-Tesla NMR Scanner. All samples were studied at room temperature. Transverse-relaxation decay curves were recorded continuously using a phase-cycled CPMG sequence. The CPMG sequence consisted of a $^{\pi}/_{2}$ rf pulse followed by a train of π pulses between each echo. The specific parameters of the pulse sequence consisted of an echo time of 1.6 ms and a repetition time of 14 s, which allowed the longitudinal magnetization to return to equilibrium after the application of the last π pulse in the echo train and before the application of the next $^{\pi}/_{2}$ pulse for the acquisition of the next FID. The time to accomplish a π pulse was set to 20 μs; it is necessary to adjust the energy deposition in the coil to obtain this pulse. After the parameters had been defined for the π pulse, using the same energy deposition and reducing the flipping time to 10 μs resulted in a $^{\pi}/_{2}$ pulse. Having these pulses set correctly is needed for an appropriate run of the CPMG sequence.

The sample, placed in the perfusion chamber centered in the RF coil, was completely excited for data acquisition. The length of the complete data acquisition for one sample varied from 1 to 6 hours. A total of 4,000 echoes were collected from which the peak of each echo was determined based on an average of 16 sample points (per echo) to obtain a data point in the FID curve. For a diagram of a CPMG sequence and echo formation, refer to fig. 1.12. Data were analyzed using a non-negative least squares fitting routine [24], explained in more detail in section 2.9.

2.8.1- Inversion Recovery-CPMG

As was mentioned before, nervous tissue may be characterized by different T_1 and T_2 component values. Inversion recovery is used to obtain information about the longitudinal (T_1) relaxation of tissue [25]. The inversion-recovery technique can be used to null signal from a specific component when the longitudinal magnetization is zero and is flipped into the transverse plane [3]. To show the intrinsic relationship between the longitudinal magnetization and the transverse magnetization, an inversion-recovery CPMG sequence was used. This sequence consisted of a 180° pulse (to flip the longitudinal magnetization into the negative z-axis) followed by an inversion time (T_I) and then a CPMG sequence (fig. 2.7). The inversion time refers to the time between the 180° pulse and the 90° pulse (starting point of CPMG sequence) and is a very important parameter to determine which component of the sample will be nulled. It is possible to eliminate signal from a specific component of the nerve or the buffer by the correct choosing of the inversion time. The longitudinal magnetization returns to thermal equilibrium according to the following equation [26]:

$$M_z(t) = M_0(1 - 2e^{-t/T_1})$$ (2.3)

where M_z is the longitudinal magnetization at a specific time t, M_0 is the magnetization at thermal equilibrium and T_1 represents the longitudinal relaxation time. Notice from this equation that the signal vanishes at $T_I = T_1 \ln2$, which corresponds to the point where the longitudinal magnetization has regrown from $-M_0$ to zero. With this sequence experiments can be performed with T_I chosen such that signal from one of the nervous tissue components is zero. That component is said to be "nulled", therefore, different components in the sample may be studied selectively.
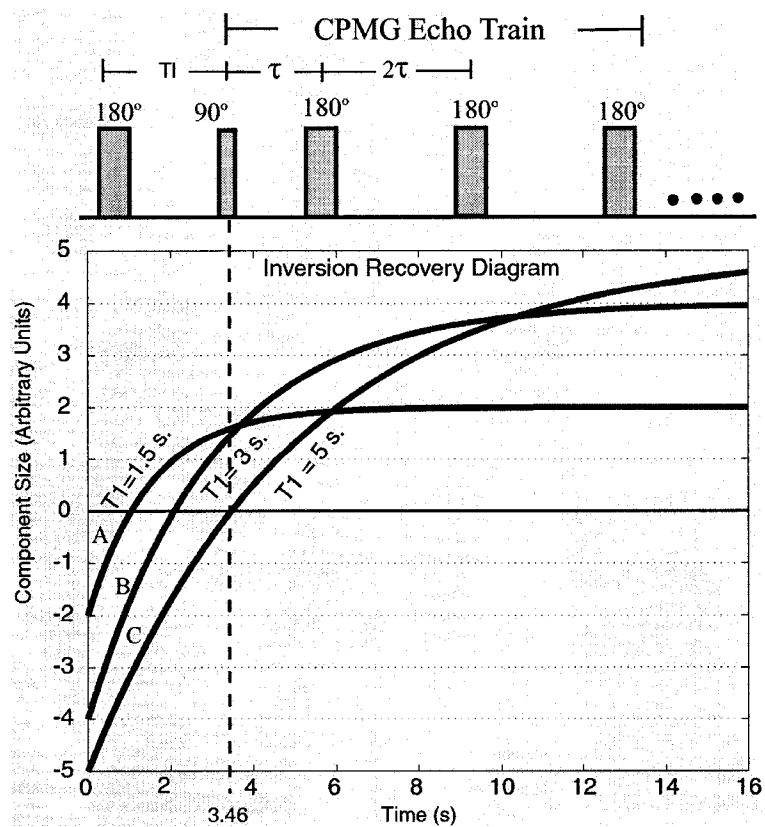
Fig. 2.7- Diagram of a theoretical example of the inversion recovery-CPMG pulse sequence. In the bottom are shown three different components with specific T_1 times A (T_1 =1.5 s) B (T_1=3 s) and C (T_1=5 s). At time 0 a 180° pulse is applied and all the longitudinal magnetizations is along the negative z-axis. At 3.46 s a 90° pulse is applied and the longitudinal magnetization is placed in the transverse plane. The component (A) has 80% of its total magnitude, the component (B) 37% and the magnitude of the component (C) has been nulled. With this technique it is possible to manipulate the magnitude of the components and the buffer.

2.9- NNLS Fitting Routine for Analyzing Data

Data from an experiment, that is, the FID as sampled by the CPMG sequence, were analyzed using a non-negative least squares (NNLS) fitting routine to convert the decay curves to T_2-relaxation spectra (fig. 2.8) [24]. The NNLS routine transforms the FID into a series of exponential decays, each characterized by a specific T_2 relaxation time and magnitude to form a T_2 spectrum. Once the T_2 spectrum was obtained we were able to get information about the different relaxation times and relative component sizes of the nervous tissue. The most common approach to the analysis of multi-exponential relaxation is to fit the decay curves with the smallest number of discrete exponential terms that provide a satisfactory representation of the experimental data. The following equations show the theory behind the fitting routine.
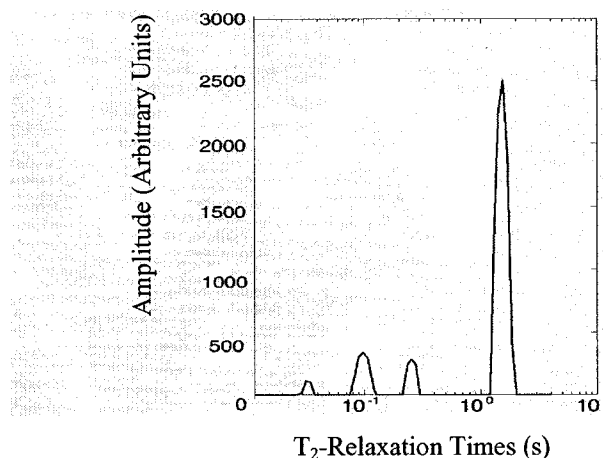
Fig. 2.8- T_2 spectrum of the rat optic nerve in a standard buffer solution

In a NMR experiment characterized by multi-exponential relaxation, the magnitude of the signal at time t_i in a FID can be described by

$$y(t_i) = \int_a^b S(T)e^{-t_i/T} dT \qquad (2.4)$$

where a and b are the limit values expected for the relaxation times T present in the sample and the unknown amplitude of the spectral component at the relaxation time T is represented by $S(T)$. The term $exp(-t_i/T)$ is the fraction of signal with relaxation time T

that has decayed by measurement time t_i [27]. In order to develop a computer algorithm, Eq. (2.4) has to be transformed into a discrete form. The signal $S(T)$ is characterized by a sum of Z delta functions, each one represented by an unknown area at a defined relaxation time T_j. The discrete form of Eq. (2.4) is described by

$$y_i = \sum_{j=1}^{Z} S_j e^{-t_i/T_j} \qquad i = 1,2...,N \qquad (2.5)$$

where N represents the number of points sampled in the FID curve. Equation (2.5) represents a linear system of equations, which can be written as:

$$y_i = \sum_{j=1}^{Z} S_j A_{ij} \qquad i = 1,2...,N \qquad (2.6)$$

where A represents a matrix with individual element values of $e^{(-t_i/T_j)}$, an array of Z columns by N rows. For this study the relaxation time T_j was chosen to have Z = 105 logarithmically spaced points between 1 ms and 10 s. Also, it was found necessary to use only 140 echoes for the T_2 algorithm in order to limit computational demands. The FID curve was logarithmically sampled to obtain more information at the beginning of the curve (sampled fine spaced) where data from all the components of the nerve are present than by the end of the curve where only the buffer is present. We can organize the information in a matrix form and solve for S_j to obtain the different magnitudes and relaxation times of the sample [24].

In any realizable experiment, the data y_i are corrupted by noise. Because of the noise contaminating y_i, Eq. (2.6) cannot be solved exactly. Proposed solutions must misfit the inaccurate data by an amount consistent with the errors. The chi-squared statistic quantifies the misfit between the measured data y_i and the data y_i^p corresponding to a particular model $S(T)$. The chi-square misfit can be represented as

$$\chi^2 = \sum_{i=1}^{N} \frac{\left(y_i^p - y_i\right)^2}{\sigma_i^2} = \sum_{i=1}^{N} \frac{\left(y_i^p - y_i\right)^2}{\left(y_i^t - y_i\right)^2} \qquad (2.7)$$

In Eq. (2.7), y_i^t is the true magnetization data point uncorrupted by noise, and σ, is the standard deviation of the noise associated with the i_{th} data point. The preferred solution is one which should misfit the noisy data by an amount which is consistent with the noise variations; therefore the chi-square preferred is when $(y_i^p - y_i) \approx (y_i^t - y_i)$

$$\chi^2 \approx \sum_{i=1}^{N} 1 \approx N \qquad (2.8)$$

The preferred model has $\chi^2 \sim N$, which is the expected value of the χ^2 statistics. If $\chi^2 \ll N$, the data are fit too accurately and may result in extra peaks, shifted peaks and incorrect amplitudes in the solution. On the other hand if $\chi^2 \gg N$ the data are not fit closely enough and information about the true spectrum contained in the data will be lost.

For relaxation data the NNLS technique is very useful because an "a priori" number of components in the spectrum does not need to be specified [28]. In other words, NNLS is a linear technique that does not require initial conditions and is guaranteed to converge to the minimum components.

Lawson and Hanson [29] developed an algorithm that introduced NNLS routines to fit data. Whittall and MacKay [24] used the NNLS routine and modified it to extract the T_2 relaxation times for decaying curves in NMR experiments. The NNLS routine finds the appropriate values of the vector S_j that minimize the least-squares misfit. The linear system of equations, Eq. (2.6), can now be solved for $S(T_j)$ by using a linear inverse technique. To minimize the least-squares misfit Eq. (2.9) is used:

$$\sum_{i=1}^{N} \left| \sum_{j=1}^{Z} S_j A_{ij} - y_i \right|^2 \qquad (2.9)$$

The signal measured during the NMR experiments is represented by y_i, and the matrix A_{ij} contains the different exponential decays with specific T_2 values used to find an appropriate fitting.

The NNLS algorithm forces the solution of the vector components S_j to be non-negative and minimizes Eq (2.9) with the minimal non-zero components for S_j. The least-squares solution that minimizes Eq. (2.9) is a discrete delta-function solution. The algorithm uses an average of the delta-function residuals around each time domain data point to estimate the standard deviation of noise, σ_i related with y_i. To overcome difficulties with noise, extra constraints can be added to the minimization function of Eq (2.9).

The extra constraints are incorporated by the addition of a smoothing term or regulariser, μ, to the minimization function of Eq. (2.9):

$$\sum_{i=1}^{N}\left|\sum_{j=1}^{Z} S_j A_{ij} - y_i\right|^2 + \mu\sum_{k=1}^{K}\left|\sum_{j=1}^{Z} H_{kj}S_j - f_k\right|^2 \qquad (2.10)$$

where H_{kj} is a matrix representing K additional constraints and f_k is the vector estimating the form of $\mathbf{H \cdot S}$. The least-squares solution is obtained when $\mu=0$. The larger the value of μ the more the algorithm attempts to satisfy the constraints involving the matrix $\mathbf{H}$ at the expense of increasing the χ^2 misfit. The value of χ^2 increases monotonically with μ. The value of μ is adjusted until the misfit is near its expected value of N. The matrix $\mathbf{H}$ can take many forms. For our studies $\mathbf{H}$ is the Z × Z identity matrix and f is the zero vector, then the K = Z extra constraints minimize the "energy" (the sum of squared amplitudes) in the spectrum:

$$\sum_{j=1}^{Z} S_j^{\,2} \qquad (2.11)$$

The smoothing factor, μ, incorporated in Eq. (2.10) consists in addition of extra rows in the matrix A_{ij}. Now it is possible to obtain a solution in a continuous distribution form by solving for $S(T)$ using the NNLS routine. The preferred solution then will have $\chi^2 > N$ since it should have a larger misfit than the delta function solution in order to avoid fitting of any noise. The degree which χ^2 is allowed to exceed N is determined by the statistics of the χ^2 distribution itself. The algorithm that handles all this information is written in MATLAB.

For experiments *in vitro* where the SNR value exceeds 1000, the resolution of nerve water components is determined by a separation between relative peaks of at least a ratio of three in the relaxation time scale to obtain a good definition between components [30]. Two peaks closely spaced may not be resolvable, thus, a change in the T_2 time of a peak in different solutions may suggest the removal of an unresolvable peak (components merging). If the valley between peaks is not zero, the peaks are still considered as T_2 components and selected in the computer algorithm for the magnitudes and relaxation times to be calculated. Linear inversion techniques, with additional smoothing constraints, give continuous distribution solutions, which are more representative of reality in biological tissues. The discrete value for T_2 times and magnitudes in the T_2 spectrum is determined as a weighted average of the T_2 times and the addition of individual signal amplitudes corresponding to each T_2 time in a specific component.

2.10- Plotting Data from the T_2 Spectrum

After a T_2 spectrum is obtained it is important to present the data in a form that is easy to understand and from which it is possible to extract information directly. Now that the data analysis has been explained it is possible to understand how the different relaxation times and component sizes in the nervous tissue are obtained. Next, an explanation on how the data (T_2 times and component sizes) are extracted from the T_2 spectrum in order to analyze the results of our experiments is described.

Figure 2.9 shows a T_2 spectrum of the optic nerve obtained from an FID curve after being analyzed with a NNLS routine. The data analyzed and plotted from the T_2 spectrum are the relaxation T_2 times (fig. 2.9 B) and the magnitudes of the different components (fig. 2.9 C). Each spectrum is obtained from the averages of 8 FID curves. It takes ≈ 2.8 min to acquire each spectrum. During the whole experiment several T_2 spectra are recorded and the data analyzed. After the addition of paramagnetic agents or salts the T_2 spectra of the nerve changes with time; this provides valuable information of the component sizes and relaxation T_2 times that can be related with the water compartments of the nervous tissue [31]. The majority of graphs in this study do not contain information about the buffer

solutions; usually the buffer is not plotted because the nervous tissue components provide more relevant information than the buffer, and therefore it is better to take a closer look at these components. In a regular experiment different T_2 spectra are recorded to obtain information about the tissue. The first T_2 spectra collected (usually 5 or 10) are used as the control parameters for the experiments, this is, data from the nervous tissue in a standard buffer solution.
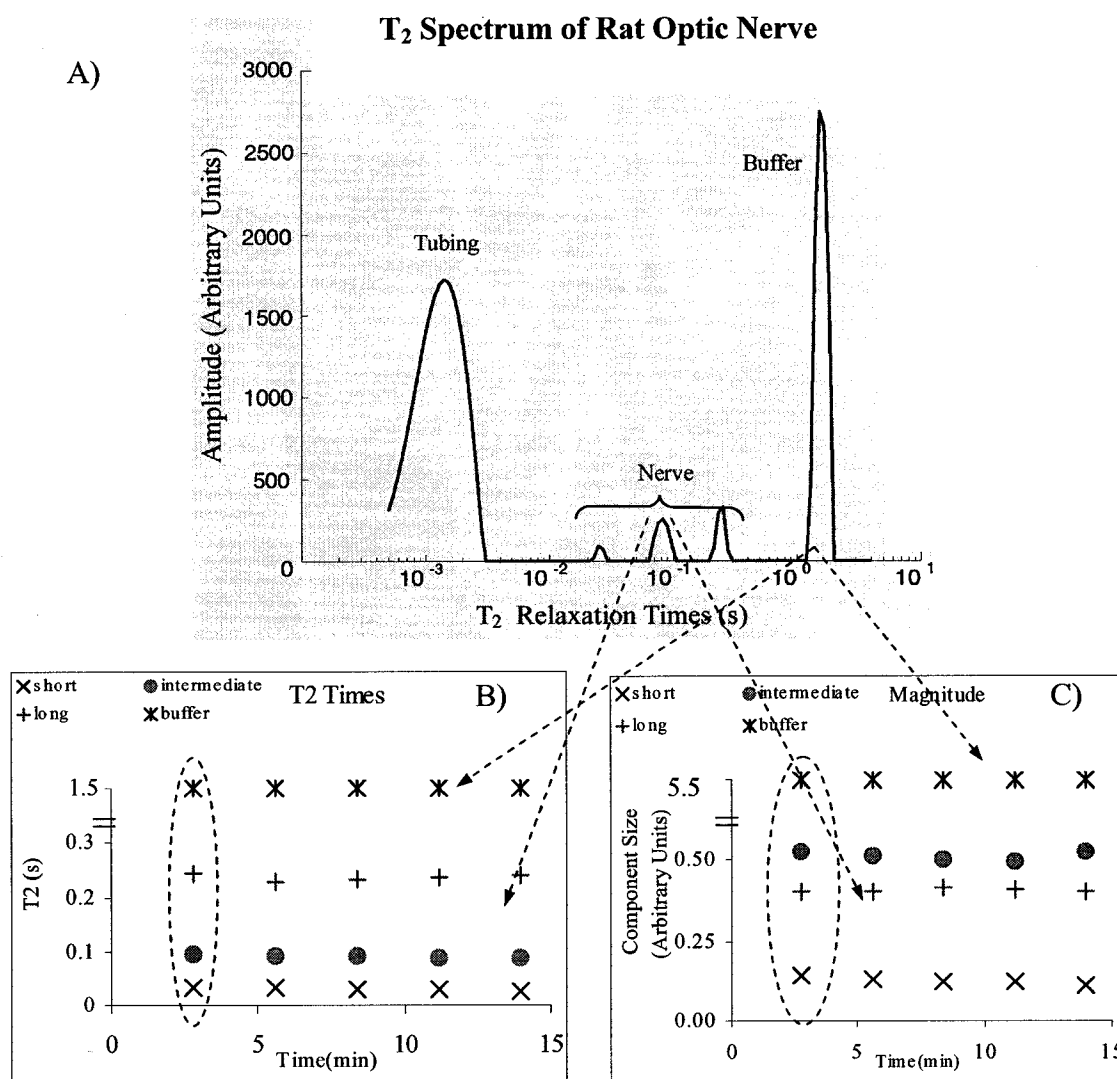
Fig. 2.9- T_2 spectrum of rat optic nerve (A). Graphs showing the way the information of the T_2 spectrum is plotted. The relaxation times are plotted vs time to collect all the data (B). In the same way the component sizes are plotted vs time (C). The time along the x-axis (min) represents the time at which a particular T_2 spectrum was collected in a particular experiment. One data set (one T_2 spectrum, information in dotted circle) is recorded in approximately 2.8 minutes. Usually in the graphs the buffer is not plotted in order to take a closer look at the nerve components.

The control data is plotted along the minus x-axis. For all the experiments in a standard buffer solution the component sizes were normalized to 100% (total signal of the nerve). After these spectrums are recorded in a standard buffer solution, different paramagnetic agents or salts can be added in order to see changes in the T_2 times or component sizes of the nervous tissue. When a standard buffer solution is about to be switched to one containing different salts or paramagnetic agents, a *time zero* is defined. After this time it is possible to observe the effects of the paramagnetic agents or salts in the nerve components. This way of plotting the data helps to follow the effects of these agents in the nervous tissue, making it easier to derive conclusions about the relaxation times and component sizes of the nerves. Figure 2.10 is an example of data from a nervous tissue in a standard buffer solution (control) prior to time zero (dotted line) and after the standard buffer solution was switched to one containing a paramagnetic agent. The advantage of this technique is that each experiment has it own control (data from the optic nerve in a standard buffer solution).
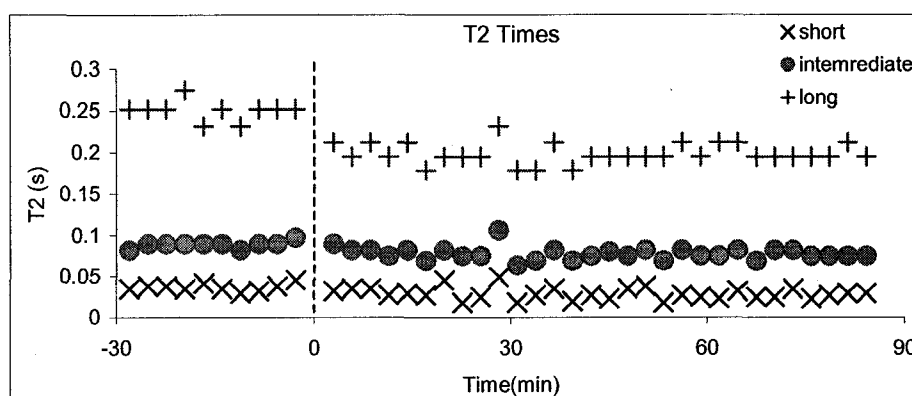
Fig 2.10- Graph showing three T_2 time components of the optic nerve. At time 0 (dotted line) the standard buffer solution was switched to one containing a paramagnetic salt.

2.11- Experimental Protocols

In our studies the experiments were performed in three different ways i) the most common one was running a CPMG sequence and recording the T_2 spectrum of the nerve in a standard buffer solution (control parameters) and in a solution after the perfusate was switched on-the-fly to another one containing paramagnetic agents or glutamate, ii)

running a inversion recovery-CPMG sequence at different inversion times (T_I) while the nerve was being perfused with a standard buffer solution, and iii) running a CPMG sequence when the nerve was placed in a NMR test tube. The information from these experiments was used to analyze changes in the T_2 spectral components and obtain a better understanding of the rat optic nerve under NMR studies.

2.12- Histology

At the completion of 4 experiments in a standard buffer solution and 8 using paramagnetic agents the nerves were fixed in fresh 4% buffered formaldehyde. All subsequent preparatory steps were performed by HistoBest Inc., (Edmonton, AB, Canada). After dehydration in graded ethanols and clearing, all tissue samples were infiltrated and embedded in ultra-pure paraffin (Poysciences, Inc., Warrington, PA, USA). Each nerve was sectioned in at least 4 segments: some oriented perpendicular in rapport with the paraffin block surface (i.e., transverse projection) while others were oriented parallel (i.e., longitudinal projection). Occasionally, HistoBest's matrix technique was employed for facilitating the precise orientation of minute multiple tissues segments [32]. Sectioning was performed at 4 μm on aminosilane-coated slides and myelin was stained with chromium trioxide. Stereology was performed on film and/or digital photographs at 400× and 1000× magnification with the aid of a stage micrometer. Some of these photographs are included in a CD for reference.

2.13- Bibliography

1. Wachowicz, K. and R.E. Snyder, *The Perfusion Chamber*. ISMRM 8th Meeting, 2000: p. 1987.

2. Bronskill, M.J. and P. Sprawis, *The Physics of MRI. 1992 AAPM Summer School Proceedings*. 1992.

3. Haacke, M.E., *Magnetic Resonance Imaging. Physical Principles and Sequence Design*. 2000: p. 665-667.

4. Landon, D.N., *The Peripheral Nerve*. 1976.

5. Young, I.R., et al., *Enhancement of relaxation rate with paramagnetic contrast agents in NMR imaging*. Journal of Computed Tomography, 1981. 5(6): p. 543-7.

6. Leawoods, J.C., B.T. Saam, and M.S. Conradi, *Polarization Transfer using hyperpolarized, supercritical xenon*. Chemical Physics Letters, 2000. 327: p. 359-364.

7. Webb, S., et al., *Is multicomponent T_2 a good measure of myelin content in peripheral nerve?* Magnetic Resonance in Medicine, 2003. 49(4): p. 638-45.

8. Wachowicz, K. and R.E. Snyder, *Assignment of the T_2 components of amphibian peripheral nerve to their microanatomical compartments*. Magnetic Resonance in Medicine, 2002. 47(2): p. 239-45.

9. Wadhwani, K.C., et al., *Saturable transport of manganese(II) across blood-nerve barrier of rat peripheral nerve*. American Journal of Physiology, 1992. 262(2 Pt 2): p. R284-8.

10. Kirsch, J.E., *Basic principles of magnetic resonance contrast agents*. Topics in Magnetic Resonance Imaging, 1991. 3(2): p. 1-18.

11. McLachlan, S.J., S. Eaton, and D.N. De Simone, *Pharmacokinetic behavior of gadoteridol injection*. Investigative Radiology, 1992. 27 Suppl 1: p. S12-5.

12. Foy, B.D. and J. Blake, *Diffusion of paramagnetically labeled proteins in cartilage: enhancement of the 1-D NMR imaging technique*. Journal of Magnetic Resonance, 2001. 148(1): p. 126-34.

13. Guiheneuf, T., et al., *Measurement of the diffusion coeficient of manganese ions in cured pork by one-dimensional H magnetic Resonance Imaging*. Intern J Food Technol, 1996. 31: p. 195-203.

14. Kriegler, S. and S.Y. Chiu, *Calcium signaling of glial cells along mammalian axons*. Journal of Neuroscience, 1993. 13(10): p. 4229-45.

15. Lehre, K.P., et al., *Differential expression of two glial glutamate transporters in the rat brain: quantitative and immunocytochemical observations*. Journal of Neuroscience, 1995. 15(3 Pt 1): p. 1835-53.

16. Matute, C., et al., *On how altered glutamate homeostasis may contribute to demyelinating diseases of the CNS*. Advances in Experimental Medicine & Biology, 1999. 468: p. 97-107.

17. Domercq, M., et al., *Expression of glutamate transporters in rat optic nerve oligodendrocytes*. European Journal of Neuroscience, 1999. 11(7): p. 2226-36.

18. Matute, C., et al., *Glutamate receptor-mediated toxicity in optic nerve oligodendrocytes*. Proceedings of the National Academy of Sciences of the United States of America, 1997. 94(16): p. 8830-5.

19. Benveniste, H., L.W. Hedlund, and G.A. Johnson, *Mechanism of detection of acute cerebral ischemia in rats by diffusion-weighted magnetic resonance microscopy.* Stroke, 1992. 23(5): p. 746-54.

20. Choi, I. and S.Y. Chiu, *Expression of high-affinity neuronal and glial glutamate transporters in the rat optic nerve.* GLIA, 1997. 20(3): p. 184-92.

21. Steinhauser, C. and V. Gallo, *News on glutamate receptors in glial cells.* Trends in Neurosciences, 1996. 19(8): p. 339-45.

22. Perez-Cerda, F. and C. Matute, *Excitotoxicidad oligodendroglial y desmielinizacion en el nervio optico.* Archivos de la Sociedad Espanola de Oftalmologia, 2000. 75(5): p. 301-4.

23. Vargova, L., et al., *Glutamate, NMDA, and AMPA induced changes in extracellular space volume and tortuosity in the rat spinal cord.* Journal of Cerebral Blood Flow & Metabolism, 2001. 21(9): p. 1077-89.

24. Whittall, K.P. and A.L. Mackay, *Quantitative Interpretation of NMR Relaxation Data.* Journal of Magnetic Resonance, 1989. 84: p. 134-152.

25. Does, M.D., et al., *Multi-component T_1 relaxation and magnetisation transfer in peripheral nerve.* Magnetic Resonance Imaging, 1998. 16(9): p. 1033-41.

26. Suetens, P., *Fundamental of Medical Imaging.* 2002: Cambridge University Press.

27. Fenrich, F., *NMR Transverse Relaxation of Water.* 2000: University of Alberta Thesis.

28. Beaulieu, C., F.R. Fenrich, and P.S. Allen, *Multicomponent water proton transverse relaxation and T_2-discriminated water diffusion in myelinated and nonmyelinated nerve.* Magnetic Resonance Imaging, 1998. 16(10): p. 1201-10.

29. Lawson, C.L. and R.J. Hanson, *Solving Least Squares Problems.* 1974: Prentice Hall, Englewood Cliffs N. J.

30. Fenrich, F.R., C. Beaulieu, and P.S. Allen, *Relaxation times and microstructures.* NMR in Biomedicine, 2001. 14(2): p. 133-9.

31. Bonilla, I., Wachowicz, K., Snyder, R.E., T_2 *spectrum of mammalian optic nerve.* ISMRM 11th Meeting, 2003: p. 1452.

32. Musat, S., et al., *Ischemia-reperfusion induces apotposis in the rat myocardium through a cycloheximide-inhibitable pathway.* J Moll Cell Cardiol, 1998. 30: p. 30.

Chapter 3

Experiments to Determine the Existence of Three T_2 Spectral Components

A main goal of this chapter is to show evidence that determines the real number of components that characterize the T_2 spectrum of the rat optic nerve. In this chapter we analyze the T_2 spectrum of the optic nerve in D_2O, in a standard buffer solution, in a solution with iron chloride and in fluorinert. We compared these results using statistical tools to see how the different solutions affect the relaxation times and the component sizes of the optic nerve. Also, we performed experiments using an inversion recovery CPMG sequence.

3.1- Identifying the T_2 Spectral Components of the Optic Nerve in a Standard Buffer Solution

3.1.1- Optic Nerve in a Standard Buffer Solution

Figure 3.1 shows a T_2 spectrum of rat optic nerve in a standard buffer solution. Four different components were identified in the T_2 spectrum ($T_2 > 10$ ms) of the nerve and the standard buffer solution, three due to signal coming from the nerve and one at ≈ 1.54 s [1, 2]. This last signal in the T_2 spectrum is assigned to be from the buffer because: i) when the nerve was removed from the chamber the only peak observed in the T_2 spectrum was at ≈ 1.54 seconds, ii) the standard buffer solution is composed mainly of water, therefore, it is expected the majority of the signal to be from the standard buffer, the signal of the buffer being approximately 83% of the total, the remaining 17% being signal from the nerve and iii) the transverse relaxation time of water (≈ 2.5 seconds) is similar to that of the standard buffer solution (≈ 1.54 s). The relaxation time of the buffer is shorter than that of the water because the addition of salts slows down the movement of water molecules, producing a more efficient relaxation [3]. As a consequence of using polyethylene for the perfusion chamber there is a T_2 component at around 1 ms; this component does not interfere with the components of the nervous tissue generally

presenting relaxation times between 10 and 500 ms. We know the polyethylene component to originate from the perfusion chamber because in experiments performed with a NMR tube this component was not present in the T_2 spectrum. Also, acquiring signal without the nerve or standard buffer solution, this component could still be seen.
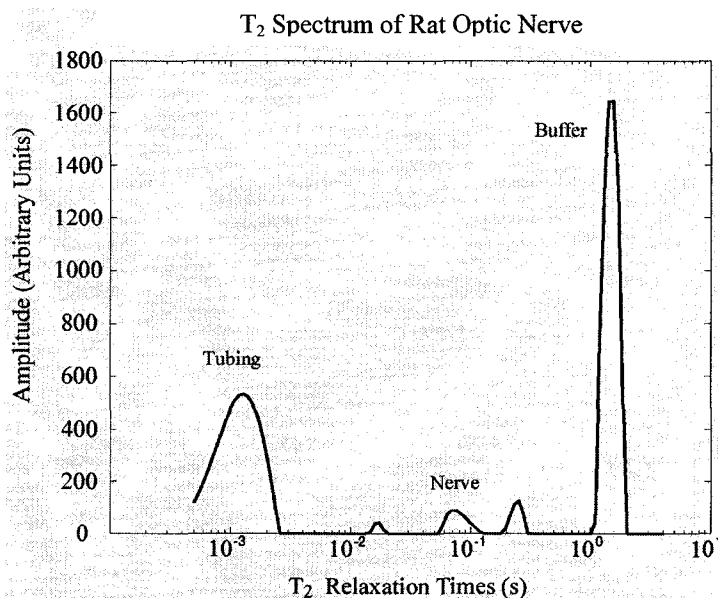
Fig 3.1- T_2 relaxation spectrum of rat optic nerve in a standard buffer solution. The larger peak (buffer) and the shorter (tubing) are the only ones observed if the nerve is removed from the perfusion chamber. It is also shown that the magnitude of the buffer is greater than that of the nerve.

3.1.1.1- Reproducibility of T_2 Times and Component Sizes

The purpose of this section is to show what difference is statistically significant in comparisons by taking one or different groups of samples that should be identical. Then when the nerve is bathed in a different solution (rather than a standard buffer) we know the changes in the T_2 times and component sizes are due to the solution and not as a result of difference in nerve samples. The different relaxation times and component sizes for a single experiment of optic nerve in a standard buffer solution are shown in Table 3.1. Ten T_2 spectra (each one composed by 8 averaged FID using phase cycling) were recorded in a single experiment when the optic nerve was bathed in a standard buffer solution. The mean and standard deviation of the T_2 times and component sizes are reported in the table in order to get an estimate of the precision of the results for one sample. The short-, intermediate-, and long-lived components of the nerve and the standard buffer solution

were analyzed. In all the experiments in a standard buffer solution the short-, intermediate- and long-lived component sizes were normalized to 100% (the total amount of signal from the nerve).

Table 3.1- Results of T_2 times and component sizes for 10 T_2 spectrum of a single sample (optic nerve) in a standard buffer solution							
	T_2 Times (ms)				Component Sizes (%)		
T_2 spectrum	Short	Inter	Long	Buffer	Short	Inter	Long	Buffer/Total
1	34.5	89.3	251.8	1.54	12.88	46.37	40.73	82.40
2	37.6	97.3	274.6	1.54	14.64	46.56	38.78	82.24
3	31.7	89.3	251.8	1.54	11.34	45.54	43.11	82.49
4	31.7	97.3	274.6	1.54	13.10	47.21	39.67	81.99
5	37.6	97.3	274.6	1.54	16.02	45.13	38.84	82.31
6	37.6	106.1	274.6	1.54	16.98	45.30	37.70	82.15
7	31.7	89.3	251.8	1.54	10.85	48.21	40.92	82.37
8	37.6	97.3	251.8	1.54	14.75	44.98	40.26	82.43
9	34.5	97.3	251.8	1.54	14.20	45.74	40.04	82.66
10	31.7	89.3	251.8	1.54	12.40	46.01	41.57	82.34
Mean	34.6	94.9	260.9	1.54	13.72	46.10	40.16	82.34
SD	± 2.7	± 5.5	± 11.7	0	± 1.96	± 1.01	± 1.54	± 0.18

The standard deviations reported for the relaxation times and component sizes were found to be similar to those from other studies of transverse relaxation in nervous tissue [3, 4]. In order to determine the variation of the T_2 times and component sizes between different optic nerve samples, we compared the results from 20 different optic nerves averaged over time in a standard buffer solution. Table 3.2 shows the different relaxation times and component sizes for these nerves.

It is shown that the inter-preparation variation is slightly greater (Table 3.2) than that of a single experiment (Table 3.1). The T_2 times and component sizes may present slight changes between different samples because the water in the compartments of the tissue may differ from one sample to another; however, these changes are minimal and do not represent a critical variable for the experiments in a standard buffer solution.

Table 3.2- T_2 times and component sizes for 20 different nerves in a standard buffer solution					
	T_2 Times (ms.)			Component Sizes (%)		
Sample	Short	Intermediate	Long	Short	Intermediate	Long
1	20.1	80.6	253.9	9.89	51.07	39.03
2	22.2	86.6	240.9	8.33	51.31	40.35
3	27.3	94.0	270.5	9.76	50.47	39.76
4	34.7	95.4	235.5	16.48	47.04	36.46
5	33.7	93.6	241.6	14.07	46.67	39.25
6	16.2	78.6	258.6	9.97	47.39	42.63
7	23.3	97.0	219.0	7.88	46.91	45.20
8	30.8	95.5	269.5	10.28	55.87	33.83
9	27.9	88.9	238.6	11.84	54.40	33.74
10	19.0	87.9	251.8	8.95	48.27	42.77
11	28.1	91.7	245.7	9.33	52.59	38.07
12	13.1	100.8	264.9	8.00	55.21	37.71
13	34.6	94.9	260.9	13.72	46.10	40.16
14	30.6	86.5	243.6	14.11	45.85	40.03
15	31.7	96.3	238.7	10.07	50.00	39.92
16	25.2	90.9	258.6	11.33	51.37	37.48
17	28.4	94.5	231.6	11.93	46.42	41.64
18	16.8	84.3	221.4	8.13	52.41	40.86
19	30.8	97.6	250.4	13.79	44.12	42.07
20	37.7	94.9	263.3	10.99	50.25	38.74
Mean	26.6	91.5	247.9	10.94	49.59	39.45
STD (σ)	± 6.9	± 5.8	± 14.8	± 2.43	± 3.29	± 2.85

To assure that the T_2 times and component sizes of the 20 experiments were similar between different nerves in the same standard buffer solution, we compared their values (Table 3.2) in different ways in order to determine if there were any statistical difference in the mean of the T_2 times and component sizes between different sample sets. The comparisons were i) the first 10 experiments with the last 10, ii) the odd experiments with the even, iii) a random sampling and iv) comparing 5 and 3 random samples out of 20, this last comparison was chosen because it will be used in the results of iron chloride and fluorinert. Table 3.3 shows a statistical comparison between the means of the relaxation times and component sizes obtained from twenty different optic nerves in a standard buffer solution. We performed a two-tailed t-test for the comparison of the mean, because it is more suitable when the population standard deviation is not known.

Table 3.3- Statistical comparisons between components in a standard buffer solution. Showing two-tailed p-values (left) and power calculations* (right).							
	T$_2$ Times				Magnitudes		
Components	i) First/ Last 10		ii) Odd/Even		i) Firs/Last 10		ii) Odd/Even
Short	0.50	0.09	0.23	0.19	0.72	0.06	0.61	0.07
Intermediate	0.24	0.12	0.26	0.18	0.65	0.07	0.34	0.14
Long	0.94	0.06	0.40	0.12	0.82	0.05	0.51	0.09
	iii) Random		iv) 3 to 5		iii) Random		iv) 3 to 5
Short	0.22	0.06	0.87	0.05	0.83	0.05	0.87	0.05
Intermediate	0.19	0.28	0.23	0.11	0.21	0.16	0.77	0.06
Long	0.95	0.12	0.14	0.14	0.14	0.25	0.68	0.08

* The power values are low because the mean of the populations are very similar

All the two-tailed p-values were greater than 0.05. This gives confidence for the following experiments that a p-value <0.05, when comparing a nerve T$_2$ time or component size for nerves bathed in different solutions, represents a real change in the value and that this change is not caused by the use of different samples.

3.2– Optic Nerve in D$_2$O

An experiment was performed where the standard buffer solution was switched to a D$_2$O based solution. D$_2$O does not give rise to any NMR signal but diffuses into the nerve. Figure 3.2 (a) shows the decay of the signal of the perfusate and fig. 3.2 (b) shows the decay of the total signal of the nerve after the standard buffer solution was switched to one containing D$_2$O. The signal of the perfusate completely vanishes in less than 5 minutes. With this experiment we were able to show that more than 98% of the signal is coming from water protons that may exchange with those present in the buffer solution.
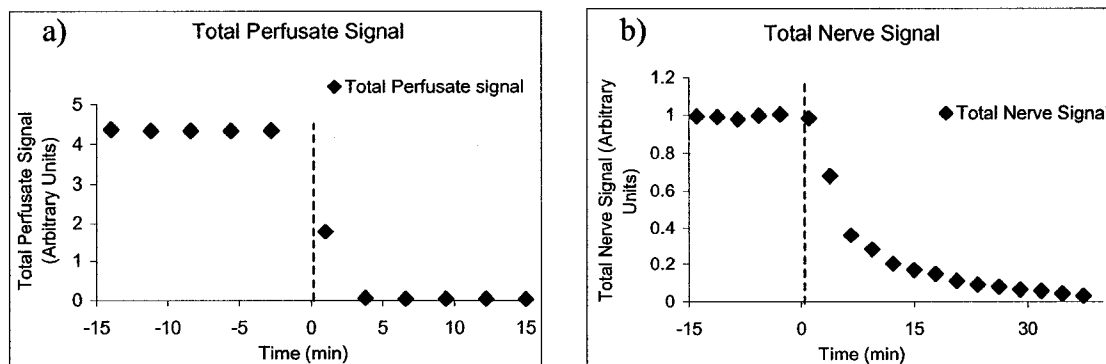
Fig. 3.2 - Graphs showing the total magnitude of a) the perfusate and b) the nerve signal. Before time 0, the optic nerve was perfused with a standard buffer solution. At time 0, the perfusate was changed to one composed of D$_2$O.

3.3- Determining if the T_2 Spectrum is Composed by 2 or 3 Components

The main objective of this chapter is to determine the real number of components that characterize the T_2 spectrum of the rat optic nerve (considered an extension of the CNS) and thus provide relevant information that may be useful in imaging or in the assessment of pathologies. In the optic nerve bathed in a standard buffer solution we have seen three different components (Table 3.2), the T_2 times of the first two similar to those identified in white matter *in vivo* [5] and bovine optic nerve *in vitro* [6]. We wanted to remove any possibility that the long-lived component might be a result of an artifact of the standard buffer solution and prove that the three components identified in our experiments are real. For this we performed two different types of experiments with specific characteristics. First, we used a paramagnetic agent ($FeCl_3$), which reduces the relaxation time of the buffer to < 5 ms, but does not permeate into the endoneurium [7] making it possible to get signal from the nerve and avoid signal from the buffer, giving the chance to observe the real number of components in the nerve. Next, we used fluorinert, which does not give rise to any proton NMR signal, the only signal obtained being from the nerve, and as a result no artifacts or contamination from the buffer would be present making it possible to identify the true number of components in the optic nerve. These two types of experiments with specific mechanisms of action were used to determine the real number of components that characterize the T_2 spectrum of the rat optic nerve.

3.3.1 Frog Sciatic Nerve with Iron Chloride

3.3.1.1- T_2 Times and Component Sizes of Frog Sciatic Nerve

Two frog sciatic nerves were used to prove that iron chloride does not permeate into the nerve, therefore this paramagnetic agent would be useful to get signal from the nerve and avoid signal from the buffer. Even though our research interest is in the optic nerve, frog sciatic nerves have been used in our studies as a model for testing different paramagnetic agents. Figures 3.3 and 3.4 show graphs of the relaxation times and component sizes of a typical frog sciatic nerve in a standard buffer solution and in a solution with $FeCl_3$.
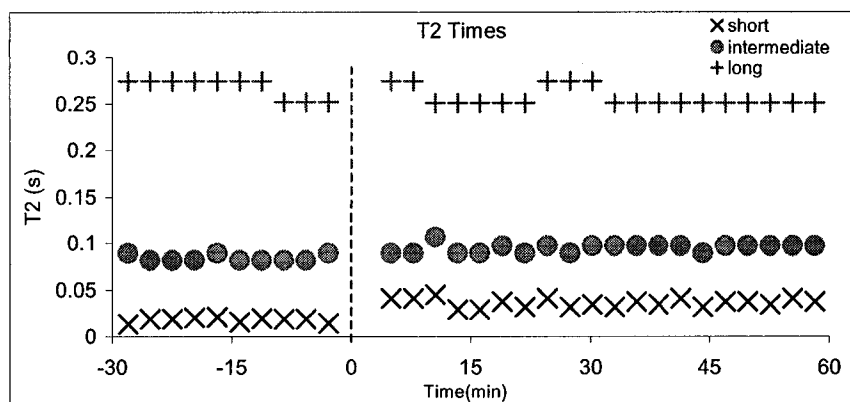
Fig. 3.3– T$_2$ times of the frog sciatic nerve before and after the addition of FeCl$_3$ (at time 0). The T$_2$ time of the standard buffer solution was ≈1.5 s. (not shown).
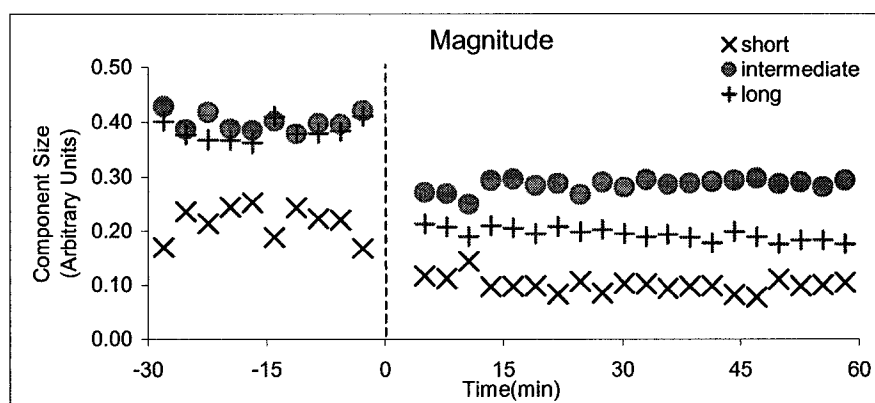
Fig. 3.4- Magnitude of the different components of the frog sciatic nerve. After 30 min, the standard buffer solution was switched to one containing 10-mM of iron chloride.

Table 3.4 shows the mean values of the relaxation time and component sizes for frog sciatic nerves before and after the addition of FeCl$_3$.

Table 3.4- Mean and SD of the T$_2$ times and magnitudes for two frog sciatic nerves in a standard buffer and in a solution with FeCl$_3$.

	T$_2$ Times		
	Short	Inter	Long
Buffer	18 ± 0.70	82 ± 2	270 ± 4
FeCl$_3$	28 ± 10.81	84 ± 14.9	252 ± 6.7
	Magnitude		
Buffer	17.53 ± 5.73	41.90 ± 2.63	40.56 ± 3.10
FeCl$_3$	15.09 ± 7.24	32.27 ± 5.37	21.62 ± 3.16

After the addition of iron chloride the long-lived component was still present for the duration of the experiments. This strong evidence for the long-lived component in frog sciatic nerve suggests that $FeCl_3$ can be used to remove any buffer artifact. Although there were changes after the addition of the paramagnetic agent, all the components were present during the whole experiment for more than 1 hr. Before the addition of the $FeCl_3$, the component sizes of the nerve looked very similar to those already obtained by Wachowicz [8]. After the addition of $FeCl_3$ the magnitude of the components experienced some changes shown in Table 3.4. The magnitudes of the short- intermediate- and long-lived components decreased with the addition of iron chloride. The long-lived component seems to be the most affected, being reduced by $\approx 50\%$.

After the addition of $FeCl_3$ to the buffer solution its relaxation time became <5 ms, so any possible artifact that may be generated by the buffer solution, which could affect the nerve components, was avoided. The buffer solution with its long relaxation time may interfere in the attribution of components in the nerve, therefore, it is important to reduce its relaxation time. Taking the buffer solution out from the nerve helps to identify the real number of components present in the T_2 spectrum. The three components found in the nerve before the addition of the paramagnetic agent remained for the duration of the experiment. These experiments showed that iron chloride was efficient in removing signal from the buffer and still leaving signal from the nerve for further analysis. After using the frog sciatic nerve as a model we decided to use this technique ($FeCl_3$) in rat optic nerve, which is our main research interest.

3.3.2- Optic Nerve with Iron Chloride

After using the frog sciatic nerve as a model to determine the effects of the iron chloride in the nervous tissue, the next step was to use this paramagnetic agent to determine the number of components present in the T_2 spectrum of the rat optic nerve.

A most extensive analysis and comparison between the T_2 times and components sizes was performed for the optic nerve. Five experiments were performed in which the standard buffer solution was changed on-the-fly to one containing 15-mM of $FeCl_3$. Prior to the addition of the paramagnetic salt to the standard buffer solution, the T_2 spectra (similar to fig. 3.1) exhibited three nerve components having relaxation times similar to those shown in Table 3.2. It is expected that dura, the outer membrane of the optic nerve, would behave similar to the perineurium in terms of allowing substances in and out of the nervous tissue.

Figure 3.5 shows the T_2 spectrum of the optic nerve after the addition of 15–mM of iron chloride to the buffer solution. The relaxation time of the standard buffer was reduced from ≈ 1.5 seconds to less than 5 ms. Three relaxation times were identified in optic nerve with and without the addition of $FeCl_3$, similar to those found in frog and rat sciatic nerves [9]. Based upon the addition of $FeCl_3$ it can be stated that the three relaxation times attributed to optic nerve are not artifactual to the buffer solution.
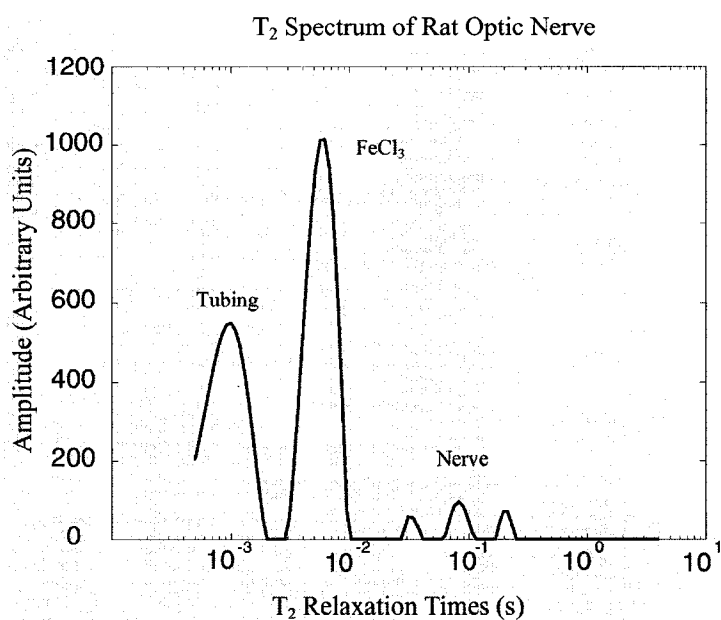
Fig. 3.5- T_2 spectrum of the rat optic nerve bathed in a $FeCl_3$ buffer solution. Here is shown signal from the tubing, signal from the buffer and signal from the nerve components after the addition of iron chloride.

3.3.2.1- T_2 Times and Component Sizes

Figures 3.6 and 3.7 show graphs with the relaxation times of the nerve components prior to (in a standard buffer solution) and after the inclusion of $FeCl_3$ into the buffer solution. All three components were clearly identified after the addition of the paramagnetic agent. The first 30 minutes of the experiments consisted of acquisition of signal from the optic nerve in a standard buffer solution, the remaining time ($\approx$ 1 to 3 hrs) consisted of acquisition of signal from the optic nerve when the standard buffer solution was switched to one containing iron chloride.
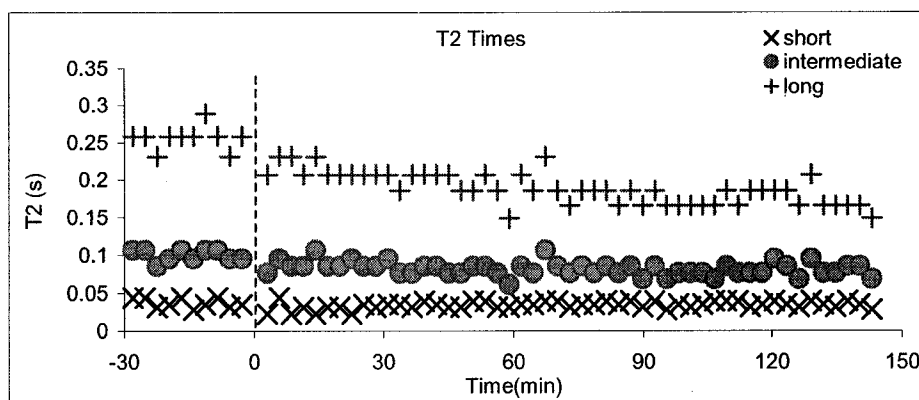
Fig 3.6- T_2 times of the optic nerve. At time 0 the standard buffer solution was changed to one containing 15-mM of iron chloride. The relaxation time of the buffer solution (not shown) was ≈ 1.5 s.
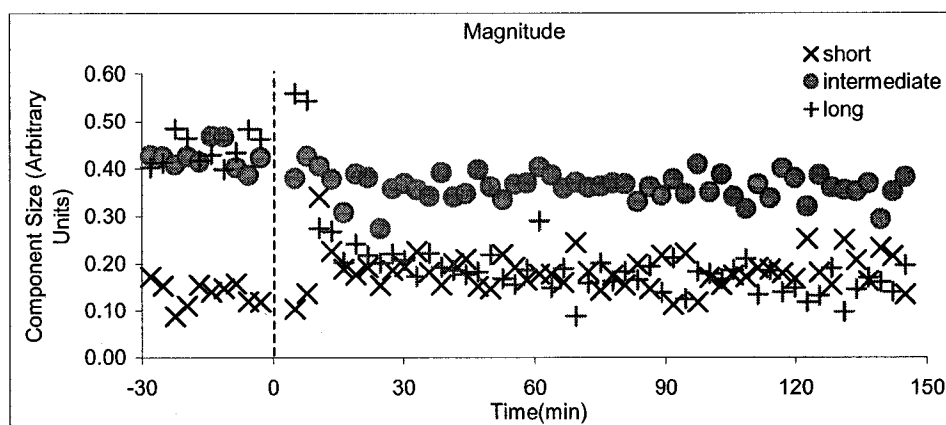
Fig 3.7– Graph showing the relative sizes of the three T_2 spectral components of optic nerve. At time zero the perfusing solution was switched from one not containing to one containing 15-mM $FeCl_3$.

In Table 3.5 are shown the relaxation times of the optic nerve before and after the addition of $FeCl_3$. For comparison purposes, after the standard buffer solution was switched to one containing $FeCl_3$ we analyzed the data points of the components until they were stable. After the addition of 15-mM of iron chloride the relaxation time of the buffer solution was successfully reduced to < 5 ms, the short-lived T_2 time did not present any change, however, the intermediate- and long-lived components were reduced in their relaxation times. The addition of the paramagnetic agent had a greater impact on the relaxation time of the long-lived component, which was initially ≈ 250 ms; after the addition of $FeCl_3$ the T_2 time of this component decreased to ≈ 200 ms.

Exp.	Soln.	T$_2$ Times (ms) Mean ± SD		
		Short	Intermediate	Long
1	B	37.4 ± 6.2	100.3 ± 7.6	256.7 ± 16.1
	Fe	34.5 ± 4.7	82.3 ± 9.3	188.7 ± 21.5
2	B	20.6 ± 3.6	82.4 ± 10.3	242.6 ± 15.0
	Fe	25.2 ± 9.1	72.5 ± 13.7	191.0 ± 20.5
3	B	28.2 ± 4.7	91.8 ± 5.3	245.8 ± 14.5
	Fe	27.9 ± 2.9	75.5 ± 12.1	193.8 ± 24.3
4	B	34.6 ± 2.8	95.0 ± 5.6	260.9 ± 11.8
	Fe	35.3 ± 3.8	81.2 ± 5.1	203.6 ± 33.3
5	B	43.3 ± 2.7	103.8 ± 1.7	240.3 ± 10.1
	Fe	39.6 ± 5.1	92.9 ± 9.8	217.6 ± 9.2
Mean ± SD	B	32.82 ± 8.72	94.66 ± 8.27	249.26 ± 9.04
Mean ± SD	Fe	32.50 ± 5.84	80.88 ± 7.83	198.94 ± 11.87

Table 3.5- T$_2$ times of the optic nerve for 5 experiments in a standard buffer (B) and FeCl$_3$ solution.

Once we evaluated the relaxation times of the components, we needed to analyze the effect of FeCl$_3$ on the component sizes. To establish a comparison between the component sizes in a standard buffer solution and in FeCl$_3$, the magnitude of the components for the optic nerve in FeCl$_3$ were normalized to the total signal of the nerve in the standard buffer solution for each of the five experiments. Then the mean values and the standard deviations were calculated for each experiment and are shown in Table 3.6. This is why the component sizes of the optic nerve in FeCl$_3$ do not add up to 100%.

Exp.	Soln.	Component Sizes (%)		
		Short	Intermediate	Long
1	B	13.57	42.49	43.92
	Fe	18.19	35.98	17.44
2	B	7.90	49.17	42.92
	Fe	14.71	39.92	17.43
3	B	9.32	52.59	38.07
	Fe	14.82	48.27	30.70
4	B	13.72	46.10	40.16
	Fe	21.04	39.55	16.44
5	B	12.83	47.65	39.50
	Fe	14.30	43.68	24.51
Mean ± SD	B	11.47±2.67	47.60±3.73	40.92±2.43
Mean ± SD	Fe	16.61±2.92	41.48±4.67	21.30±6.16

Table 3.6- Component sizes of the optic nerve for 5 experiments in a standard buffer (B) and FeCl$_3$ (Fe) solutions.

After the inclusion of the paramagnetic agent the short-lived component increased in its magnitude, different from the results observed in the intermediate- and long-lived components that decreased. Similar to what was found in frog sciatic nerve, the long-lived component magnitude was reduced to approximately half after the addition of the paramagnetic agent. Reduction in the relative size of the long-lived component in the optic nerve after adding $FeCl_3$ suggests this component is real, but may be composed in part of a signal related to the buffer solution or the dura.

In order to determine changes in the relaxation times and component sizes of the optic nerve in a standard buffer solution and after the addition of $FeCl_3$, we looked carefully at each experiment and the mean of the relaxation times. Magnitudes of the experiments were compared with a two-tailed t-test to see if the paramagnetic agent was having an effect on the nerve components. The results of the statistical analysis for the T_2 times and component sizes (magnitudes) are shown in Table 3.7.

Table 3.7- P-values of a statistical comparison (two-tailed t-test) between the components in a standard buffer and in $FeCl_3$ solutions.

Experiment	T_2 Times			Magnitude		
	Short	Inter	Long	Short	Inter	Long
1	0.098	<0.0001	<0.0001	0.0001	<0.0001	<0.00001
2	0.28	0.15	<0.0001	0.0089	0.0007	<0.00001
3	0.85	0.001	<0.0001	<0.0001	<0.0001	<0.00001
4	0.66	<0.001	<0.0001	<0.0001	<0.0001	<0.00001
5	0.05	0.002	<0.0001	0.003	<0.0001	<0.00001

For each of the five experiments a statistical comparison was performed in order to determine which relaxation times or magnitudes of the optic nerve presented a statistical difference between bathing in a standard buffer or a $FeCl_3$ solution. Table 3.7 shows that the addition of the paramagnetic agent has an implication in the relaxation times and magnitudes of the optic nerve components. The only parameter not presenting a statistical difference was the relaxation time of the short-lived component. The relaxation times of the intermediate- and long-lived components as well as the magnitudes of the short-, intermediate- and long-lived components present a statistical difference with p-values < 0.01.

In order to establish that there was a substantial difference between the components of the optic nerve in a standard buffer solution and in $FeCl_3$, we determined that the relaxation times and magnitudes were consistent in a standard buffer solution and in $FeCl_3$; therefore, the change of the components in these two solutions was real. We compared 10 data points (5 vs 5) in a standard buffer solution and 40 (20 vs 20) in iron chloride. Table 3.8 shows the p-values after a t-test was performed for comparison of the mean.

Table 3.8- Different p-values of a statistical comparison between T_2 times and magnitudes in a standard buffer and between T_2 times and magnitudes in $FeCl_3$.					
	T_2 Times			Magnitude		
	Short	Intermediate	Long	Short	Intermediate	Long
Buffer	0.22	0.96	0.58	0.95	0.60	0.79
$FeCl_3$	0.48	0.84	0.22	0.34	0.37	0.06

Based on the results shown in Table 3.8, it can be determined that there is no statistical difference between values in a standard buffer solution or $FeCl_3$. All the p-values > 0.05 show that the data points can be considered stable during the period of the experiments when the nerve is in a standard buffer or in $FeCl_3$ solution. As a result, the difference found in the components comparing results in a standard buffer solution and in one containing $FeCl_3$ is real.

3.3.3- Optic Nerve in Fluorinert

The T_2 spectrum of the optic nerve in fluorinert is shown in fig. 3.8. For these experiments three optic nerves were excised and used for the relaxation analysis. Three experiments were performed in which the optic nerves were bathed in fluorinert.

T₂ Spectrum of Rat Optic Nerve
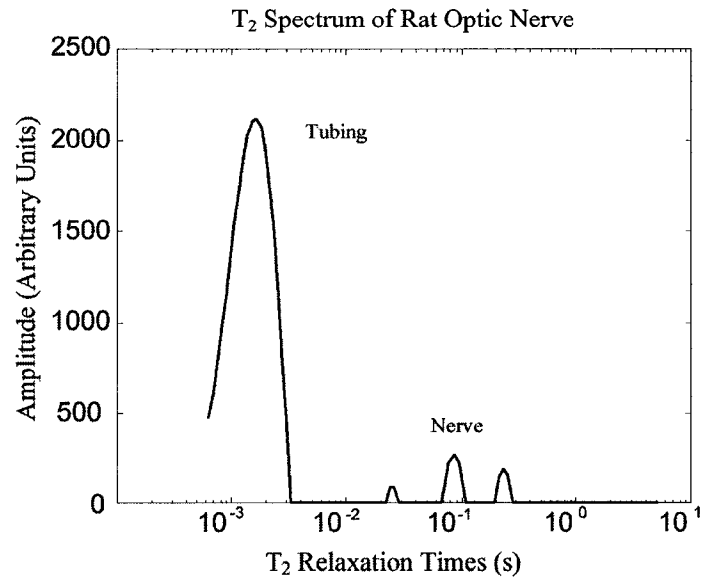
Fig. 3.8- T_2 spectrum of rat optic nerve bathed in fluorinert. The component at ≈ 1 ms is signal coming from the tubing of the perfusion chamber. Three T_2 spectral components are shown when the optic nerve is in a fluorinert solution. Note that there is no presence of the standard buffer signal at ≈ 1.5 s.

3.3.3.1– T_2 Times and Component Sizes

The relaxation times and component sizes of the nervous tissue in fluorinert are similar to those for experiments in a standard buffer solution shown in Table 3.2. Figures 3.9 and 3.10 are graphs of the relaxation times and the component sizes for a typical optic nerve in fluorinert.
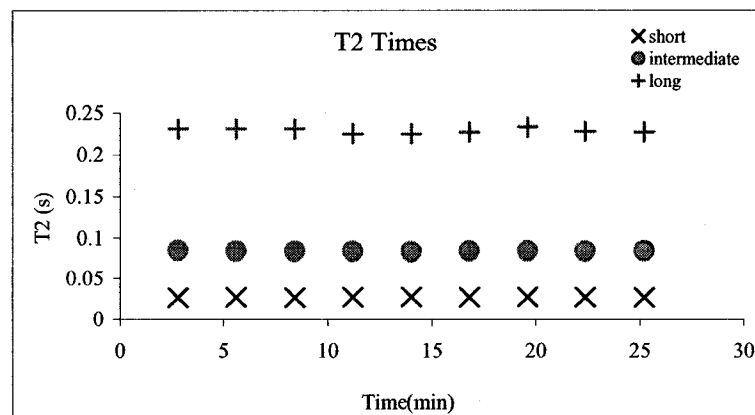
Fig. 3.9- Graph showing the T_2 times of rat optic nerve in fluorinert. Note that signal from the standard buffer at ≈ 1.5 s is not present and the three components are from the nerve.
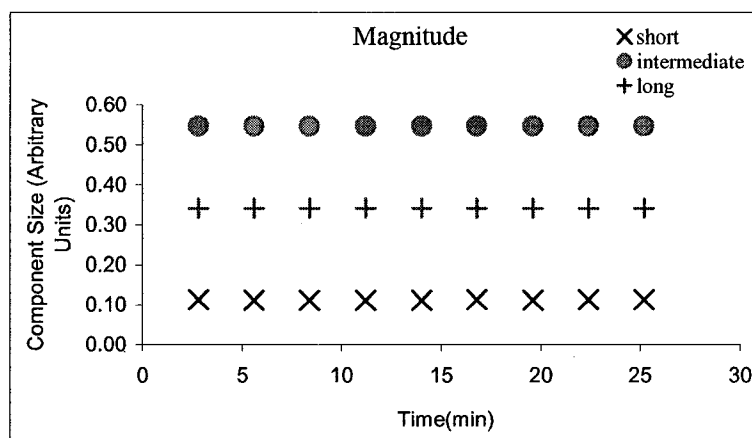
Fig. 3.10- Component sizes of rat optic nerve in fluorinert. Note that signal from the standard buffer is not present and the three components shown are from the nerve.

The relaxation times and component sizes for three optic nerve experiments in fluorinert are shown in Table 3.9.

Table 3.9- Mean and SD of the T_2 times and component sizes for 3 optic nerve experiments (Exp) in fluorinert.					
Exp	T_2 Times			Magnitudes		
	Short	Intermediate	Long	Short	Intermediate	Long
1	19.2	73.9	235	10.11	53.44	36.43
2	22.8	75.1	240.2	7.70	54.77	37.50
3	26.7	84.7	228.6	11.11	54.72	34.16
Mean±SD	22.9 ± 3.75	77.9 ± 5.92	234.6 ± 5.81	9.64 ± 1.75	54.31 ± 0.75	36.03 ± 1.70

In these experiments there is no presence of signal from the standard buffer, therefore, it is assured that the presence of the long-lived component is real and is not a consequence of an artifact created by the standard buffer solution

3.4- Comparison of the T_2 components in Different Solutions

Once we performed experiments in fluorinert, we wanted to compare these results with the ones obtained in a standard buffer solution. Table 3.10 shows a comparison between the mean of the T_2 times and component sizes for optic nerve in a standard buffer solution and in fluorinert.

	Short component			Intermediate component			Long component		
Solution	Mean	SD	p-value	Mean	SD	p-value	Mean	SD	p-value
				T_2 Times					
Buffer	26.60	±6.90	0.40	91.50	±5.80	0.001	247.90	±14.80	0.15
Fluorinert	22.90	±3.75		77.90	±5.92		234.60	±5.81	
				Magnitude					
Buffer	10.94	±2.43	0.38	49.59	±3.29	0.03	39.45	±2.85	0.05
Fluorinert	9.64	±1.75		54.31	±0.75		36.03	±1.70	

Table 3.10- Statistical comparison of T_2 times and component sizes in a standard buffer solution and fluorinert.

Neither the T_2 times for the short- and long-lived components nor the magnitude of the short-lived component present a statistical difference between the means in a standard buffer and fluorinert with p-values > 0.05. The magnitudes of the intermediate- and long-lived components are marginal in the statistical analysis with p-values between 0.01 and 0.05. Taking a closer look at the magnitude of the long-lived component, it is shown that it is smaller in fluorinert than in a standard buffer, supporting the assumption that the long-lived component for the optic nerve in a standard buffer solution may be composed in part by signal from the dura or by an interaction between the surface of the optic nerve and the buffer because its magnitude decreases when the buffer is removed. The only parameter presenting a significant statistical difference is the relaxation time of the intermediate-lived component with a p-value of 0.001. Based on these results it can be stated that the T_2 times and magnitudes of the nerve components are very similar in a standard buffer solution and fluorinert.

In order to make an extensive analysis of the nerve components in different solutions, we compared results from the nerve components in $FeCl_3$ and fluorinert. Table 3.11 is similar to Table 3.10, but now comparing $FeCl_3$ and fluorinert. The T_2 times of the short- and intermediate-lived components as well as the magnitude of the intermediate-lived component did not present statistical differences. The magnitudes of the short- and long-lived components as well as the T_2 time of the long-lived component present statistical differences with p-values <0.01. From comparisons of optic nerve in a standard buffer solution, $FeCl_3$ and fluorinert, it is clear that the T_2 times of the components and their magnitudes are definitely affected by the paramagnetic agent.

The results of the optic nerve in $FeCl_3$ compared to the standard buffer solution and fluorinert adds evidence to the belief that the long-lived component might be signal in part coming from the dura, or may be related with an interaction between the buffer and the surface of the nerve.

Table 3.11- Statistical comparison of T_2 times and component sizes in a $FeCl_3$ buffer solution and fluorinert.								
	Short component			Intermediate component			Long component		
Solution	Mean	SD	p-value	Mean	SD	p-value	Mean	SD	p-value
T_2 Times									
$FeCl_3$	32.50	±5.84	0.046	80.87	±7.84	0.59	198.74	±12.05	0.0031
Fluorinert	22.90	±3.75		77.90	±5.92		234.60	±5.81	
Magnitude									
$FeCl_3$	21.16	±4.89	0.008	52.06	±2.26	0.15	26.74	±4.46	0.01
Fluorinert	9.64	±1.75		54.31	±0.75		36.03	±1.70	

For the statistical analysis of the magnitudes and the comparisons between standard buffer and fluorinert, and $FeCl_3$ and fluorinert, we had to normalize the magnitudes of the components to 100% (total amount of signal in the nerve). We also analyzed the ratios of the magnitudes between the different components with non-normalized data. Table 3.12 shows the different ratios of the relaxation times and the magnitudes of the components in a standard buffer solution and in $FeCl_3$. Also are shown the p-values to compare the results of the component ratios in a standard buffer solution and $FeCl_3$. As it was shown before, the paramagnetic agent has an evident effect on the long-lived component. The ratios showing statistical difference p-values < 0.01 comparing the results of the components of the nerve in a standard buffer solution and iron chloride are the ones related with the magnitude of the long-lived component (LG/SH, LG/IN).

Table 3.12- Ratios of the different T_2 times and component sizes for optic nerve in a standard buffer solution and $FeCl_3$. Ratios of components, Long/Short (LG/SH), Long/Intermediate (LG/IN), Intermediate/Short (IN/SH).						
	T_2 Times			Magnitudes		
	LG/SH	LG/IN	IN/SH	LG/SH	LG/IN	IN/SH
Exp #	Buffer					
1	6.86	2.56	2.68	3.23	1.03	3.13
2	11.77	2.94	4.00	5.43	0.87	6.22
3	8.72	2.68	3.26	4.08	0.72	5.64
4	7.54	2.75	2.75	2.93	0.87	3.36
5	5.55	2.32	2.40	3.08	0.83	3.71
Mean ± SD	8.09±2.36	2.65±0.23	3.01±0.63	3.75±1.04	0.86±0.11	4.41±1.41
Exp #	$FeCl_3$					
1	5.46	2.29	2.39	0.96	0.48	1.96
2	7.58	2.64	2.88	1.18	0.44	2.71
3	6.95	2.57	2.71	2.07	0.64	3.26
4	5.77	2.51	2.30	0.78	0.42	1.88
5	5.49	2.34	2.35	1.71	0.56	3.05
Mean ± SD	6.25±0.95	2.47±0.15	2.52±0.25	1.34±0.54	0.51±0.09	2.57±0.62
p-value	0.14	0.18	0.14	0.001	0.0005	0.029

The other ratios do not present statistical differences. However, the ratios of the relaxation times involving the long-lived component are smaller in $FeCl_3$ than in experiments in a standard buffer solution, indicating that the relaxation time of this component decreases after the addition of the paramagnetic agent. It is demonstrated then, that analyzing the true values of the magnitude consistently indicates that $FeCl_3$ has a direct effect on the relaxation time most evident in the magnitude of the long-lived component. Table 3.13 shows the ratios of the relaxation times and magnitudes for experiments in a standard buffer solution and flurorinert.

Table 3.13- Ratios of the different T_2 times and component sizes for optic nerve in a standard buffer solution (n=20) and fluorinert (n=3). Ratio of components, Long/Short (LG/SH), Long/Intermediate (LG/IN), Intermediate/Short (IN/SH).						
	T_2 Times			Magnitudes		
	LG/SH	LG/IN	IN/SH	LG/SH	LG/IN	IN/SH
Buffer	10.09±3.43	2.72±0.23	3.70±1.18	3.78±0.91	0.80±0.09	4.77±1.17
Fluorinert	10.44±1.84	3.02±0.28	3.43±0.36	3.84±0.92	0.66±0.03	5.77±1.17
p-values	0.86	0.05	0.71	0.91	0.03	0.18

In Table 3.13 it is shown that all the ratios are very similar except for the T_2 times and magnitudes of ratios (LG/IN). The change in the T_2 ratio (LG/IN) is due to a decrease in the T_2 time of the intermediate-lived component when the sample is in fluorinert. The change in the ratio (LG/IN) is a result of the decrease of the long-lived component magnitude when the sample is placed in fluorinert (similar effect observed when the sample is in $FeCl_3$). The results of the ratio comparisons indicate that there is a small difference between the T_2 times and magnitudes in a standard buffer solution compared with fluorinert.

In order to have a complete analysis of the relaxation times and component sizes in all the different solutions (standard buffer, $FeCl_3$ and fluorinert) we compared the ratios of the components of the optic nerve in fluorinert and $FeCl_3$. Table 3.14 shows the ratios of the different relaxation times and magnitudes. The ratios of the long- and short-, and the intermediate- and short-lived components differ by as much as a factor of two, showing substantial differences between the experiments in fluorinert and iron chloride as it was shown before. Among the three solutions (standard buffer, $FeCl_3$ and fluorinert) the T_2 times and magnitudes of the optic nerve components differ the most when $FeCl_3$ was present in the solution.

Table 3.14- Ratios of the different relaxation times and component sizes for optic nerve in fluorinert (n=3) and $FeCl_3$ (n=5). Ratios of components, Long/Short (LG/SH), Long/Intermediate (LG/IN), Intermediate/Short (IN/SH).

	T_2 Times			Magnitudes		
	LG/SH	LG/IN	IN/SH	LG/SH	LG/IN	IN/SH
Fluorinert	10.44±1.84	3.02±0.28	3.43±0.36	3.84±0.92	0.66±0.03	5.77±1.17
$FeCl_3$	6.25±0.95	2.47±0.15	2.52±0.25	1.34±0.54	0.51±0.09	2.57±0.62
p-values	0.004	0.009	0.005	0.002	0.032	0.002

3.5- Relationship Between Transverse and Longitudinal Relaxation

3.5.1- Optic Nerve and Inversion Recovery-CPMG

The importance of inversion recovery is to demonstrate that it is possible to manipulate and even eliminate different components in the T_2 spectra of the optic nerve and the standard buffer by choosing the appropriate inversion recovery time (T_I). Three optic nerves were used for Inversion Recovery-CPMG experiments. In section 2.8.1 we explained how to eliminate a component and avoid getting signal from it using the inversion recovery technique together with a CPMG sequence. The use of this technique is primarily to avoid signal from a certain component. In these experiments it is shown how the signal from the different components and the standard buffer solution changes with modification of the (T_I) values. The potential value of this observation lies in the connection between transverse- and longitudinal-relaxation components with the tissue microanatomy and the potential to manipulate the intensity of the signal for different components.

3.5.2-Results of Hybrid T_I-CPMG Sequence

It is demonstrated that depending on the T_I chosen it is possible to manipulate the presence of different components and the standard buffer. Also, it is shown that the magnitude of the components change as well. Experiments were run at different T_I times. Table 3.15 shows these results. In these experiments the optic nerve was perfused with a standard buffer solution. The experiments relating the longitudinal relaxation with the transverse relaxation using a hybrid T_I-CPMG sequence show that the optic nerve is composed by three different components. The inversion-recovery experiments provide additional evidence to support the presence of three components in the T_2 spectrum of the optic nerve and showed that the longer the T_I time the greater the effect in the size of the longer-relaxation time components as was expected.

Table 3.15- True values of the magnitude (arbitrary units) of the different components of the optic nerve and the standard buffer solutions at specific inversion times (ms).				
Inversion Time (ms)	Short	Intermediate	Long	Buffer
TI=50	0.0543	0.4422	0.3786	3.7924
TI=200	----	0.3335	0.3399	3.3623
TI=500	----	----	0.2262	2.6057
TI=800	----	----	----	1.8891
TI=1000	----	----	----	1.3569
TI=1400	----	----	----	0.4547
TI=1700	0.0508	0.4208	----	----
TI=2000	0.0464	0.3322	0.1774	0.4412
TI=2500	0.0506	0.3678	0.2879	1.1694
TI=3000	0.0542	0.4230	0.3036	1.7239
TI=4000	0.0768	0.4974	0.3152	2.5825
CPMG	0.1271	0.5033	0.4411	4.1390

3.6- Conclusion

At this point we were interested in establishing the real number of components in the T_2 spectrum of the optic nerve. For the accomplishment of this goal, we performed different experiments i) using a paramagnetic agent that reduced the relaxation time of the buffer solution to a few ms ($FeCl_3$) and ii) using a solution that does not give rise to any NMR signal from the buffer (Fluorinert). Both types of experiments successfully established that the T_2 spectrum of the rat optic nerve is characterized by three different components. This information is essential for our studies, because there is no point in going further in the analysis of the nerve components until it was substantially determined the real number of components present in the optic nerve. The following chapter pursues the establishment of the relationship between the T_2 components and the water compartments of the nerve, defined in a model as axonal, myelinic and interaxonal water. The difference in the relaxation times and magnitudes of the components when the optic nerve was bathed in a standard buffer solution, a buffer solution with $FeCl_3$ or fluorinert, provided valuable information useful for the further analysis of the T_2-spectral components of the nerve discussed in the following chapters.

3.7- Bibliography

1. Bonilla, I., K. Wachowicz and R.E. Snyder, T_2 spectrum of mammalian optic nerve. ISMRM 11th Meeting, 2003: p. 1452.

2. Wachowicz, K. and R.E. Snyder, A look at the transverse relaxation spectra of mammalian optic nerve at 3.0 T. ISMRM 10th Meeting, 2002: p. 1211.

3. Beaulieu, C., F.R. Fenrich, and P.S. Allen, Multicomponent water proton transverse relaxation and T_2-discriminated water diffusion in myelinated and nonmyelinated nerve. Magnetic Resonance Imaging, 1998. 16(10): p. 1201-10.

4. Does, M.D. and R.E. Snyder, T_2 relaxation of peripheral nerve measured in vivo. Magnetic Resonance Imaging, 1995. 13(4): p. 575-80.

5. Whittall, K.P., et al., In vivo measurement of T_2 distributions and water contents in normal human brain. Magnetic Resonance in Medicine, 1997. 37(1): p. 34-43.

6. Stanisz, G.J. and R.M. Henkelman, Diffusional anisotropy of T_2 components in bovine optic nerve. Magnetic Resonance in Medicine, 1998. 40(3): p. 405-10.

7. Landon, D.N., The Peripheral Nerve. 1976.

8. Wachowicz, K. and R.E. Snyder, Assignment of the T_2 components of amphibian peripheral nerve to their micro-anatomical compartments. Magnetic Resonance in Medicine, 2002. 47(2): p. 239-45.

9. Wacowicz, K. and R.E. Snyder, Relationship between the Proton T_2 Relaxation Components of Peripheral Nerve and their Micro-anatomical Compartments. ISMRM 10th Meeting, 2002(1024).

Chapter 4

Experiments to establish the Component-Compartment Relationship

After assuring that the T_2 spectrum of the optic nerve is characterized by three components (chapter 3), in this chapter it is intended to establish the relationship between the T_2 spectral components and the water compartments of the optic nerve. To accomplish this objective we followed three different techniques: 1) checking the percentage of water in each compartment and comparing it with the amplitude of signal obtained in each component of the T_2 spectrum, 2) using paramagnetic agents that reduce the relaxation times of the components and therefore determine which regions are affected first by the paramagnetic agent and 3) using glutamate that induces swelling in the glial cells and axons. Comparing this information with the signal in the spectrum we can determine which components are affected by the addition of glutamate. In our studies the optic nerve in the standard buffer solution works as the control parameter, therefore it is possible to compare the implications of adding paramagnetic agents or salts to the buffer solution. It is important to establish a relationship between the compartments of the nerve and the components of the T_2 spectrum. If nervous tissue is damaged, an altered state of relaxation times may occur [1]. Therefore, finding the relationship between the components and compartments opens the opportunity to explore in more detail diseases related with the myelin, ECS and axons of the nerves. In the optic nerve we saw three different components with relaxation times similar to those found in the frog and rat sciatic nerves. There is enough evidence to attribute the short-lived component to signal from the myelin [2-4]. Therefore, the focus of this chapter is the identification of the intermediate- and long-lived components.

4.1- Analyzing Water Compartments in Optic Nerve and White Matter

A compartment in a tissue is a region (e.g., myelin, axoplasm) where the relaxation (T_1 & T_2) is the same everywhere. But, if H_2O can diffuse between two compartments, the observed relaxation time will be some mixture of the two. If the diffusion time between compartments is on the order of or greater than the relaxation time of either, then there will be two distinct relaxation times [5]. Water behaves differently in different micro-anatomical regions of the nerve due to the presence of proteins or other molecules that affect its relaxation [6]. Evidence suggests that myelin separates the axoplasm and ECS, hence three compartments may be identified [7]. The point of this section (sec. 4.1) is that the physical H_2O compartment sizes agree with the component sizes obtained during NMR experiments. This information suggests that the short-lived component can be related to myelin; however, it is not possible to assign the components for the axoplasm and ECS since their water content and component sizes are very similar. However, since compartments and component sizes are in approximate agreement, this supports the hypothesis that there are three water compartments with different relaxation times in the optic nerve. These results are shown next.

Water Compartments in Rat Optic Nerve

We combined data by Matheson [8] and Stys et al. [9] to estimate the water compartment sizes in rat optic nerve. In their studies the nerves were analyzed from the point at which the nerves enter the optic chiasm to the bulb. The length of the optic nerve was ≈ 1.3 cms. Their results indicated that the distribution of myelinated fibers is relatively uniform along the optic nerves. Table 4.1 shows information about the axons and myelin content in the rat optic nerve and Table 4.2 specific characteristics of the dimensions of the optic nerve as well as the myelin volume.

Table 4.1- Anatomical characteristics of rat optic nerve.					
Age (days)	Fiber diameter range (μm)	Estimated # of myelinated fibers per group	≈Axon radius (μm)	Volume of Axons (μm^3)	Total Volume of axoplasm (μm^3)
70	0-2	27,000	0.42	154x10^6	1034x10^6
	2-4	13,600	1.14	571x10^6	
	4-8	1,600	2.44	308x10^6	

Data from [8].
For the calculations of the areas and volumes of the nerve fibers it was assumed they had cylindrical shapes. Also a fiber is considered as a bare axon.

Table 4.2- Volumes of different compartments in rat optic nerve.	
Total Volume	$2{,}750{\times}10^6\ \mu m^3$
Total myelin volume	$700{\times}10^6\ \mu m^3$
Total axoplasm volume	$1034{\times}10^6\ \mu m^3$
Total ECS/glial cells volume	$1016{\times}10^6\ \mu m^3$

Data from [8].

Table 4.3 shows the water content of different micro-anatomical compartments of the optic nerve.

Table 4.3- Water content (%) of myelinated axons, myelin and ECS.	
Axons	91
Myelin	53
ECS/glial cells	95

Data from [9].

Grouping the information from previous tables, we were able to come up with an approximation of the water content in each micro-anatomical compartment of the optic nerve (Table 4.4). Also, Table 4.5 shows data of the component sizes in NMR experiments of the optic nerve.

Table 4.4- Volume and water content of myelin, axoplasm, ECS/glial cells of the rat optic nerve.				
Region	Volume (%)	Water (%)	Water content (%)	Normalized (%)
Myelin	25.45	53	13.48	16.28
Axoplasm	37.60	91	34.21	41.32
ECS/glial cells	36.95	95	35.10	43.39

Table 4.5- Mean of the component sizes (%) of the rat optic nerve for 20 experiments in a standard buffer solution* and 3 experiments in a fluorinated solution**.		
Component	Standard buffer	Fluorinert
Short	10.94	9.46
Intermediate	49.59	54.31
Long	39.45	36.03

* Refer to section 3.1.
** Refer to section 3.3.3.

This comparison between the water compartmentalization and NMR signal is the first approach to establish a relationship between the components in the T_2 spectrum and the compartments in the nerve. It is shown (Tables 4.4 & 4.5) that the short-lived component is most likely signal from water in the myelin, in accordance with studies from other laboratories [3, 4]. For the intermediate- and long-lived components, the relationship is

more challenging because the ECS and axoplasm have similar water contents. However, it is important to note that two components identified in NMR experiments (intermediate & long) are similar in size to the water compartments of the rat optic nerve (ECS & axoplasm).

In experiments realized by Fenrich [10] the total water population of different compartments in the optic nerve of the garfish showed myelin with $\approx16\%$, the axoplasm $\approx37\%$ and the extracellular space and glial cells $\approx47\%$. This water compartmentalization is similar to that in the rat optic nerve. The histology of the rat optic nerve observed by light microscope is similar to the garfish optic nerve except for the arrangement of connective tissue channels (fig. 4.1).
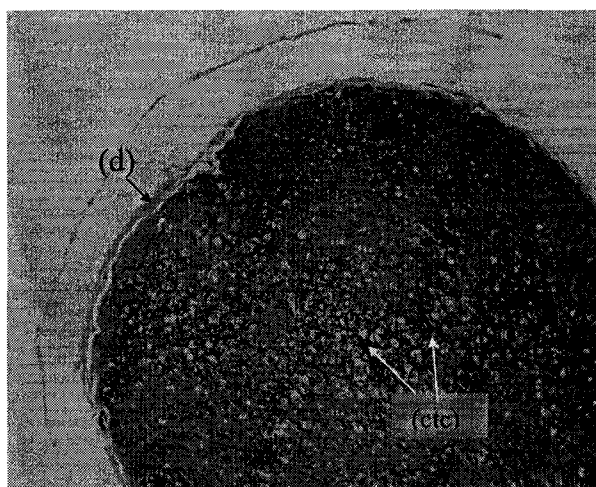
Fig. 4.1- Light microspcopic section of the rat optic nerve. The nerve is enclosed by a sheath of dura (d), the connective tissue channels (ctc) serving as a framework for the optic nerve present a random arrangement. The histology of the optic nerves used for the experiments looked normal.

Water Compartments in White Matter

In NMR experiments, signal is obtained from ^1H of water molecules, therefore the amount of water in the compartments can be related with the signal intensity of the different components. In humans, approximately 40% of the myelin is water; in CNS myelin forms $\approx 15\%$ of all the water in white matter [11]. Approximately 40% of the water in white matter is contained in the axoplasm [12]. Thus $\approx 45\%$ of the total water volume in white matter is from the ECS.

4.2- The Use of Paramagnetic Agents

In previous experiments we used $FeCl_3$ to determine the real number of components in the T_2 spectrum of the optic nerve. Here we use other paramagnetic agents (Mn^{2+} and Gd-DTPA) in order to attempt to establish the relationship between the T_2-spectral components and the water compartments of the nerve. For all the experiments with paramagnetic agents the T_2 times and component sizes of the nerve in a standard buffer solution were similar to those presented in section 3.1. The component sizes of the optic nerve in a solution with Mn^{2+} or Gd-DTPA were normalized to 100% (total signal from the nerve in a standard buffer solution, control.).

4.2.1- Optic Nerve with Manganese

In previous experiments performed by Wachowicz [13], the use of manganese as a paramagnetic agent helped to identify the relationship between the components of the T_2 spectrum and the compartments of the frog sciatic nerve (Refer to section 2.6.1). The same technique was applied in the optic nerve in order to attempt to establish a relationship between the components and the compartments. Three optic nerves were used for analysis with Mn^{2+}. Experiments were ran with a standard buffer solution, then the perfusate was changed on-the-fly to a solution containing 10-mM of $MnCl_2$, which decreased the T_2 time of the buffer solution to < 3 ms.

4.2.1.1- T_2 Times and Component Sizes

Figure 4.2 shows the different T_2 times for a typical optic nerve in a standard buffer solution and in a solution with $MnCl_2$. Note the rapid decay of the relaxation times in the first 10 minutes. Figure 4.3 shows the magnitude of the different components of a typical optic nerve before and after the addition of manganese.
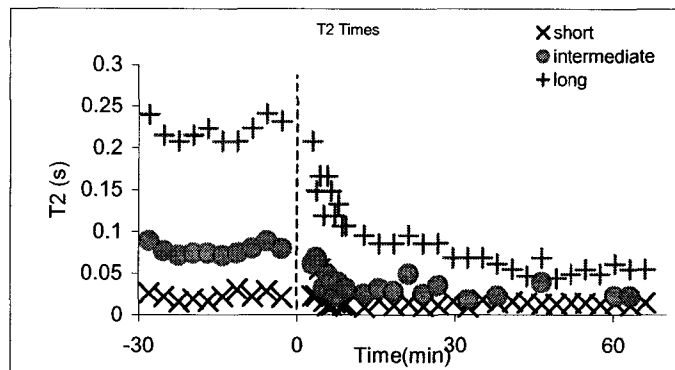
Fig 4.2- Graph showing the T_2 times of the optic nerve. At time zero the standard buffer solution was switched to one containing 10-mM $MnCl_2$.
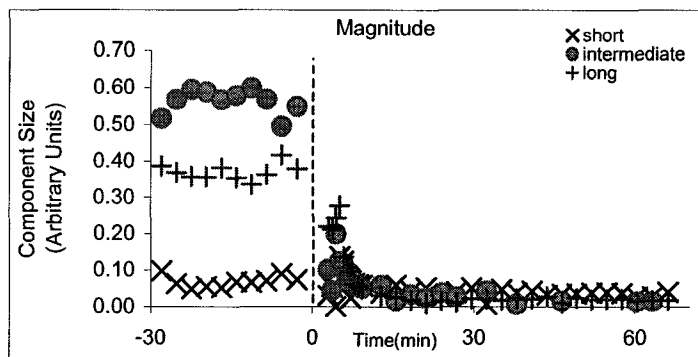
Fig. 4.3- Magnitude of the optic nerve components. At time zero the perfusing solution was switched to one containing 10-mM $MnCl_2$. Note the rapid decline in the intermediate- and long-lived components.

Table 4.6 shows the T_2 times of the optic nerve in a standard buffer solution and in a solution with 10-mM of $MnCl_2$. The table shows the average of the T_2 times of the components after 30 minutes of the inclusion of Mn^{2+}, when the T_2 times and component sizes become stable.

Table 4.6- Mean and SD of the T_2 times of the optic nerve in a standard buffer solution and in a solution with 10-mM of $MnCl_2$.					
Exp	T_2 Times in a standard buffer			T_2 Times in $MnCl_2$		
	Short	Intermediate	Long	Short	Intermediate	Long
1	22	78	221	14	25	57
2	34	101	265	16	27	88
3	35	110	243	16	24	39
Mean	31	96	243	15	25	61
SD	± 7	± 16	± 22	± 1	± 2	± 25

The relaxation times of all the components were affected by the addition of the paramagnetic agent. Table 4.7 is similar to Table 4.6, but in this case the table presents the component sizes of the optic nerve.

Table 4.7- Mean and SD of the component sizes of the optic nerve in a standard buffer solution and in a solution with 10-mM of $MnCl_2$.					
Exp	Component size in a standard buffer (%)			Component sizes in $MnCl_2$ (%)		
	Short	Intermediate	Long	Short	Intermediate	Long
1	6.83	56.18	36.97	3.46	1.87	2.00
2	15.33	41.43	43.22	9.04	9.92	5.27
3	17.22	55.63	27.14	4.99	1.81	2.05
Mean	13.13	51.08	35.78	5.83	4.53	3.11
SD	± 5.53	± 8.35	± 8.10	± 2.88	± 4.66	± 1.87

After the addition of Mn^{2+}, the signal started to decay very rapidly; it was not possible to identify which component was affected first by the paramagnetic agent, making it difficult to determine which component gives rise to the signal from the ECS and which from the axoplasm. All the components presented a drastic change in their signal intensity due to the presence of Mn^{2+}. In order to quantify the change in the T_2 times and component sizes after the addition of Mn^{2+}, we compared the values in the standard buffer solution with the values in a solution with manganese. The change (%) for the T_2 times and the component sizes are shown in Table 4.8.

Table 4.8- Change (%) comparing the T_2 times and component sizes of the optic nerve in a standard buffer solution and in a solution with Mn^{2+}. Change = (Data buffer – Data Mn^{2+}) / Data buffer x 100.					
Exp	Changes of T_2 Times			Changes of Component sizes		
	Short	Intermediate	Long	Short	Intermediate	Long
1	37.54	67.66	74.33	49.25	96.66	94.58
2	54.72	72.93	66.69	41.02	76.05	87.79
3	55.78	78.28	84.07	71.00	96.73	92.43
Mean	49.35	72.96	75.03	53.76	89.81	91.60
SD	± 10.23	± 5.30	± 8.71	± 15.49	± 11.91	± 3.47

The presence of Mn^{2+} decreased the relaxation times and magnitudes of all the components of the optic nerve. The intermediate- and the long-lived components are similarly affected by the paramagnetic agent in the T_2 times ($\approx$74%) and component sizes ($\approx$90%), thus it is difficult to extract information that may lead to the identification of the water compartment that is being affected first by the paramagnetic agent, which makes more challenging the establishment of the component-compartment relationship. In order

to determine the concentration, C (t), of paramagnetic agent based in changes of the relaxation times we modified Eqs. 2.1 and 2.2 to obtain

$$C(t) = \frac{\dfrac{1}{T_2(t)} - \dfrac{1}{T_2(0)}}{\alpha_2}$$

(4.1)

where $T_2(t)$ is the T_2 value of any components at time t after the paramagnetic agent has been added to the solution and $T_2(0)$ is the relaxation time of the component in the standard buffer solution. Figure 4.4 shows the concentration of Mn^{2+} for the intermediate and long-lived components.
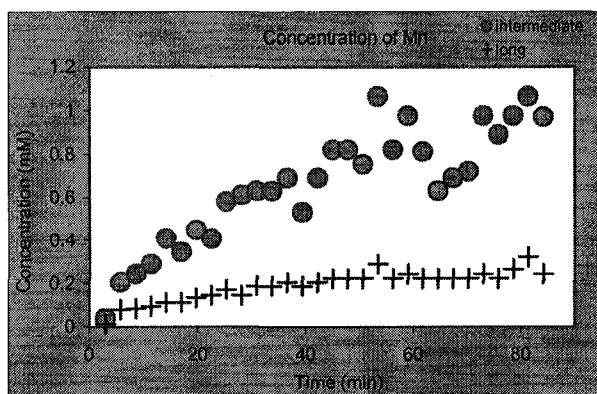
Fig. 4.4- Concentration of Mn^{2+} for the intermediate- and long-lived components. Note that there is a higher concentration for the intermediate- than the long-lived component. Even if the signal decrease to <10% after the addition of the paramagnetic agent, it is possible to observe changes in the concentration of the agent in the different components.

It is shown that the concentration of the intermediate lived-component is higher than the long-lived component during the time of the experiment represented in fig. 4.4. The results using Mn^{2+} to identify the components and compartments of the optic nerve were different than the ones obtained for frog peripheral nerves [13]. As a result of its rapid action, the use of Mn^{+2} as a paramagnetic agent did not reveal rather the intermediate- or the long-lived component was being affected first, thus not allowing a determination of which of the two components results from the axonal water; however, we could extract some information based in the concentration analysis. Other paramagnetic agents with similar characteristics as Mn^{2+} were used for this study.

4.2.2- Optic Nerve with Gd-DTPA

It is known that Gd-DTPA diffuses at a slower rate than Mn^{2+} [14, 15]. Therefore, as a result of the different diffusion characteristics it was expected to show slower changes in the spectrum due to Gd-DTPA than Mn^{2+}. Two optic nerves were used in experiments with 35-mM Gd-DTPA, one with a lower concentration (20-mMol), and four in experiments with 30-mM (which provided the most valuable information).

4.2.2.1- Optic Nerve Using 35-mM Gd-DTPA

After the addition of the paramagnetic agent and during the first 15 minutes the intermediate- and the long-lived components seemed to merge into one (fig. 4.5). The buffer solution decreased from ≈ 1.5 s to <3ms. After another 15 minutes all 3 components merged in one. The intermediate-lived seemed to be affected faster than the long-lived component.

The averaged T_2 time for the remaining component was ≈ 30 ms. The averaged magnitude of the remaining component was $\approx 10\%$ of the total signal from the nerve in a standard buffer solution (fig. 4.6). The results of these experiments were similar to the ones obtained using Mn^{2+} (sec. 4.2.1). It is believed that the concentration of 35-mM was too high, so that the paramagnetic agent diffused very rapidly into the nerve making the components merge into one.
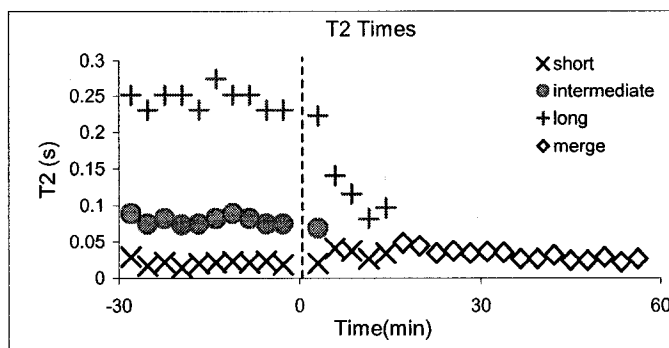
Fig. 4.5- Graph showing the T_2 times of the optic nerve in a standard buffer solution and after time 0, in a solution with 35-mM of Gd-DTPA.
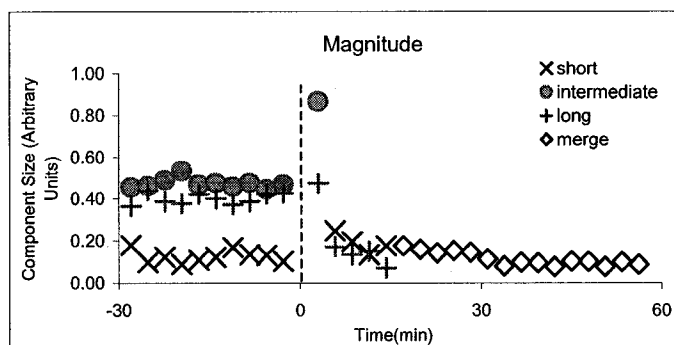
Fig. 4.6- Graph showing the component sizes of the optic nerve in a standard buffer solution and after time 0, in a solution with 35-mM of Gd-DTPA.

4.2.2.2- Optic Nerve Using 20-mM Gd-DTPA

The use of 20-mM of Gd-DTPA reduced the relaxation time of the buffer combined with the short-lived component to ≈ 8 ms. The T_2 component of the 20-mM Gd-DTPA buffer could not be resolved from the short-lived component. We were more interested in the assessment of changes in the intermediate- and long-lived components; therefore the interference of the 20-mM Gd-DTPA buffer with the short-lived component was acceptable. Figures 4.7 and 4.8 are graphs showing the T_2 times and magnitudes of the nerve components.
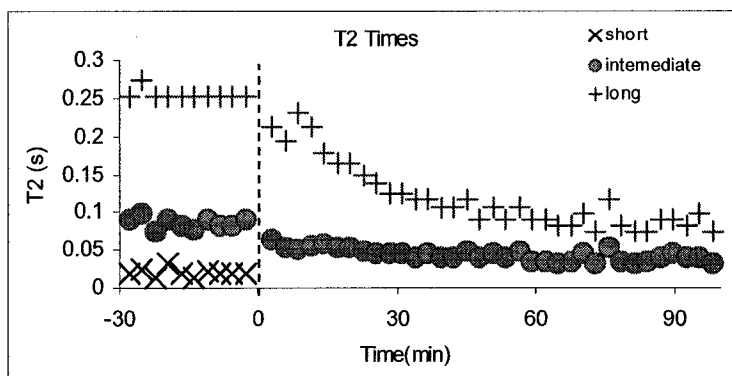
Fig.4.7- Graph of the T_2 times of the optic nerve. At time 0, the standard buffer solution was switched to one containing 20-mM of Gd-DTPA. At this time the buffer and the short-lived component merge in a T_2 time of $\approx$8ms (not shown).
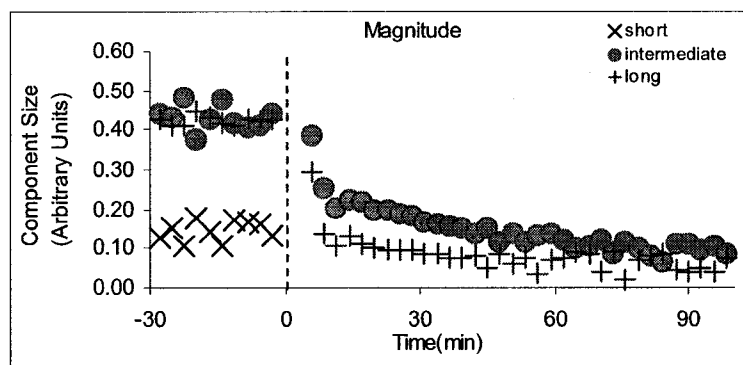
Fig.4.8- Graph of the magnitudes of the components of the optic nerve. At time 0, the standard buffer solution was switched to one containing 20-mM of Gd-DTPA. Note that the intermediate- and long-lived components decay at a similar rate.

Forty minutes after adding Gd-DTPA, when the decay was stable, the averaged T_2 time of the intermediate-lived decreased to $\approx$55% and the long-lived component to $\approx$66% of their original values. The short-lived component merged with the buffer. After the addition of Gd-DTPA the magnitude of the intermediate-lived component decreased to $\approx$76% of its original value, and the long-lived component to $\approx$85%. The change in the size of the short-lived component could not be determined as this component merged with the buffer. In these experiments the components of the spectrum remained for more than one hour after the addition of the paramagnetic agent. Using Gd-DTPA in optic nerve is very valuable because it diffuses at a slower rate than Mn^{2+}, thus more

information can be extracted. The long-lived component seems to be affected dramatically in the first 15 minutes of the experiment after the addition of Gd-DTPA, this characteristic was observed also in experiments with $FeCl_3$. These results are valuable in order to get a better understanding of the nervous tissue from a NMR perspective; in this experiment the long-lived component seemed to be slightly more affected by the paramagnetic agent than the intermediate.

4.2.2.3- Optic Nerve Using 30-mM Gd-DTPA

After using different concentrations of paramagnetic agents we decided that 30-mM of Gd-DTPA might be more appropriate to extract information from the components of the T_2 spectrum in order to establish a component-compartment relationship, as 35-mM seemed to be too high a concentration and 20-mM too low.

4.2.2.3.1- T_2 Times and Component Sizes

The relaxation times and the magnitudes of the nerve components prior to time zero were similar to previous experiments. The relaxation times and component sizes of a typical optic nerve in a standard buffer solution and in a solution with 30-mM of Gd-DTPA are shown in figs. 4.9 and 4.10, respectively.

Table 4.9 shows the T_2 times of the components in a standard buffer solution and in a solution with 30-mM of Gd-DTPA (30 min following the addition Gd-DTPA when the relaxation decay had become stable).
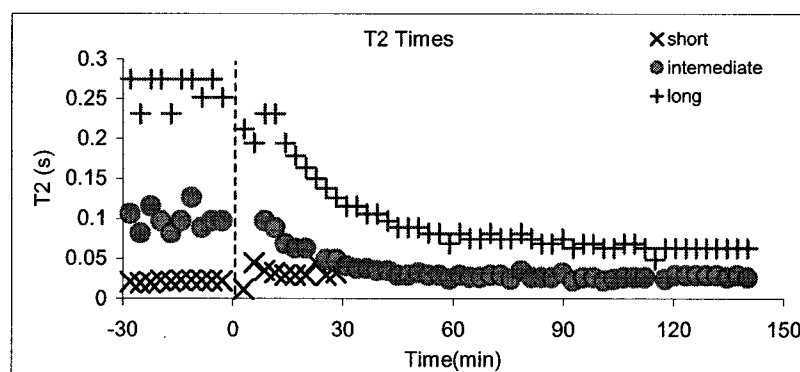
Fig. 4.9- Graph of the different T_2 times of the optic nerve in standard buffer solution. At time 0 the solution was switched to one containing 30-mM of Gd-DTPA. The T_2 time of the buffer decreased from ≈ 1.5 s to < 3ms. Note the intermediate- and long-lived components merge at ≈ 30 min.
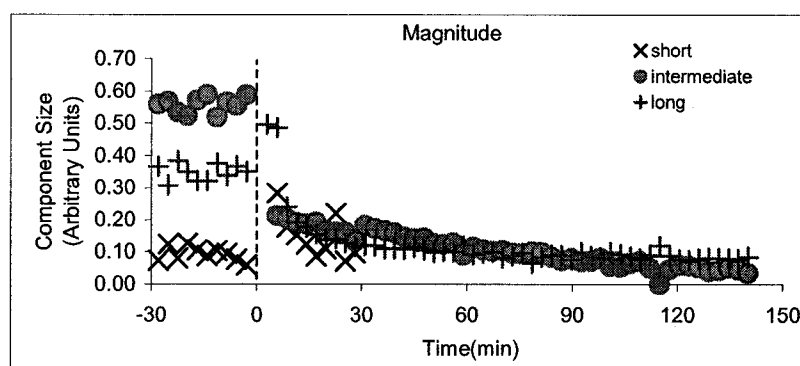
Fig. 4.10- Magnitudes of the different components of the optic nerve in standard buffer solution and after the addition of 30-mM of Gd-DTPA at time 0. Note that the intermediate-lived component is smaller than the long-lived at ≈ 90 min.

Table 4.9- Mean and SD of the T_2 times of the optic nerve in a standard buffer solution and in a solution with 30-mM Gd-DTPA (> 30 min) for 4 experiments. Note that only the T_2 times of the short/intermediate and long-lived component are shown (Gd-DTPA).

Exp	T_2 times in standard buffer solution			T_2 times in Gd-DTPA	
	Short	Intermediate	Long	Short/Intermediate	Long
1	22 ± 1	99 ± 14	261 ± 18	27 ± 3	68 ± 7
2	38 ± 6	95 ± 13	268 ± 16	37 ± 5	75 ± 12
3	38 ± 7	96 ± 6	270 ± 10	35 ± 3	89 ± 5
4	31 ± 6	88 ± 10	239 ± 11	36 ± 4	54 ± 7
Mean ± SD	± 32 ±8	94 ±5	259 ±14	34 ±5	71 ±14

All the T_2 times decreased after the addition of the paramagnetic agent. The T_2 time of the short-lived component is not shown in the table because it seemed to merge with the intermediate-lived component approximately 30 min after the addition of Gd-DTPA. Table 4.10 is similar to 4.9 but shows the component sizes.

Table 4.10- Mean and SD of the component sizes of the optic nerve in a standard buffer solution and in a solution with 30-mM Gd-DTPA (> 30 min) for 4 experiments. Note that only the component sizes of the short/intermediate and long-lived component are shown (Gd-DTPA).

Exp	Component size in standard buffer solution (%)						Component sizes in Gd-DTPA (%)			
	Short		Intermediate		Long		Short/Intermediate		Long	
*1	9.37	± 2.18	55.74	± 2.50	34.89	± 2.56	6.93	± 2.68	8.72	± 1.01
2	12.55	± 2.05	41.68	± 1.62	45.77	± 1.55	10.47	± 3.23	5.61	± 2.43
3	10.50	± 2.91	53.87	± 1.67	35.64	± 2.09	10.39	± 0.99	7.93	± 1.05
*4	10.22	± 1.18	49.36	± 2.06	40.42	± 1.63	5.94	± 2.26	9.17	± 2.62
Mean SD	10.66	±1.35	50.16	±6.26	39.18	±5.03	8.43	±2.34	7.86	±1.58

Note that in two experiments (*) the magnitude of the intermediate component is smaller than the long-lived component after the addition of Gd-DTPA.

Following the time the paramagnetic agent was added, the intermediate- and long-lived components decayed very rapidly during the first 25 minutes. Then, after 30 min the short-lived and intermediate-lived components merged into one. In two experiments the decay of the intermediate-lived component was greater than the long-lived (1 & 4). This was a good indication that the intermediate-lived component was being affected to a greater degree by the paramagnetic agent than the long-lived component. In order to clearly see the effect of the paramagnetic agent on the components, we compared their T_2 times and magnitudes in a standard buffer solution and in a solution with Gd-DTPA, and calculated the change (Table 4.11). Information of the short-lived component is not shown because it merged with the intermediate, thus it is not possible to compare.

Table 4.11- Changes (%) comparing the T_2 times and magnitudes of the components in a standard buffer solution and in a solution with 30-mM Gd-DTPA. Change = (data buffer – data Gd-DTPA) / data buffer x 100.

Exp	T_2 Times		Magnitudes	
	Intermediate	Long	Intermediate	Long
1	72.43	73.87	87.56	75.00
2	60.45	71.91	74.88	87.73
3	63.36	67.03	80.71	77.75
4	58.71	77.52	87.97	77.32
Mean	63.74	72.58	82.78	79.45
SD (σ)	± 6.11	±4.37	6.23	± 5.65

The decrease in the T_2 times of the long-lived component (≈73%) is greater than the intermediate-lived component (≈63%), however, the averaged magnitude of the component sizes for the intermediate-lived component was affected in a greater scale (≈83%) than the long-lived component (≈79%).

In order to analyze the concentration of Gd-DTPA in the nerve to relate information of the components to water compartments we followed the same procedure as in section 4.2.1. Figure 4.11 shows the concentration of the paramagnetic agent in the intermediate- and long-lived components of a typical optic nerve in a solution with Gd-DTPA.
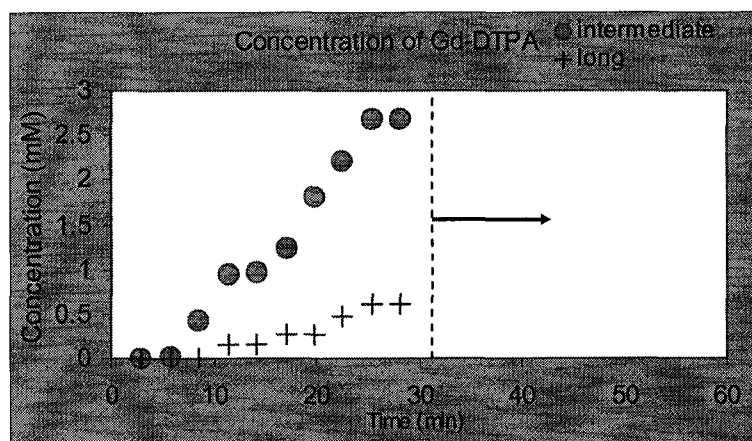
Fig 4.11- Concentration of Gd-DTPA of the intermediate- and long-lived components. The graph is truncated at ≈ 30 min because the short and intermediate components seem to merge making difficult to determine which region has a higher concentration of Gd-DTPA.

It is shown that the concentration of Gd-DTPA is higher in the intermediate-lived than in the long-lived component during the first 30 min.

4.2.3- Optic Nerves with Iron Chloride + Mn^{2+} or Gd-DTPA

It was noticed that high concentrations of Mn^{2+} and Gd-DTPA diffused very rapidly into the nerve. Thus we decided to use $FeCl_3$ and Mn^{2+} or $FeCl_3$ and Gd-DTPA because in this case a lower concentration of Mn^{2+} or Gd-DTPA was needed to reduce the relaxation time of the buffer to <3ms. Two optic nerves were analyzed, the solutions used for these experiments being 15-mM of $FeCl_3$ and 10-mM of Gd-DTPA or 15-mM of $FeCl_3$ and 8-mM of Mn^{2+}. Experiments were run with standard buffer solution, then with $FeCl_3$ and finally with $FeCl_3$ and Mn^{2+} or Gd-DTPA. The T_2 times and component sizes were similar to previous experiments using $FeCl_3$ (section 3.3.2). We had extensively analyzed

the optic nerve with $FeCl_3$, now after the addition of Gd-DTPA or Mn^{2+} it was observed that Gd-DTPA and Mn^{2+} reacted with $FeCl_3$ and precipitated. This may have an implication in the relaxation time of the solution and also the way it diffuses into the nerve. For these experiments it was not clear which component was affected first by the paramagnetic agent, therefore it was difficult to derive conclusions except that mixing Mn^{2+} or Gd-DTPA with iron chloride it is not recommended.

4.3- Cell Swelling

4.3.1- Rat Optic Nerve with Glutamate

In frog sciatic nerves the relationship between the components of the T_2 spectrum and the compartments of the nerve has been established. The short-, intermediate and long-lived components are related to myelinic, interaxonal and axonal water respectively. In optic nerve this relationship has not been established, and with this study we intended to prove from which compartments of the optic nerve signal is arising. We used six optic nerves for these experiments. Ten-mM of glutamate was added to the buffer solution that bathed the optic nerve. Axonal swelling as a result of the interaction of the glutamate with the optic nerve leads to an extracellular space volume decrease. It has been suggested that the accumulation of potassium ions during neuronal activity and neuronal depolarization in response to the application of glutamate is accompanied by axonal swelling, which may be caused by a Na and water influx into the axons [16-18].

4.3.1.1- T_2 Times and Component Sizes

Figures 4.12 and 4.13 show the relaxation times and component sizes of a typical optic nerve before and after the addition of glutamate.
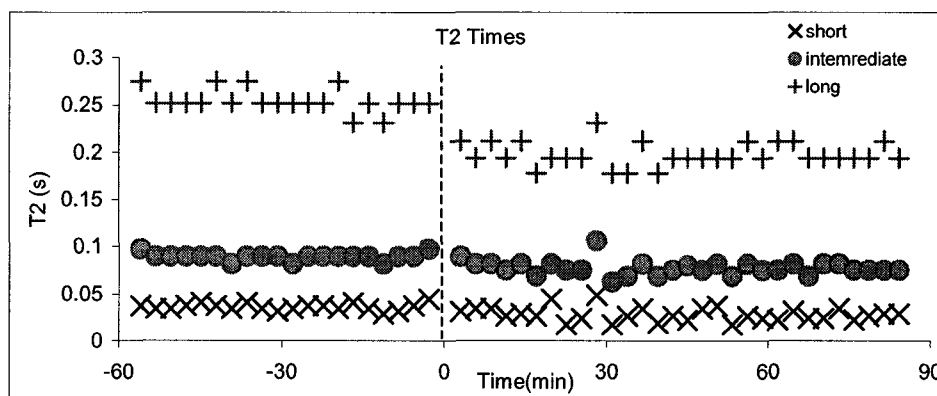
Fig. 4.12-Graph showing the different T_2 times of the optic nerve in a standard buffer solution. At time 0, 10-mM of glutamate was added to the solution.
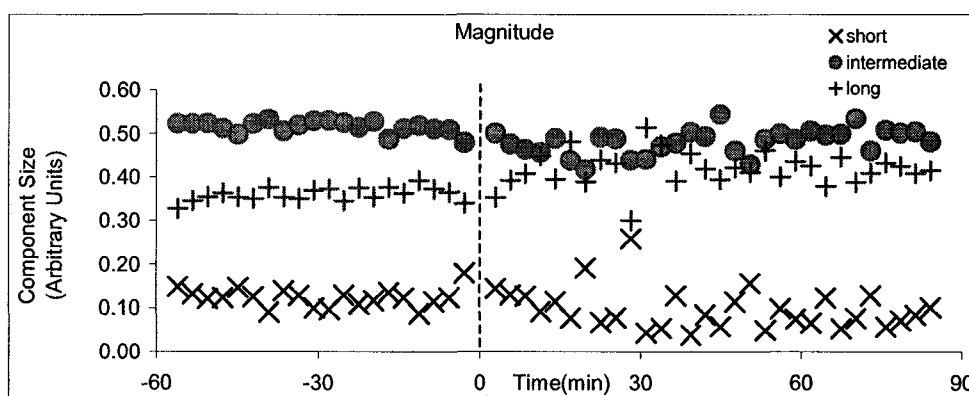
Fig. 4.13- Graph showing the magnitude of the optic nerve components in a standard buffer solution. At time zero, 10-mM of glutamate were added to the solution.

Table 4.12 shows the mean and standard deviation of the different T_2 times of the optic nerve in a standard buffer solution and in one containing glutamate (30 min after addition). Table 4.13 is similar to 4.12 but showing the magnitudes of the components. A two-tailed t-test was performed in order to compare the results in a standard buffer solution and in a solution with glutamate [19]. The p-values to establish a significant difference between solutions are shown as well in the tables. Ten spectrums (each one composed of 8 averages) of the optic nerve in a standard buffer solution were compared with 10 spectrums in glutamate after 30 minutes of the salt being added to the solution.

Table 4.12- Mean and SD of the T_2 times for 6 experiments of optic nerve in a standard buffer solution (B) and in glutamate (G). The two-tailed p-values comparing each component in these two solutions are shown as well.

Exp	Sln	Short		p-value	Intermediate		p-value	Long		p-value
1	B	38	±4	0.12	95	±5	<0.001	263	±16	<0.001
	G	34	±4		82	±6		225	±15	
2	B	38	±2	0.001	100	±6	<0.001	282	±11	<0.001
	G	27	±7		84	±11		238	±17	
3	B	36	±3	<0.001	89	±3	<0.001	259	±11	<0.001
	G	27	±4		76	±4		200	±8	
4	B	28	±4	0.14	91	±5	<0.001	257	±10	<0.001
	G	25	±3		78	±4		226	±10	
5	B	31	±7	0.028	91	±7	<0.001	245	±10	<0.001
	G	25	±4		78	±5		210	±10	
6	B	39	±3	0.37	95	±4	<0.001	238	±11	<0.001
	G	37	±3		86	±4		205	±4	

Table 4.13- Mean and SD of the component sizes (%) for 6 experiments of optic nerve in a standard buffer (B) and glutamate (G) solution. The two-tailed p-values comparing each component in these two solutions are shown as well.

Exp	Sln	Short		p-value	Intermediate		p-value	Long		p-value
1	B	11.00	± 2.30	0.24	50.26	± 1.00	0.006	38.74	± 2.10	0.007
	G	9.84	± 2.10		47.90	± 1.90		42.26	± 2.50	
2	B	17.82	± 2.50	<0.001	46.15	± 0.94	0.40	36.10	± 2.00	<0.001
	G	10.95	± 3.50		45.79	± 1.42		42.14	± 2.10	
3	B	12.57	± 1.80	0.002	51.95	± 1.00	0.034	35.48	± 1.30	<0.001
	G	8.39	± 2.60		49.88	± 1.90		41.73	± 2.10	
4	B	13.15	± 2.30	0.061	51.94	± 1.00	0.012	34.91	± 1.60	0.003
	G	11.03	± 2.00		50.61	± 0.80		38.36	± 1.90	
5	B	13.83	± 4.20	0.028	45.21	± 2.90	0.23	40.96	± 2.40	<0.001
	G	9.39	± 2.60		43.80	± 1.00		46.81	± 2.70	
6	B	15.58	± 2.10	0.51	47.07	± 1.30	0.074	37.35	± 1.50	0.02
	G	14.78	± 2.10		45.87	± 1.00		39.34	± 1.50	

As is shown in Table 4.12, the majority of the components present a statistical difference in the T_2 times with p-values < 0.01. After the addition of glutamate all the components present shorter T_2 times. The relaxation time of the buffer decreased as well from ≈ 1.5 s to ≈ 1.09 s. The decrease in the relaxation times might be caused by the addition of salts (glutamate), which may slow down the movement of the water molecules resulting in a more efficient relaxation process. From information in Table 4.13 we can determine that in the 6 experiments the short-lived component decreased in size, as well as the intermediate-lived. The long-lived component presents an opposite reaction, increasing in magnitude after the standard buffer solution was switched to one containing glutamate. Once we had collected data from 6 experiments using glutamate,

we decided to compare the controls for these experiments (data of the components in a standard buffer solution) with the controls of other experiments shown in section 3.1. Table 4.14 shows the results of the comparison of the T_2 times and Table 4.15 shows the comparison of the component sizes. Also the two-tailed p-values are shown, indicating a statistical comparison with a t-test of independent samples.

Table 4.14- Comparison between the T_2 times of the 3 components in the optic nerve of 6 controls (standard buffer) for experiments with glutamate (C-6) and 20 controls for different experiments in a standard buffer solution (C-20).							
	Short		p-value	Intermediate		p-value	Long		p-value
C-6	35	±6	0.006	93	±6	0.38	257	±18	0.16
C-20	26	±7		91	±6		248	±15	

Table 4.15- Comparison between the component sizes of the 3 components in the optic nerve of 6 controls (standard buffer) for experiments with glutamate (C-6) and other 20 controls for different experiments in a standard buffer solution (C-20).							
	Short		p-value	Intermediate		p-value	Long		p-value
C-6	14.00	±3.41	0.01	48.76	±3.13	0.55	37.25	±2.76	0.09
C-20	10.94	±2.43		49.59	±3.29		39.45	±2.85	

These results (Table 4.14 & 4.15) show the majority of the components and the buffer (data not shown) present no statistical difference. We can conclude that the results for the controls of experiments with glutamate are similar to those of the optic nerve in a standard buffer solution (sec. 3.1). From the information in Table 4.12 and 4.13 we compared the results from the 6 experiments of the optic nerve in a standard buffer solution and glutamate. We are interested in determining which components changed after the addition of glutamate. Data from 10 spectrums for each of the 6 experiments in a standard buffer solution and in glutamate were used to compare the T_2 times and component sizes. Table 4.16 shows the mean and standard deviation of the T_2 times for the 6 different experiments. Table 4.17 is similar to 4.18 but showing the component sizes. The two-tailed p-values obtained with a t-test are also show in these tables.

Table 4.16- Comparison between the mean of the T_2 times of the optic nerve in a standard buffer solution (B) and glutamate (G) for all the 60 (10 per experiment) data points.							
Exp	Short		p-value	Intermediate		p-value	Long		p-value
B	35	± 6	< 0.001	93	± 6	<0.001	257	± 18	< 0.001
G	29	± 6		81	± 7		217	± 17	

Exp	Short		p-value	Intermediate		p-value	Long		p-value
B	14.00	± 3.41	<0.001	48.76	± 3.13	0.008	37.25	± 2.76	< 0.001
G	10.73	± 3.20		47.31	± 2.78		41.77	± 3.44	

Table 4.17- Comparison between the mean of the component sizes (%) of the optic nerve in a standard buffer solution (B) and glutamate (G) for all the 60 (10 per experiment) data points.

From Table 4.16 we can determine that all the relaxation times decrease and present statistical differences. The T_2 time of the short-lived component, comparing all the 6 experiments, decreased by ≈17%, the intermediate-lived by ≈13% and the long-lived component by ≈ 15%. All the components are affected by the addition of glutamate.

In these experiments we focused on the magnitude of the signal for each component. It is important to remember that the NMR signal is obtained from water in the different compartments; therefore, the more water present in the compartment, the more signal is detected from that component. As a result of the action of glutamate in the nerves we expected to see an increase in the signal from the axoplasm and a decrease in the signal from the ECS. Based on results for the optic nerve, shown in Table 4.17, the magnitudes of the short and long-lived component decreased after the addition of glutamate showing significant differences. On the other hand, the long-lived component increased in magnitude, showing a significant difference as well. To have another way of comparing the results we analyzed ratios between the different components of an optic nerve in a standard buffer solution and in a solution with glutamate (Table 4.18).

Table 4.18- Ratios of the T_2 times and magnitudes comparing the components in a standard buffer solution and in glutamate. Ratio = (glutamate/buffer).

	T_2 Times			Magnitudes		
	Short	Intermediate	Long	Short	Intermediate	Long
Mean (n=6)	0.83	0.86	0.84	0.77	0.97	1.12
SD (σ)	± 0.10	± 0.02	± 0.04	± 0.13	± 0.01	± 0.04

The ratios (<1) for the T_2 times reaffirm the results shown before where the T_2 times of the components were shorter in glutamate than in a standard buffer solution. The ratios of the short-lived and intermediate-lived components (<1) indicate that the components decrease in size and the ratios (>1) indicate that the long-lived component increased in size from a standard buffer solution to a solution containing glutamate. These results are consistent with the previous analysis.

4.3.2- Rat Sciatic Nerve with Glutamate

The decrease in the relaxation times of the components of the optic nerve in a glutamate solution may have an effect on the component sizes when analyzing the data with the NNLS routine. Therefore, we decided to analyze rat sciatic nerve as well. The optic nerve has glutamate receptors and transporters in the axons and glia, these cells may become swollen after exposure to large amounts of glutamate; on the other hand, in peripheral nerves even if axons may communicate with Schwann cells via release of glutamate these nerves are not constituted by astrocytes or oligodendrocytes therefore, the effect of glutamate was expected to be less evident. It was interesting to observe how sciatic nerves reacted when they were exposed to 10-mM of glutamate. Three rat sciatic nerves were used for these experiments.

4.3.2.1- T_2 Times and Component Sizes

The samples were perfused with a standard buffer solution, and then the solution was switched on-the-fly to one containing 10-mM of glutamate. Figures 4.14 and 4.15 show the relaxation times and the magnitudes of the sciatic nerve components before and after the addition of glutamate.
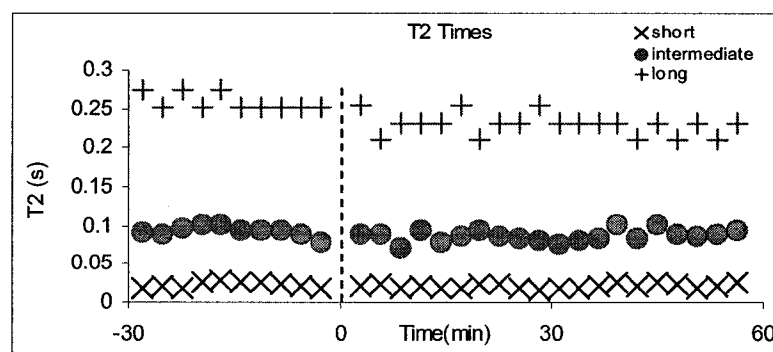
Fig. 4.14-Graph showing the T_2 times of the sciatic nerve components in a standard buffer solution. At time zero, 10-mM of glutamate was added to the solution.
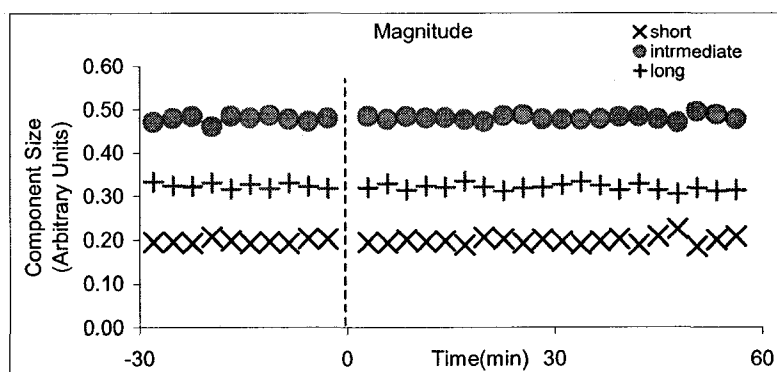
Fig. 4.15- Graph showing the magnitude of the sciatic nerve components in a standard buffer solution. At time zero, 10-mM of glutamate was added to the solution.

Table 4.19 shows the relaxation times of the components and Table 4.20 shows the component sizes for the different experiments. We followed the same method as for the optic nerve in the comparison of 10 spectrums (each one composed of 8 averages) in a standard buffer solution with 10 spectrums from the nerve in a glutamate solution after 30 min of the addition of the salt. A two-tailed t-test was used to identify changes in the components after the solution was changed.

Table 4.19- Mean and SD for the T_2 times of rat sciatic nerve in a standard buffer solution (B) and in glutamate (G). Also are shown the p-values of a comparison of the different components with a two-tailed t-test.

Exp	Short		Intermediate		Long	
B	19	± 3	92	± 7	282	± 16
G	17	± 2	88	± 4	268	± 11
p-value	0.069		0.10		0.076	
B	18	± 1	100	± 5	279	± 10
G	16	± 1	102	± 3	277	± 13
p-value	0.06		0.24		0.61	
B	22	± 4	93	± 7	259	± 11
G	21	± 3	90	± 8	245	± 10
p-value	0.50		0.21		0.076	

Table 4.20- Mean and SD for the magnitudes of rat sciatic nerve in a standard buffer solution (B) and in glutamate (G). Also are shown the p-values of a comparison of the different components with a two-tailed t-test.			
	Short	Intermediate	Long
B	15.22 ± 1.48	55.66 ± 2.07	29.12 ± 1.14
G	12.59 ± 3.62	58.01 ± 3.99	29.40 ± 0.78
p-value	0.04	0.12	0.49
B	17.92 ± 3.35	52.92 ± 2.73	29.16 ± 0.94
G	13.28 ± 1.85	56.31 ± 1.52	30.41 ± 1.40
p-value	0.01	0.01	0.08
B	19.74 ± 0.54	47.78 ± 0.76	32.48 ± 0.60
G	20.00 ± 1.16	48.07 ± 0.72	31.93 ± 0.86
p-value	0.51	0.47	0.11

From Table 4.19 we can see that all the T_2 times decreased, showing similar characteristics than the optic nerve, however, these changes were not as large and do not show statistical differences. The glutamate seemed to have less of an effect on the T_2 times of the sciatic nerves than on the optic nerve. The T_2 time of the buffer decreased from ≈1.5 s to ≈1.09 s, similar to experiments of optic nerve. A reason for the difference in the T_2 times between the optic nerve and sciatic nerve may be because different membranes engulf them, perineurial sheath in sciatic and dura in optic nerves, which may present a different permeability to glutamate. From Table 4.20 it can be seen that the component sizes of sciatic nerves did not show significant differences in a standard buffer solution and in a solution with glutamate. These results differ from the ones obtained for optic nerve. We also compared all results from the 3 experiments. For this comparison we analyzed 30 spectrums (10 per experiment) in a standard buffer solution and 30 in a solution with glutamate. Table 4.21 shows the mean and standard deviation of the T_2 times and Table 4.22 shows the magnitudes. A t-test of independent samples was used for comparison. Two-tailed p-values are presented in the tables as well.

Table 4.21- Mean and SD for the T_2 times for the 3 experiments of rat sciatic nerve in a standard buffer solution (B) and in glutamate (G). Also are shown the p-values of a comparison of the different components with a t-test of independent samples.				
Exp	Sln	Short	Intermediate	Long
1-3	B	20 ± 3	95 ± 7	273 ± 16
1-3	G	18 ± 3	93 ± 9	263 ± 17
	p-value	0.073	0.30	0.027

Exp	Sln	Short		Intermediate		Long	
1-3	B	17.62	± 2.79	52.12	± 3.85	30.25	± 1.83
1-3	G	15.28	± 4.13	54.12	± 5.03	30.58	± 1.46
	p-value	0.012		0.088		0.44	

Table 4.22- Mean and SD for the magnitudes for the 3 experiments of rat sciatic nerve in a standard buffer solution (B) and in glutamate (G). Also are shown the p-values of a comparison of the different components with a t-test of independent samples.

After the addition of glutamate all T_2 times of the sciatic nerve decreased as in the optic nerve, however, the long-lived component is the only one that presents statistical difference. Another way to analyze changes in the components is with ratios. In this case we calculated the ratios of the components in a standard buffer solution and in a solution with glutamate. Table 4.23 shows the ratios of the relaxation times and component sizes. Also are shown the mean values and the standard deviation for the 3 experiments.

Table 4.23- Ratios of the T_2 times and the component sizes in a standard buffer solution and in glutamate. Also are shown the mean values and SD of the 3 experiments. Ratio = glutamate / buffer.

	T_2 Times			Magnitude		
Exp	Short	Intermediate	Long	Short	Intermediate	Long
1	0.90	0.95	0.95	0.83	1.05	1.01
2	0.92	1.03	1.00	0.74	1.08	1.05
3	0.96	0.96	0.95	1.02	1.01	0.99
Mean	0.93	0.98	0.97	0.86	1.05	1.02
SD (σ)	± 0.03	± 0.04	± 0.03	± 0.14	± 0.03	± 0.03

The ratios for the intermediate-lived and long-lived components are very close to one. A ratio of one indicates no change in the component sizes before and after the addition of glutamate. Thus, as it was stated before, even analyzing the raw data of the magnitudes, it was shown that the intermediate- and long-lived components do not change after the addition of glutamate.

4.4- Conclusion

After analyzing the effect of $MnCl_2$ and Gd-DTPA in the optic nerve it was difficult to establish the component-compartment relationship; however we obtained valuable information that together with experiments using glutamate allow the determination of this relationship. After analyzing the effect of glutamate in the optic nerve where axons and glial cells swell, and the ECS decreases in volume, it is believed that the decrease in the magnitude of the intermediate-lived component and increment in the long-lived component showed evidence to assign the signal from the intermediate-lived component to be originated by water in the extracellular space and signal in the long lived-component to be signal coming from the axoplasm. In the optic nerve, the relaxation time of the long-lived component was affected by the addition of glutamate; this may have an implication on the magnitude of this component, however, in the sciatic nerve the relaxation time of this component was affected as well but in lesser degree, showing no change in the magnitude for this component in sciatic nerve. This characteristic may suggest that changes in the magnitudes of the optic nerve can be attributed to water movement in the micro-anatomical compartments instead of as a consequence of a more efficient relaxation process after the addition of glutamate. Based on the results of these experiments described in this chapter, it is believed that signal of the intermediate-lived component in the T_2 spectrum of the optic nerve is originated from water in the ECS and signal of the long-lived component is from water in the axoplasm.

4.5- Bibliography

1. Bronskill, M.J. and P. Sprawls, *The Physics of MRI. 1992 AAPM Summer School Proceedings.* 1992.

2. Beaulieu, C., et al., *Changes in water diffusion due to Wallerian degeneration in peripheral nerve.* Magnetic Resonance in Medicine, 1996. **36**(4): p. 627-31.

3. Does, M.D. and R.E. Snyder, *Multiexponential T_2 relaxation in degenerating peripheral nerve.* Magnetic Resonance in Medicine, 1996. **35**(2): p. 207-13.

4. Stewart, W.A., et al., *Spin-spin relaxation in experimental allergic encephalomyelitis. Analysis of CPMG data using a non-linear least squares method and linear inverse theory.* Magnetic Resonance in Medicine, 1993. **29**(6): p. 767-75.

5. Menon, R.S., M.S. Rusinko, and P.S. Allen, *Proton relaxation studies of water compartmentalization in a model neurological system.* Magnetic Resonance in Medicine, 1992. **28**(2): p. 264-74.

6. Elster, A.D., *Questions and Answers in Magnetic Resonance Imaging.* 1994.

7. Does, M.D. and R.E. Snyder, *T_2 relaxation of peripheral nerve measured in vivo.* Magnetic Resonance Imaging, 1995. **13**(4): p. 575-80.

8. Matheson, D.F., *Some quantitative aspects of myelination of the optic nerve in rat.* Brain Research, 1970. **24**(2): p. 257-69.

9. Stys, P.K. and R.M. Lopachin, Jr., *Elemental composition and water content of rat optic nerve myelinated axons during in vitro post-anoxia reoxygenation.* Neuroscience, 1996. **73**(4): p. 1081-90.

10. Fenrich, F., *A simulation and experimental study of water proton relaxation in a white matter model.* Master of Science, Thesis. 1992: University of Alberta.

11. Knaap, M.S.V.d. and J. Valk, *Magnetic Resonance of Myelin, Myelination and Myelin Disorders.* 1995.

12. Fenrich, F., *NMR Transverse Relaxation of Water.* 2000: University of Alberta Thesis.

13. Wachowicz, K. and R.E. Snyder, *Assignment of the T_2 components of amphibian peripheral nerve to their microanatomical compartments.* Magnetic Resonance in Medicine, 2002. **47**(2): p. 239-45.

14. Foy, B.D. and J. Blake, *Diffusion of paramagnetically labeled proteins in cartilage: enhancement of the 1-D NMR imaging technique.* Journal of Magnetic Resonance, 2001. **148**(1): p. 126-34.

15. Guiheneuf, T., et al., *Measurement of the diffusion coeficient of manganese ions in cured pork by one-dimensional H magnetic Resonance Imaging.* Intern J Food Technol, 1996. **31**: p. 195-203.

16. Vargova, L., et al., *Glutamate, NMDA, and AMPA induced changes in extracellular space volume and tortuosity in the rat spinal cord.* Journal of Cerebral Blood Flow & Metabolism, 2001. **21**(9): p. 1077-89.

17. Anderson, A.W., et al., *Effects of osmotically driven cell volume changes on diffusion-weighted imaging of the rat optic nerve.* Magnetic Resonance in Medicine, 1996. **35**(2): p. 162-7.

18. Rothman, S.M., *Glutamate and anoxic neuronal death in vitro*. Advances in Experimental Medicine & Biology, 1986. **203**: p. 687-95.

19. Dawson-Saunders, B. and R.G. Trapp, *Basic & Clinical Biostatistics*, ed. 2. 1994: Lange Medical Book.

Chapter 5

Water Compartments and T_2 Components of the Optic Nerve

The main goal of this chapter is to discuss the results obtained in this study where the real number of components in the T_2 spectrum (chapter 3) and the relationship between the components and the water compartments of the optic nerve were established (chapter 4). With this discussion we intend to propose a model that relates three T_2 spectral components with the water compartments. In order to assess sensitivity and specificity in the appropriate diagnosis of pathologies using NMR techniques, it is important to obtain detailed information about the micro-anatomical regions of nervous tissue and establish a relationship with their NMR parameters [1].

5.1- Three Components Characterize the T_2 Spectrum of the Optic Nerve

As the decay time of the standard buffer solution is longer than that of the nerve components, it is possible that the buffer could alter the T_2-spectral components attributed to the nerve. To prove that the long-lived component in the rat optic nerve was real and not caused by any artifacts from the buffer we used $FeCl_3$ and fluorinert. In our experiments three components were identified in the T_2 spectrum of the rat optic nerve; these components are believed to come from three different water compartments, the myelin, the extracellular space and the axoplasm. These compartments can be distinguished individually in NMR experiments because water diffuses slowly (compared with the T_2 times) from different regions due to myelin acting as a diffusion barrier [2].

5.1.1- Myelin Acting as a Diffusion Barrier Between Compartments

Evidence shows that myelin engulfing the axons acts as a diffusion barrier between the axoplasm and the extracellular space. This is shown in Wallerian degeneration where myelin is broken down by macrophages and Schwann cells and the distinction between the intra- and extra-cellular signal disappears [3]. The limited permeability of myelin

decreases the diffusion rate of water from the intra-axonal to the extra-axonal space; therefore it is possible to see these two components separated in a time scale of a NMR experiment as two different components in the T_2 spectrum. There is enough evidence showing that myelin is the main diffusion barrier between different compartments in the nerve [4].

5.1.2- Characteristics of the Components Using $FeCl_3$ and Fluorinert

Table 5.1 summarizes information from different experiments showing the optic nerve to be characterized by three T_2-spectral components. From this table it is shown that the T_2 times and component sizes in $FeCl_3$ are different compared with the results in a standard buffer and fluorinert. This is a clear indication that the paramagnetic agent is having an effect on the different components of the optic nerve.

Table 5.1- Mean and SD for the T_2 times and component sizes of the optic nerve in a standard buffer (n=20) solution, $FeCl_3$ (n=5) and fluorinert (n=3).

	T_2 Times (ms)			Component sizes (%)		
	Short	Intermediate	Long	Short	Intermediate	Long
Buffer	26.6 ± 6.9	91.5 ± 5.8	247.9 ± 14.8	10.94 ± 2.43	49.59 ± 3.29	39.45±2.85
Fluorinert	22.9±3.75	77.9±5.92	234.6±5.81	9.64±1.75	54.31±0.75	36.03±1.70
$FeCl_3$	32.5 ± 5.84	80.88 ± 7.83	198.94±11.87	16.61 ± 2.92	41.48 ± 4.67	21.30±6.16

Note: The magnitude of the components in buffer and fluorinert is normalized to the total signal in the nerve (100%). The magnitude of the components in $FeCl_3$ is normalized to the total signal in their controls ($\neq$ 100%).

Three relaxation nerve components were found for the optic nerve in a standard buffer solution for experiments *in vitro* [5, 6]. When the buffer solution was switched to one containing iron chloride or the nerve was bathed in a fluorinert solution we found that:

- Three components are shown in the T_2 spectrum of the optic nerve. This suggests that the long-lived component in the spectrum of the optic nerve is real.

- The reduction in the relative size of the long-lived component after adding $FeCl_3$ suggests this component is real but:

i) It may be composed in part by a signal related to an interaction of the buffer solution with the surface of the nerve.

ii) Because $FeCl_3$ penetrates into the perineurium [7] (which may behave similar to dura) in a few minutes, the decrease in the relaxation time and size of this component may be an indication of this effect.

iii) The rationale in assumptions i) and ii) is based in the decrease of the long-lived component in ≈ 3 min (time it takes for the buffer to wash out from the chamber demonstrated with D_2O) showing the effect the buffer may have in the long lived component in i) or the effect of the paramagnetic agent in ii) due to the proximity of dura with the outer environment.

iii) The slow changes in the other components suggest that iron chloride diffuses slowly into the different regions of the nerve, its rate of entrance being retarded by the dura.

- The T_2 spectrum of the optic nerve bathed in fluorinert gives rise to three components (similar results to that using iron chloride), assuring that the T_2 spectrum of the optic nerve is characterized by three real components.

- The results using fluorinert were very similar to those obtained with a standard buffer solution, adding confidence that using a buffer solution does not add substantial artifacts to the relaxation times and component sizes of the optic nerve, except for the long-lived component that showed a decrease in size as in experiments with iron chloride.

- The difference in the number of components between experiments *in vitro* (optic nerve) and *in vivo* (white matter) may be due to differences of the tissue or the SNR. The SNR for experiments *in vivo* is ≈ 100, while for experiments *in vitro* is >1000; a greater SNR gives a better resolution of the peaks in the T_2 spectrum [8].

- In experiments of bovine optic nerve where only two components where identified [9], the analysis routine used to obtain the data was defined to fit two components; therefore, even if the raw data may have information about three components, only two would be identified.

5.2- The Component-Compartment Relationship

Once it was determined that the T_2 spectrum of the rat optic nerve is characterized by three components, the next step was to determine from which micro-anatomical regions signal was arising.

5.2.1- Myelin and its Relationship with the Short-lived Component

In peripheral and optic nerve the signal from the short-lived component has been strongly associated with myelin. This signal has a T_2 time of ≈ 10-50 ms, and its relative magnitude is $\approx 15\%$; this value is very similar to the relative amount of water within myelin in nervous tissue [10]. The following statements support that the short-lived component is signal coming from water in the myelin:

i) In experiments performed in the non-myelinated olfactory nerve of the garfish, the short T_2 component (10-50 ms) was not present in the T_2 spectrum [2].

ii) In experiments where Wallerian degeneration was induced in frog sciatic nerve, it was shown that myelin can be related to the short-lived component because the magnitude of this components decreased while the injury was progressing [3].

iii) The amplitude of the short-lived component in experiments were multiple sclerosis (MS) was induced in Hartley guinea pigs decreased; this decrease was also shown in pathologic samples with extent demyelination demonstrated by histology [11].

iv) The presence of lipids, proteins and macromolecules in myelin slows down the motion of water molecules; this characteristic causes the relaxation process to be more efficient, agreeing with the fact that the short-lived component originates from water in the myelin because it has the shortest relaxation time among the different T_2 time components of the nervous tissue [11, 12].

v) The short-lived component was not seen in experiments of gray matter *in vivo* where there is no myelin [13].

5.2.2- Characteristics of T_2 Components in a Standard Buffer Solution, Glutamate, Mn^{2+} and Gd-DTPA

A potential relationship between structural compartments in neural tissue and NMR parameters may increase the specificity of MRI in diagnosis of pathologies. It is very important then to determine in the optic nerve from which micro-anatomical regions signal is arising. The establishment of the relationship between the components of the T_2 spectrum and the compartments of the nerve are still under debate. There are several groups that have attempted to establish the component-compartment relationship for peripheral nerve; however to the best of our knowledge, no group has attempted to establish a relationship for optic nerve. As it was shown in the previous section, the short-lived component is agreed to be signal from the myelin. In two-component T_2 spectra, the longer-lived component is then attributed to the axoplasm and the extracellular space [4, 14, 15]. In neuronal structures such as frog sciatic nerve [1, 16-18], guinea pig [11], garfish [2] and optic nerve [5, 6] an intermediate- and a long-lived component have been observed. To establish the relationship in rat optic nerve we 1) compared NMR data with the amount of water in the different regions of the nerve, 2) used paramagnetic agents (Mn^{2+} and Gd-DTPA) and 3) glutamate. In this section we discuss the results obtained using these three different techniques to establish the component-compartment relationship.

The most relevant information obtained from comparing the amount of water in the optic nerve with the magnitude of the components in the T_2 spectrum is:

- Myelin water has a very similar magnitude to the short-lived component, $\approx 15\%$. This suggests, as it was mentioned before, that the short-lived component is signal coming from water in the myelin.

- The intermediate- and long-lived components have similar magnitudes to the extracellular space and the axoplasm water compartments. This is important as it was shown that the T_2 spectral components could be related with the water compartments of the optic nerve. However, due to the similarity of the magnitudes it is not possible to make a component-compartment assignment.

Analyzing the water compartments of the optic nerve does not provide sufficient information to establish the component-compartment relationship. Other techniques such as the use of glutamate to induce cell swelling (information that was compared with the changes in the T_2 spectrum) provided relevant information to establish this relationship in the optic nerve. We also performed experiments using rat sciatic nerve. After analyzing the results from these experiments we found that the short-, intermediate- and long-lived components can be related to signal from water in the myelin, extracellular space and axoplasm, respectively, because:

- After the addition of glutamate (presence of glutamate in the nerve causes water to be moved from the extracellular space into the axons, causing swelling) the short- and the intermediate-lived components decreased in size; however, the long-lived component increased. This suggests, based on a model of the optic nerve in which axons swell and the extracellular space decreases, that the intermediate-lived component may be signal from water in the extracellular space and the long-lived component from water in the axoplasm.

- Glial cells, specifically astrocytes, swell in the presence of glutamate as well as the axons. Glial cells are supposed to exchange water very rapidly through their membrane. Therefore, a single T_2 component should be detected with the glial cells and ECS [2]. In our model it may be possible that the T_2 times from the glial cells would be similar to that of axoplasm, and therefore this increase results in an increment in the size of the long-lived component; or, if the signal from glial cells is a result of a single component with the ECS, then this change would not be detected as the water in the ECS-glial cells compartment would remain the same just with different proportions.

- Experiments in rat sciatic nerve showed no statistical difference in the T_2 components comparing results in a standard buffer solution and a solution with glutamate. These results differ for what we have seen in the optic nerve because:

    i) The nerves have different engulfing membranes, which may have different permeabilities to glutamate.

    ii) The sciatic nerve lacks glutamate receptors and glial cells (astrocytes and oligodendrocytes), therefore the presence of glutamate should not have any effect on the nervous tissue. As a consequence of the difference in anatomical structures between the optic nerve (physiologically similar to white matter) and the sciatic nerve (part of the peripheral nervous system), we obtained different results in the component sizes after the addition of glutamate.

- The relaxation times of the optic nerve decreased after the addition of glutamate, while the relaxation times of the rat sciatic nerve decreased as well but to a lesser degree. Glutamate reduces the T_2 times of the buffer, therefore could be that glutamate also reduces the T_2 times of any component it enters. Changes in the relaxation times may have an implication on the component sizes, however, based on the comparison of the rat sciatic and optic nerve in a solution with glutamate, we believed that the changes in the components of the optic nerve reflects the effect that glutamate has in the nervous tissue.

Also, experiments with paramagnetic agents (Mn^{2+} and Gd-DTPA) were performed in order to provide evidence to support the previous component-compartment assignment, the relevant information for discussion is:

- The T_2 spectrum of the rat optic nerve is similar to that of the frog sciatic nerve in a standard buffer solution, however, after the addition of Mn^{2+} or Gd-DTPA the two spectrum profiles are very different throughout time as it is shown below.

- Mn^{2+} was used in frog sciatic nerves experiments by Wachowicz [17] to determine changes in the relaxation times of the components and analyze their magnitudes. This technique was used to establish a relationship between the T_2 spectrum components and the compartments in the frog sciatic nerves (fig. 5.1 a). We followed the same technique in order to establish the relationship in the rat optic nerve, however the results were very different (fig. 5.1 b).
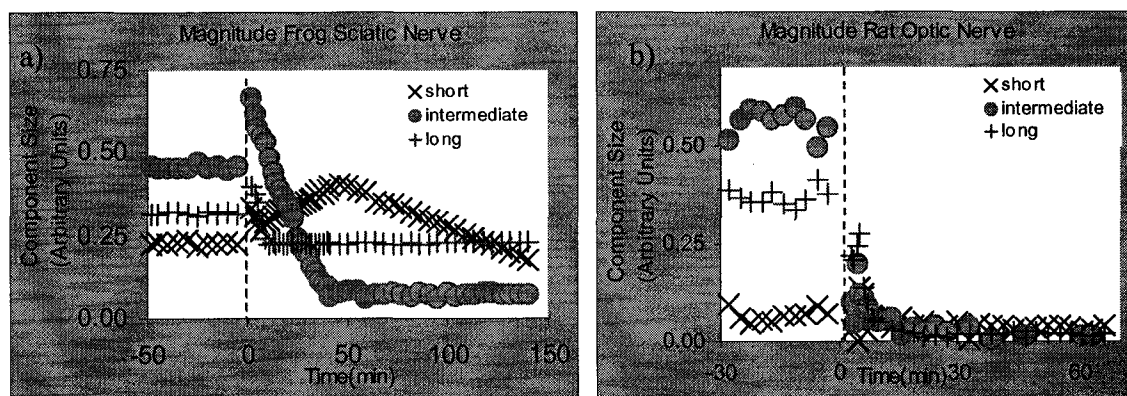
Fig. 5.1- In a) Magnitude of the frog sciatic nerve showing three components (short, intermediate and long) that can be related to three water compartments (myelin, ECS and axoplasm). Note that the intermediate component is the most affected one after the addition of a paramagnetic agent (Mn^{2+}) at time 0, indicating this component can be related to the ECS due to its proximity with the outer environment of the nerve. Data provided by Wachowicz. In b) Magnitude of the rat optic nerve showing the signal of the components vanishing after the addition of Mn^{2+}.

- The anatomical structure of the nerve plays an important role in determining which region of the nerve is being affected first by the paramagnetic agent. Based on the anatomy of nerves it is believed that Mn^{2+} will diffuse first into the ECS, then into the myelin and the axoplasm through the Nodes of Ranvier. After the addition of Mn^{2+} in experiments with optic nerve the signal decayed too rapidly, in less than 8 minutes, making it difficult to establish the component-compartment relationship. We believe this rapid decay might be caused by:

i) A difference in the nerve dimensions; the diameter of the optic nerve is approximately half that of the sciatic nerve. This difference has an implication in the diffusion rate, causing manganese to diffuse more rapidly into the optic nerve, vanishing the signal of the components. Based on the nerve dimensions the time it takes for the paramagnetic agent to diffuse into the center of the optic nerve is reduced roughly by four times compared to that in sciatic nerve. In diffusion $t \approx x^2$, where t = time to diffuse and x = distance.

ii) A difference in the membranes engulfing the nerves; the optic nerve is engulfed by meningeal sheaths of dura and the sciatic nerve by the perineurium. These membranes may have specific characteristics of permeability to the diffusion of paramagnetic salts.

iii) Smaller axons have a larger surface to volume ratio and higher rates of metabolism [19].

iv) In the central nervous system (CNS) the lengths of the nodes of Ranvier seem to be greater than in peripheral nerve [19] (fig. 5.2), thus the diffusion into the axons may be faster in optic nerve.

v) In the CNS, the axonal node is bare and the axolemma has an undercoating of dense material. A similar undercoating is also present at the peripheral node, but here the axon is covered by processes that extends from the outer layer of

cytoplasm of the Schwann cells [19] (fig. 5.2), suggesting that diffusion into the axons through the nodes of Ranvier should be more difficult in the peripheral nerve than in the CNS.
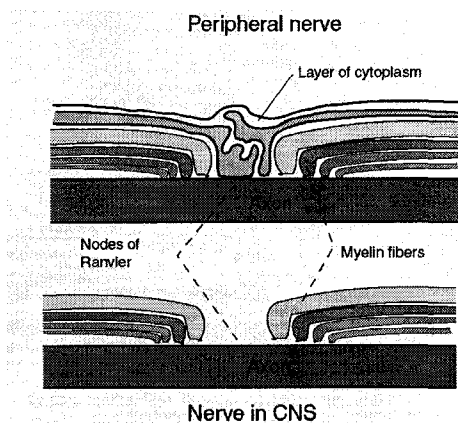

Fig. 5.2- Diagram comparing the nodal region of myelinated axons in the peripheral and central nervous systems. Note that the peripheral node is covered by an outer layer of cytoplasm that extends from the Schwann cells. Figure similar to [19].

- A higher concentration of paramagnetic agent (fig. 4.4) in the intermediate-lived component may suggest that this component could be related with the ECS, because in our model of the nervous tissue we believe that the paramagnetic agent will diffuse from the ECS to the axoplasm. For this to happen, a higher concentration of the paramagnetic agent should be present in the ECS. Even if the signal of the components decreased in <10% this observation provides valuable information of the optic nerve and $MnCl_2$.

- Rat sciatic and optic nerve exhibit similar three-component T_2-relaxation spectra; however, after the addition of $MnCl_2$ the two profiles seen by the T_2 relaxation analysis of the optic and sciatic nerve are quite different, so even if these nerves have similar characteristics and water compartments they are different from an NMR perspective.

- In experiments with 20-mM of Gd-DTPA the long-lived component was more affected than the intermediate component. This may reflect the action of the buffer solution and the paramagnetic agent in the long-lived component, decreasing it as it was shown with $FeCl_3$.

- After the addition of 30-mM of Gd-DTPA the intermediate-lived component was affected to a greater degree than the long-lived component; this suggests that the intermediate-lived component is due to signal coming form the extracellular space (due to its proximity to outer environment) and the long-lived component from the axoplasm.

- The decrease in the T_2 times of the long-lived component ($\approx 73\%$) is greater than the intermediate-lived component ($\approx 63\%$), however, the averaged magnitude of the component sizes for the intermediate-lived component was affected to a greater degree ($\approx 83\%$) than the long-lived component ($\approx 78\%$). Comparing these results with the ones obtained in frog sciatic nerves, these experiments may be an indication that the intermediate-lived component comes from the ECS and the long-lived component is due to signal coming from the axoplasm, as a result of the proximity of the ECS to the outer environment, which is affected to a greater degree by Gd-DTPA (also shown below).

- When analyzing the concentration of Gd-DTPA in the intermediate- and long-lived components of the optic nerve (fig. 4.11), we found that the results were similar to the optic nerve with Mn^{2+}. This may be an indication as well that the intermediate-lived component is signal from water in the ECS.

5.3- A Closer Look at Different Nervous Tissues and Experiments

Peled et al. [1] performed diffusion experiments in frog sciatic nerve at 2.35 Tesla and found three different T_2 components with values similar to our laboratory. In the Peled diffusion experiments, the water mobility of the intermediate-lived component ($T_2 \approx 100$ ms) was unrestricted, while restricted diffusion was observed in the long-lived component ($T_2 \approx 280$ ms), thus assigning this component to signal from the axoplasm because it is known that more cells and microtubules are present in this region which may decrease the movement of water. These findings agreed with the relationship found in our group. Other groups have suggested that the intermediate-lived component is signal from

the axoplasm and the long-lived component is signal from the extracellular space [18, 20]. However, they have not attempted to establish this relationship. They base their assignment on assumptions that are mainly sustained by the fact that the relaxation time of the long-lived component is the closest among all the T_2 components to that of water, and the ECS should be similar to water. However, in the ECS there is a large amount of collagen, which is known to reduce the water relaxation time [1, 21], so it is possible that collagen may have an influence on the reduced relaxation time present in the ECS. Collagen is a relaxing factor in tendons, and studies have shown that tumors having more collagen exhibit a shorter T_2 time than tumors with other histological composition. One thing that groups agree upon in peripheral nerve is that the T_2 spectrum is composed of three different relaxation times. Table 5.2 shows the results of T_2 relaxation analysis of peripheral nerve from different research groups.

Table 5.2- T_2 times and component sizes of different peripheral nerves.

	Short-lived		Intermediate-lived		Long-lived	
	T_2 (ms)	(%)	T_2 (ms)	(%)	T_2 (ms)	(%)
[a]Peled	18±1	17±4	68±16	54±3	281±34	29±4
[b]Does et al.	16	16	78	48	317	36
[c]Does and Gore	12	19	33	47	105	34
[d]Vasilescu et al.	17±6	29	70±14	50	310±21	21
[e]Wachowicz et al.	18	18	90	48	240	34

a Frog sciatic nerve for experiments in vitro at 2.35 T [1]. d Frog sciatic nerve in vitro [18].
b Frog sciatic nerve for experiments in vitro at 3.0 T [16]. e Frog sciative nerve for experiments in vitro at 3.0 T [17].
c Rat trigeminal nerve in vivo at 4.7 T [22]

Even though our study is based on the analysis of optic nerve, it is important to take a look at data from other nervous tissue such as peripheral nerve and white matter. Various research groups have identified the T_2 relaxation times of white matter at different field strengths; these results are shown in Table 5.3.

Table 5.3- T_2 times and component sizes ( ) for white matter and optic nerve.

Reference	Bo (T)	Short	Intermediate	Long
[a]Beaulieu et al.	2.35	49 (16)	140 (53)	480 (25)
[b]Lancaster et al.	1.9	10 (0.17)	40 (0.53)	130 (0.30)
[c]Stanisz et al.	1.5	22	176	
[d]MacKay et al.		10-55 (0.16)	>55 (0.84)	
[e]Stewart et al.	2.1	10 (0.04)	92 (0.96)	
[f]Vavasour et al.	1.5	20	80	120

a garfish optic nerve in vitro [2]. d white matter in human brain in vivo [23].
b white matter in human brain in vivo [24]. e brain and spinal cord of guinea pig in vitro [11].
c bovine optic nerve in vitro at 1.5 Tesla [9]. f human brain in vivo [25].

Three T_2-relaxation components are seen in peripheral nerve *in vivo* and *in vitro* which are similar to those found in optic nerve. The study by Does and Snyder [16] includes the identification of a long-lived component ($T_2>200$ ms) that was previously found only *in vitro*. There is enough evidence showing the T_2 spectrum of peripheral nerve to be characterized by three components, this characteristic was found in the optic nerve as well. Experiments with white matter have shown two and three components; this may be a result of the difference in the techniques to acquire data, the types of species and/or the field strength used for these studies.

5.4- Bibliography

1. Peled, S., et al., *Water diffusion, T_2, and compartmentation in frog sciatic nerve.* Magnetic Resonance in Medicine, 1999. **42**(5): p. 911-8.

2. Beaulieu, C., F.R. Fenrich, and P.S. Allen, *Multicomponent water proton transverse relaxation and T_2-discriminated water diffusion in myelinated and nonmyelinated nerve.* Magnetic Resonance Imaging, 1998. **16**(10): p. 1201-10.

3. Does, M.D. and R.E. Snyder, *Multiexponential T_2 relaxation in degenerating peripheral nerve.* Magnetic Resonance in Medicine, 1996. **35**(2): p. 207-13.

4. MacKay, A., et al., *In vivo visualization of myelin water in brain by magnetic resonance.* Magnetic Resonance in Medicine, 1994. **31**(6): p. 673-7.

5. Bonilla, I., Wachowicz, K., Snyder, R.E., *T_2 spectrum of mammalian optic nerve.* ISMRM 11th Meeting, 2003: p. 1452.

6. Wachowicz, K., and Snyder, R. E., *A Look at the Transverse Relaxation Spectra of Mammalian Optic Nerve at 3.0 T.* ISMRM 10th Meeting, 2002: p. 1211.

7. Landon, D.N., *The Peripheral Nerve.* 1976.

8. Fenrich, F.R., C. Beaulieu, and P.S. Allen, *Relaxation times and microstructures.* NMR in Biomedicine, 2001. **14**(2): p. 133-9.

9. Stanisz, G.J. and R.M. Henkelman, *Diffusional anisotropy of T_2 components in bovine optic nerve.* Magnetic Resonance in Medicine, 1998. **40**(3): p. 405-10.

10. Does, M.D. and J.C. Gore, *Compartmental study of diffusion and relaxation measured in vivo in normal and ischemic rat brain and trigeminal nerve.* Magnetic Resonance in Medicine, 2000. **43**(6): p. 837-44.

11. Stewart, W.A., et al., *Spin-spin relaxation in experimental allergic encephalomyelitis. Analysis of CPMG data using a non-linear least squares method and linear inverse theory.* Magnetic Resonance in Medicine, 1993. **29**(6): p. 767-75.

12. Elster, A.D., *Questions and Answers in Magnetic Resonance Imaging.* 1994.

13.   Fischer, H.W., et al., *Nuclear relaxation of human brain gray and white matter: analysis of field dependence and implications for MRI*. Magnetic Resonance in Medicine, 1990. **16**(2): p. 317-34.

14.   Gareau, P.J., et al., *In vivo measurements of multi-component T_2 relaxation behaviour in guinea pig brain*. Magnetic Resonance Imaging, 1999. **17**(9): p. 1319-25.

15.   Gareau, P.J., et al., *Magnetization transfer and multicomponent T_2 relaxation measurements with histopathologic correlation in an experimental model of MS*. Journal of Magnetic Resonance Imaging, 2000. **11**(6): p. 586-95.

16.   Does, M.D. and R.E. Snyder, *T_2 relaxation of peripheral nerve measured in vivo*. Magnetic Resonance Imaging, 1995. **13**(4): p. 575-80.

17.   Wachowicz, K. and R.E. Snyder, *Assignment of the T_2 components of amphibian peripheral nerve to their microanatomical compartments*. Magnetic Resonance in Medicine, 2002. **47**(2): p. 239-45.

18.   Vasilescu, V., et al., *Water compartments in the myelinated nerve. III. Pulsed NMR results*. Experientia, 1978. **34**(11): p. 1443-4.

19.   Davison, A.N. and A. Peters, *Myelination*. 1970: Charles C. Thomas.

20.   Shinar, H., Y. Seo, and G. Navon, *Discrimination between the different compartments in sciatic nerve by 2H double-quantum-filtered NMR*. Journal of Magnetic Resonance, 1997. **129**(1): p. 98-104.

21.   Sundaram, M., M.H. McGuire, and F. Schajowicz, *Soft-tissue masses: histologic basis for decreased signal (short T_2) on T_2-weighted MR images*. AJR. American Journal of Roentgenology, 1987. **148**(6): p. 1247-50.

22.   Does, M.D. and J.C. Gore, *Compartmental study of T_1 and T_2 in rat brain and trigeminal nerve in vivo*. Magnetic Resonance in Medicine, 2002. **47**(2): p. 274-83.

23.   Whittall, K.P., et al., *In vivo measurement of T_2 distributions and water contents in normal human brain*. Magnetic Resonance in Medicine, 1997. **37**(1): p. 34-43.

24.   Lancaster, J.L., et al., *Three-pool model of white matter*. Journal of Magnetic Resonance Imaging, 2003. **17**(1): p. 1-10.

25.   Vavasour, I.M., et al., *Different magnetization transfer effects exhibited by the short and long T_2 components in human brain*. Magnetic Resonance in Medicine, 2000. **44**(6): p. 860-6.

Chapter 6

Conclusion

6.1 Conclusion

Based upon the addition of $FeCl_3$ and fluorinert it is concluded that the long-lived component in optic nerve is not an artifact of the buffer solution. Thus it can be stated that the T_2-relaxation spectrum of the optic nerve is characterized by three real T_2 components.

Three different relaxation times were identified in rat optic nerve similar to those found in frog and rat sciatic nerves in a standard buffer solution; however, after the addition of Mn^{2+} the nerves exhibited different profiles, making it difficult to establish for the optic nerve the component-compartment relationship.

After performing experiments where Gd-DTPA was added to the buffer solution it was determined that the changes in the T_2 spectrum of the optic nerve were similar to those found in rat and frog sciatic nerves. Therefore, we believe they may share the same component-compartment relationship.

It was found in experiments were cellular swelling was induced in the optic nerve using glutamate that the component-compartment relationship agreed with previous experiments of frog sciatic nerve. Therefore, the suggested relationship is determined as the short-lived component to be signal from water in the myelin, the intermediate-lived component to be signal from water in the extracellular space and glial cells and the long-lived component to be signal from water in the axoplasm.